COMPUTATIONALLY EFFICIENT HYDROPOWER OPERATIONS OPTIMIZATION FOR LARGE CASCADED HYDROPOWER SYSTEMS REFLECTING MARKET POWER, FISH CONSTRAINTS, MULTI-TURBINE POWERHOUSES, AND RENEWABLE RESOURCE INTEGRATION

A Dissertation
Presented to the Faculty of the Graduate School
of Cornell University
In Partial Fulfillment of the Requirements for the Degree of
Doctor of Philosophy

by
Sue Nee Tan
August 2017

COMPUTATIONALLY EFFICIENT HYDROPOWER OPERATIONS OPTIMIZATION FOR LARGE CASCADED HYDROPOWER SYSTEMS REFLECTING MARKET POWER, FISH CONSTRAINTS, AND RENEWABLE RESOURCE INTEGRATION

Sue Nee Tan, Ph. D.

Cornell University 2017

Hydropower generation, though a centuries-old technology, is gaining new relevance as a way to integrate renewable energy sources into the power grid. This dissertation describes the development of two efficient models for optimizing hydropower operations to address the competing priorities of maximizing the value of hydropower generation, renewable generation integration, economically efficient hydropower generation, and environmental stewardship. The models are demonstrated using the 10-reservoir Federal Columbia River Power System in the Pacific Northwest in the U.S.A.

First, a computationally efficient nonlinear optimization model that maximizes the value of hydropower generation is built for the 10-reservoir system. This model incorporates forecasted inflow, hydropower plant operation, contracted energy loads, and the hydropower utility's interaction with wholesale energy markets. When applicable the model also includes special seasonal constraints for fish addressing specified turbine operations and upper and lower bounds on spills. The opportunity cost of meeting these environmental constraints can be quantified. Efficient features include variable time step lengths and precomputed powerhouse functions. For a 21-day horizon, having 8-hour time steps in the first few days of the model then transitioning to a coarser 24-hour time step for flow routing in the later stages results in

optimization runtimes being decreased to $1/6^{th}$ of the time it takes to run the optimization with all 8-hour time steps. Powerhouse functions reduced the many dispatch and loading decisions for multiple turbines at a hydropower project into a single generation function with respect to total flow. Additionally, the market power of a very large hydropower producer in a regional market is modeled. For an entity with market power, maximizing societal benefits will result in energy prices that are very similar across periods, which is the economically efficient solution. In contrast, maximizing revenue will result in prices that are not balanced across periods, a typical result from monopolistic behavior.

To address renewable integration, a second stochastic dynamic programming and nonlinear programming model builds upon the aforementioned framework with a time decomposition approach to maximize the value of hydropower generation of a subset of the 10-reservoir hydropower system under wind generation uncertainty. This model also includes the effect that wind generation has on market prices, in addition to the hydro utility market power. The results show that the hydro utility will hedge by decreasing its commitment to the wholesale electricity market under wind generation uncertainty. The model estimates the opportunity costs to the hydropower utility of providing hour-by-hour balancing of the wind generation to a wind power generation owner.

BIOGRAPHICAL SKETCH

Sue Nee Tan is a model builder and data visualization enthusiast currently at Pacific Gas and Electric (PG&E) in San Francisco, CA. As an Expert Quantitative Analyst with the Energy Procurement Modeling and Analysis team at PG&E, Sue Nee works on building models and performing analysis to answer some of the utility energy procurement questions around energy and reliability for both the California Independent System Operator's system and PG&E customers. She received an M.S. in Environmental and Water Resources Systems Engineering from Cornell University in 2013, and double Bachelor of Science degrees in Civil and Environmental Engineering (B.Sc. CEE) and Earth and Environmental Science (B.Sc. EES) from Lehigh University in 2009. In her spare time she enjoys hiking in the San Francisco Bay Area and beyond, and attempting to replicate childhood favorite dishes of her native Malaysia.

To God who made all things possible

with Your provision and grace,

for allowing me to surrender my trials to You;

To my husband, Kevin for nourishing me

and for your patience, understanding,

late-night counseling and support; and

To my parents, for their sage counsel and unfailing encouragement

ACKNOWLEDGMENTS

Thank you to my advisor Dr. Christine A. Shoemaker for her inspiring legacy as pioneering woman professor of engineering, and for her continued support, time and guidance.

Thanks to Prof. Jery R. Stedinger for his attention to detail and invaluable feedback as an expert in the hydropower optimization field – the rigor with which you viewed the results made the dissertation stronger.

Much appreciation to Steve Barton, currently at the U.S. Army Corps of Engineers, and his colleagues at the Bonneville Power Administration for all their industry knowledge, data, and for helping us to provide a useful product for their system.

To my collaborators Dr. Jonathan Lamontagne, Dr. Esther Chiew, and Liang Chen: this work would not have happened without your contributions, input, support, and friendship.

Thank you to my committee members Drs. Phillip Liu and Huseyin Topaloglu for their mentorship and support.

Finally, thank you to Enrique Mejorada, Yumi Oum, Jan Grygier, and all my other colleagues at PG&E for creating a challenging academic environment at the workplace, and for their unflagging support as I cross this threshold.

This research was made possible through financial support from the Hydro Research Foundation and the Cornell School of Civil and Environmental Engineering. We also thank the Bonneville Power Administration for their support of this work through the grant "Computationally efficient, flexible, short-term hydropower optimization and uncertainty analysis (SHOA) for the BPA system," TIP# 265: SHORT TERM HYDROPOWER OPTIMIZATION PROJECT, COOP. AGREEMENT 59612.

TABLE OF CONTENTS

LIST OF FIGURES

LIST OF TABLES

CHAPTER 1

INTRODUCTION

Hydropower operations optimization is an issue that has been a concern for many decades [*Becker and Yeh*, 1974; *Stedinger et al.*, 1984; *Tejada-Guibert et al.*, 1993; *Labadie*, 2004; *Li et al.*, 2013a, 2013b], by many eminent researchers in the field of water resources, applied mathematics, operations research, and electrical engineering. Power is sold with the price varying by season, by week, and from hour-to-hour making operations planning very important. This problem is especially challenging for systems with many connected reservoirs, or when hydropower generation is coupled with a thermal system generation [*Jacobs et al.*, 1995] or renewable energy resources such as wind [*Matevosyan et al.*, 2009]. Hydropower operations optimization continues to be an important and challenging problem, especially given new requirements associated with the incorporation of renewal energy sources and the increasing constraints associated with preserving aquatic life.

As part of a portfolio of solutions to combat climate change, many U.S. states have begun to adopt increasingly stringent renewable portfolio standards, which set targets for a certain percentage of generation from renewable resources by a prescribed date. Hawaii and possibly California have set ambitious targets to have 100% of their renewable generation come from renewable or non-GHG emitting sources by 2045 [*Maloney*, 2017]. According to the 2016 Annual Status Report of the U.S. Renewables Portfolio Standard (RPS) by the Lawrence Berkeley National Laboratory [*Barbose*, 2016], RPS policies collectively apply to 55% of total U.S. retail electricity sales. The same report also states that most of the 29 states that have set

their RPS goals are on their way to meeting roughly 95% of their interim RPS targets in recent years.

The inherent unpredictability of wind and solar can wreak havoc on a fragile electric grid that was built to run best on constant levels of supply and demand [*Bakke*, 2016]. As of 2016 California had about 10% of its energy served by wind and about 7% of its energy served by solar. At these penetration levels, the stochastic nature of wind becomes a significant issue, requiring large power reserves to prevent sags in supply should wind drop out suddenly [*Tuohy et al.*, 2009]. The forecast errors as a fraction of the wind power plant capacity usually average about 5 percent on an hour-ahead basis, and between 15 to 25 percent on a day-ahead basis [*Acker*, 2011]. Additionally, large amounts of solar generation have caused negative energy prices to occur in the middle of the day, indicative of supply-side inflexibilities and must-take energy contracts for solar and wind. This is the so-called duck curve [*St. John*, 2016].

Existing hydropower systems with large storage capabilities can provide flexible generation that can adjust for these forecast errors or act as grid-scale energy storage to shift energy in hours when there is overgeneration at a low environmental and economic cost [*Trabish*, 2017]. However, in some systems like the Federal Columbia River Power System (FCRPS) in the Pacific Northwest, the hydropower operators are legally bound to operate to meet the needs for navigation and operations that enhance and preserve endangered aquatic life [*US Army Corps of Engineers*, 2012]. Therefore, power production is not necessarily the highest priority for the operation of those systems. These and other constraints (e.g. recreation) may conflict with policies that seek to maximize the benefits from generation alone. Thus, careful

coordination is required in order to prevent the violation of these constraints [*Howard and Stedinger*, 2012].

The trade-offs between the meeting the constraints and maximizing the benefits are difficult to guess for large systems over many time steps. Changing the operations at upstream reservoirs will affect the operations of a reservoir downstream at a later time, which in turn affects the operations of the reservoirs further downstream at even later times. Consequently, this cascading effect makes it difficult to determine the optimal operation policy by trial-and-error in a short amount of time. Thus, the use of mathematical programming can provide a baseline or recommendation for the operators who seek to maximize the value from power generation while meeting all the constraints of the system. The chapters in this dissertation describe these mathematical models for hydropower system operation considering cascaded hydropower systems.

Choosing an efficient and effective mathematical programming algorithm for short-term hydropower production optimization is not a trivial task. The combination of many time steps, possibly nonlinear or multi-modal generation functions, and perhaps a need for integer variables leads to a difficult problem for deterministic analysis. The effects of unpredictability of renewable generation on the grid is perhaps most profound at smaller timescales (such as on the hourly time scale needed to model variations in wind power). The optimization time steps are shortened to take into account these effects, which then increases the size of the computational problem. The generation function for a hydropower plant made up of many generating units is nonlinear could be nonconvex, which may lead to a need for integer variables to ensure that the

optimum is found *[Li et al., 2013b]*. This further increases the difficulty of the problem. Additionally, there are sources of uncertainty that need to be taken into account, such as uncertainty in load (which is increased if renewable generation is subtracted from load), price, and inflows into the reservoir system. The need to run an algorithm many times to represent many scenarios makes choosing an efficient algorithm even more important.

The chapters in this dissertation develop efficient models for optimizing hydropower operations that can be used to as part of the solution for integrating renewables, accounting for the uncertainty in renewable energy generation and reflecting the behavior of market energy prices.

The second chapter describes the development of powerhouse functions which can be used as part of a larger model of a system; a powerhouse generation function describes power generation as a function of the total flow through the powerhouse, which may contain many turbines or different types where each type has its own characteristics. Scheduling many heterogeneous hydropower generating units at many projects using integer values leads to a very large and difficult problem; this is a tremendous burden if the analysis is to be repeated over many time steps. However, it is possible to precompute the optimal loading of the many different hydropower generation units at a powerhouse for a fixed time period. In addition, the powerhouse function can implicitly consider operations for preserving aquatic life, as well and constraints on the individual operating units. This powerhouse function generally eliminates the need for integer variables used in mixed-integer linear programming and greatly reduce the

difficulty of the optimization problem. Powerhouse functions can easily be recomputed to reflect anticipated maintenance of unanticipated forced outages.

The third chapter develops a variable time-step short-term scheduling optimization algorithm for a 10-reservoir hydropower system including the major facilities in the Federal Columbia River Power System in the Pacific Northwest. The output of the short-term scheduling optimization algorithm will serve to inform the operators of the optimal decisions for the operation of the 10-reservoir system that maximize benefits given an inflow, load, and price scenario. The computational burden of the optimization algorithm is greatly reduced because the optimal scheduling of the individual generation units within a project has already been considered, as described in the chapter 2. An efficient sequential quadratic programming routine is used so that the algorithm can be applied to both deterministic and stochastic optimization of the short-term hydropower scheduling problem.

Finally, the fourth chapter presents a computationally-efficient method of optimizing hydropower operations given a stochastic wind input into the system. Models developed in the second and third chapters are utilized in the development of this model. The algorithm will take a time-decomposition approach: on a daily timestep, the stochastic dynamic programming (SDP) optimizes the sequential day-to-day day-ahead power commitments for a horizon of one week; and on an hourly timestep, a nonlinear programming (NLP) algorithm receives the day-ahead power commitment as a constraint and optimizes the 24 hourly releases in a one day time horizon. This approach is expected to be more computationally efficient and realistic than a traditional stochastic dynamic programming algorithm with a one-hour time step. This is because

for a time horizon of T days, the number of stages are reduced from 24*T to T, while the multiple hourly scenarios can be solved for each day in parallel.

The models developed here also incorporate descriptions of the power markets and price variations with hydropower generation. Big systems like the mid-Columbia Federal power system affect the price in their regional market. To ignore such relationships can misrepresent the value of the generated power. Price variation over a day clearly impacts hydropower generation. In Chapter 3, we develop two functions that describe the value of hydropower when the hydropower utility has market power: revenue and avoided cost. Chapter 4 enhances this by modeling the interaction of dynamic hydropower operations with intermittent wind generation and a price model responsive to energy generation levels thereby providing an important description of the interaction of these players.

Clearly hydropower operations will be a challenge for some time here. This thesis research develops modeling methods that can be used to describe different operational issues, powerhouse operations, the variability of wind energy systems, and a dynamic energy price model.

1.1 References

Acker, T. L. (2011), Hydroelectric Industry's Role in Intergrating Wind Energy.

Bakke, G. (2016), The Grid: The Fraying Wires Between Americans and Our Energy Future, Bloomsbury Publishing.

Barbose, G. (2016), U.S. Renewable Portfolio Standards: 2016 Annual Status Report.

Becker, L., and W. W.-G. Yeh (1974), Optimization of Real Time Operation of a Multiple-Reservoir System, Water Resour. Res., 10(6), 1107–1112.

Howard, C. D. D., and J. R. Stedinger (2012), Hydroelectric Power and the Future, in Toward a Sustainable Water Future, edited by W. Grayman, D. P. Loucks, and L. Saito, pp. 234–242, ASCE Press.

Jacobs, J., G. Freeman, J. Grygier, D. Morton, G. Schultz, K. Staschus, and J. R. Stedinger (1995), SOCRATES: A system for scheduling hydroelectric generation under uncertainty, Annals, 59, 99–133.

St. John, J. (2016), The California Duck Curve is Real, and Bigger Than Expected, Green Tech Media.

Labadie, J. W. (2004), Optimal Operation of Multireservoir Systems : State-of-the-Art Review, J. Water Resour. Plan. Manag., 130(2), 93–111.

Li, F., C. A. Shoemaker, J. Wei, and X. Fu (2013a), Estimating Maximal Annual Energy Given Heterogeneous Hydropower Generating Units with Application to the Three Gorges System, J. Water Resour. Plan. Manag., 139(June), 265–276, doi:10.1061/(ASCE)WR.1943-5452.0000250.

Li, X., T. Li, J. Wei, G. Wang, and W. W.-G. Yeh (2013b), Hydro Unit Commitment via Mixed Integer Linear Programming : A Case Study of the Three Gorges Project , China, IEEE Trans. Power Syst., 1–10.

Matevosyan, J., M. Olsson, and L. Söder (2009), Hydropower planning coordinated with wind power in areas with congestion problems for trading on the spot and the regulating market, *Electr. Power Syst. Res.*, *79*(1), 39–48, doi:10.1016/j.epsr.2008.05.019.

Maloney, P. (2017), California Assembly Committee clears measure for 100% renewables goal, Util. Dive. Available from: http://www.utilitydive.com/news/california-assembly-committee-clears-measure-for-100-renewables-goal/447277/

Stedinger, J. R., B. F. Sule, and D. P. Loucks (1984), Stochastic dynamic programming models for reservoir operation optimization, Water Resour. Res., 20(11), 1499 – 1505, doi:10.1029/WR020i011p01499.

Tejada-Guibert, J. A., S. A. Johnson, and J. R. Stedinger (1993), Comparison of Two Approaches for Implementing Multireservoir Operating Policies Derived Using Stochastic Dynamic Programming, Water Resour. Res., 29(12), 3969–3980.

Trabish, H. K. (2017), Prognosis negative: How California is dealing with below-zero power market prices, Util. Dive, 1–12. Available from: http://www.utilitydive.com/news/prognosis-negative-how-california-is-dealing-with-below-zero-power-market/442130/

Tuohy, A., P. Meibom, E. Denny, and M. O. Malley (2009), Unit Commitment for Systems with Significant Wind Penetration, IEEE Trans. Power Syst., 24(2), 592–601.

US Army Corps of Engineers (2012), Fish Passage Plan.

CHAPTER 2

PRECOMPUTED MULTI-TURBINE POWERHOUSE GENERATION FUNCTIONS WITH OR WITHOUT FISH CONSTRAINTS

2.1 Introduction

The operation of cascaded reservoirs on major river systems with hydropower objectives is an economically and environmentally important problem in many parts of the world. Examples of such systems include the PG&E hydropower system in Northern California [*Jacobs et al.*, 1995], the BC Hydro system in British Columbia, Canada [*Shawwash et al.*, 2000], the Brazilian hydropower system [*Barros et al.*, 2003], the Federal Columbia River Power system in Washington and Oregon [*Schwanenberg et al.*, 2014], the Ume River hydropower system in Sweden [*Matevosyan et al.*, 2009], and the Nile River in Africa [*Digna et al.*, 2017]. The multi-period optimization of such system poses a very large-scale and highly nonlinear problem with different components of the system operating on different temporal and spatial scales: system operation requires looking weeks and months into the future, whereas the operation of powerhouses and turbines can consider decisions made on hourly and sub-hourly time scales.

Hydropower system operators turn to models such as those described in Jacobs et al [1995] and Shawwash et al [2000] to inform daily operation of their reservoir system. Since these models will be run frequently (at least daily), computational efficiency is a key factor in the usability of a proposed modeling system if operators are to have the ability to look at many options and/or a stochastic future. In our analysis to capture different temporal-spatial scales, we consider the case wherein the optimization of a system of reservoirs with hydropower generation

is broken down into three temporal - spatial levels: (1) the overall system level addresses the quantity and timing of the flows between individual reservoirs and total system energy generation in different periods that result from those releases, (2) the power plant level, where the quantity and timing of the flows among different turbines each with their own generation characteristics are optimized given a total reservoir releases, and (3) the turbine level, where turbine generation as a function of head and flow through the turbine is characterized to enable optimization of power plant operations. This chapter develops an algorithm that addresses the latter two problem formulations. Chapter 3 addresses the overall system level optimization problem.

Previous incorporations of multiple types of turbines in the hydropower system level optimization have used approximations of the power generation function as a series of piecewise linear functions of turbine flows [*Becker and Yeh*, 1974], [*Yeh*, 1985], [*Labadie*, 2004], [*Hamann et al.*, 2017]. However, linearization results in approximations that may be unacceptable to hydropower systems operators. For example, powerhouse generation functions derived using multi-regression analysis to fit two-dimensional piecewise linear lookup tables [*Schwanenberg et al.*, 2014] results in the inability to explicitly account for turbine outages in a powerhouse and the inability to explicitly model operations that dictate a specific turbine order, as required on the Columbia River in some periods. Additionally, Perez-Diaz et al. [2010] demonstrates that failing to account for turbine nonlinearities could result in an overestimation of powerhouse generation). For piecewise linear functions that do take into account head effects and turbine overdrive opportunities [*Chang et al.*, 2001] [*Li et al.*, 2013a], [*Li et al.*, 2013b], the resulting number of decision variables that would be taken into account for a mixed-integer linear program (MILP)

for multi-stage multi-reservoir operating accounting for heterogeneous units within each powerhouse would be intractable for stochastic optimization.

This chapter develops a powerhouse function as a computationally efficient way to solve the power plant level and turbine level problems and uses it to develop such functions for different projects in a large system of hydropower reservoirs with or without fish constraints on powerhouse operations. The powerhouse function has four important characteristics: (1) reduction of many turbine-level decision variables to one powerhouse release per project for a multi-reservoir optimization model, (2) precomputation of the plant-level powerhouse function, (3) incorporation of operational constraints, and (4) continuity and convexity of the powerhouse generation function. This analysis has been performed using actual turbine efficiency data from the large Federal Columbia River hydropower system: 10 projects with 1 to 4 turbine types per project and several turbines of each type, and includes complex legal restrictions for fish protection. These will be discussed in more detail in Section 2.2.

The remainder of the chapter is laid out as follows: first, a brief overview of powerhouse operations is provided in Section 2.3. Section 2.5 provides a general algorithm for constructing powerhouse function when no restrictions on turbine dispatch order or load are imposed. In this case, the resulting powerhouse function maximizes powerhouse generation for a particular flow and head. Section 2.6 addresses the cases where there are restrictions on the turbine dispatch order; methods are provided that identify near-optimal powerhouse generation as a function of flow for a fixed head. Section 2.7 summarizes the findings and insights for the case study. Section 2.8 provides conclusions.

2.2 Powerhouse Function Features

The hydropower functions developed here need to have several critical functions and features. First, the powerhouse function must calculate the most energy that can be generated with a given release at a given reservoir storage level, reflecting an optimal dispatch and allocation of water to the different turbines (loading). As a result, a reservoir system model will need only one powerhouse function release variable per project per time step, eschewing the need to assign decision variables for each individual turbine type. Incorporating models of individual turbines can results in a mixed-integer programming model, which are very involved to solve. Finer details will be implicit, and in most cases there are many possible allocations of flows among turbines that would yield the same results.

Pre-computation of powerhouse functions results in a smaller optimization problem for the mutli-reservoir system optimization model. The powerhouse function can be used with efficient nonlinear programming methods such as sequential quadratic programming (SQP) [*Boggs and Tolle*, 1995] and other programming methods such as Stochastic Dynamic Programming (SDP), Approximate Dynamic Programming (ADP), and Model Predictive Control(MCP) that aim to maximize the value of generations by the hydropower system overall subject to constraints.

The second feature of the powerhouse function is that it can be "precomputed;" that is, the powerhouse functions are calculated in advance of their use in a systems optimization algorithm. In our example, first a least-squares spline was fit to actual turbine generation data available for alternative turbine types. This allowed computation of the most efficient operating

point for each turbine type and generation as a function of release. Our approach will treat turbines of the same type as identical, which greatly simplifies the solution space for the plant level optimization problem compared to Lagrangian relaxation or dynamic programming, as used previously in Ponrajah et al. [1998], Li et al. [1997], and Perez-Diaz et al. [2010]. The BC Hydro model in Shawwash et al.[2000] also uses a precomputed generation function which is obtained using dynamic programming[*Siu et al.*, 2001]. We dispatch turbines at their maximum efficiencies, following a heuristic that is much faster than solving the dispatch and loading problem using dynamic programming or mixed-integer linear programming. .

The third characteristic of our powerhouse functions is that different powerhouse functions can be quickly computed to reflect three situations that may occur at different times of the year: a) optimal "economic" operations with all turbines available and operations are not constrained by legislation, b) operations that are dictated by legislation to protect endangered anadromous fish populations, and c) operations with planned and unplanned outages of turbines. In the first operation type (a), the turbine dispatch and loading is unconstrained and can be run optimally. In the second type of operation (b), different policy and regulatory constraints limit the dispatch order of the turbines within a powerhouse. Finally, the operation type (c) can occur concurrently with operation types (a) and (b). Hydropower turbines routinely undergo planned outages as part of regular maintenance. Moreover, unplanned outages can occur and can last for several weeks. Our methodology is flexible and can quickly develop new powerhouse functions that reflect changes in unit availability. This is not the case if powerhouse functions result from fitting a regression to historical data, as in Schwanenberg et al. [2014].

The fourth feature of the powerhouse function result from it being the solution to a continuous maximization problem that is convex in the decision vector, which is the amount of water going through each turbine. Concave powerhouse functions will expedite the computation time for a nonlinear programming algorithm to solve the system operation problem, thus eliminating the need to simplify the powerhouse function by linearization, as done by Catalao et al. [2009] and Perez-Diaz et al. [2010]. This convexity is important because it means the continuous optimization can be much more computationally efficient. In SDP and ADP, the future value function is computed by solving a "subproblem", which is optimizing the decision for each value of the state space sample, an operation that occurs many times in each time period. The convexity of the powerhouse function means we can employ convex nonlinear programming methods with continuous variables that solve the subproblem very quickly. In addition, convexity is necessary to assure convergence of the continuous nonlinear programming methods typically used in MPC for hydropower optimization. As discussed later, non-convexity occurs with fish constraints that dictate turbine loading order which is not economic. We have developed an approximation approach to generating convex powerhouse functions that are generally sufficiently accurate to provide good policies while retaining convexity.

2.3 Federal Columbia River Power System

The operation of 10 reservoirs in the Federal Columbia River Power System is used as a case study for the development of powerhouse functions for projects with different numbers of turbine types and operational constraints. The Bonneville Power Administration, US Army Corps of Engineers, and the U.S. Bureau of Reclamation jointly operate and manage the 10 reservoir with a combined generation capacity of 20 GW. Figure 2-1 shows a schematic of the

reservoirs and their relationship to one another. The powerhouses at a reservoir in the hydropower system have several turbines grouped into different types. For example, there are 24 turbines grouped into four types at Grand Coulee (GCL) with a total generation capacity of about 6.8 GW [*Bonneville Power Administration et al.*, 2001]. The powerhouse function at Grand Coulee should represent the total generation for a given flow through the project. Note that there will be only one powerhouse function per project, even though physically there may be more than one powerhouse function at a particular project, as would be the case for Grand Coulee which has three. A dispatch order to produce optimal amount of power for a given release of water from the reservoir needs to be determined, and is called "economic" dispatch. The optimal dispatch and allocation of flows and the constraints on turbine flows are implicitly represented by the powerhouse function.

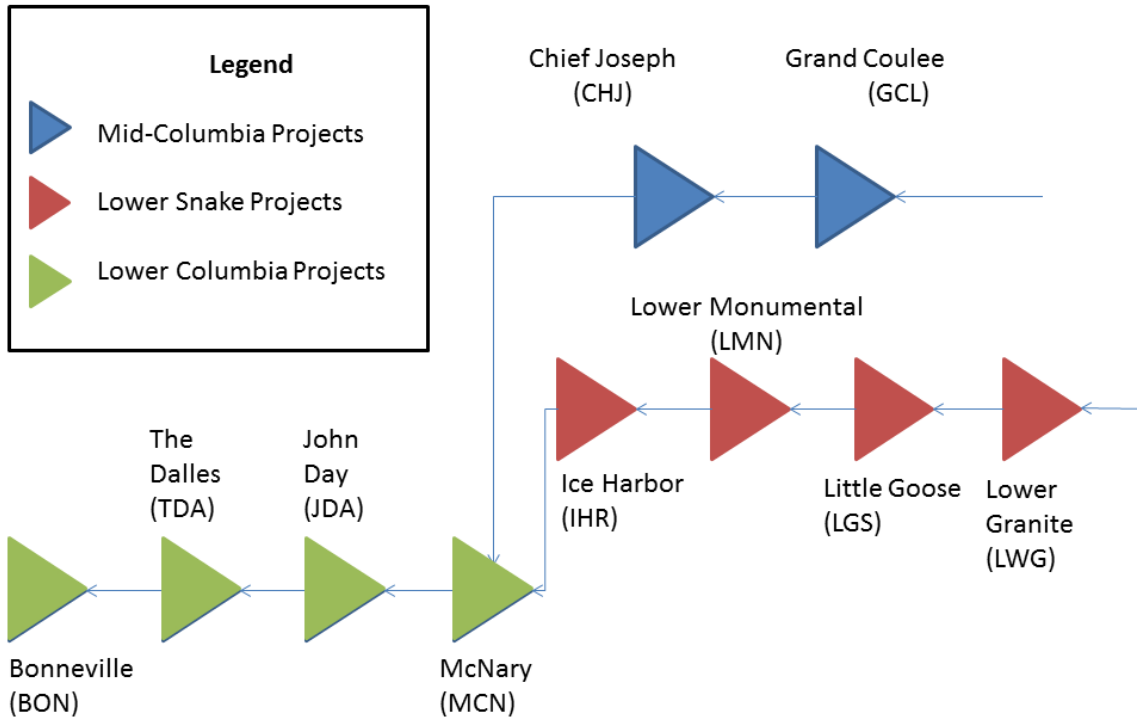

Figure 2-1: Schematic of the 10-reservoir system for the Federal Columbia River Power System.

Operation of the 10 reservoirs are also subject to a number of requirements; among the most important is the seasonal operation of the system to meet water quality standards and provide attraction flows for endangered anadromous fish that spawn in the Columbia River basin. In these operations, the "fish" dispatch order does not always maximize the combined efficiency of the units; instead dispatch is selected to improve flow patterns in the vicinity of the dam, or to provide attraction flow for fish ladders. Figure 2-2 summarizes the powerhouse operations for each reservoir project and for each monthly period. The green shaded cells show times where there are no dispatch restrictions, and so the reservoir project operates with economic dispatch, which maximizes the efficiency of generation for each level of flow through that powerhouse [*Ponrajah et al.*, 1998]. The yellow shaded cells describe reservoir powerhouse

operations with fish dispatch to encourage fish migration through and maximize the survival rate of the fish travelling through the Columbia River. This includes fish screens at certain reservoirs at certain times, which also affect the generation characteristics of the turbines.

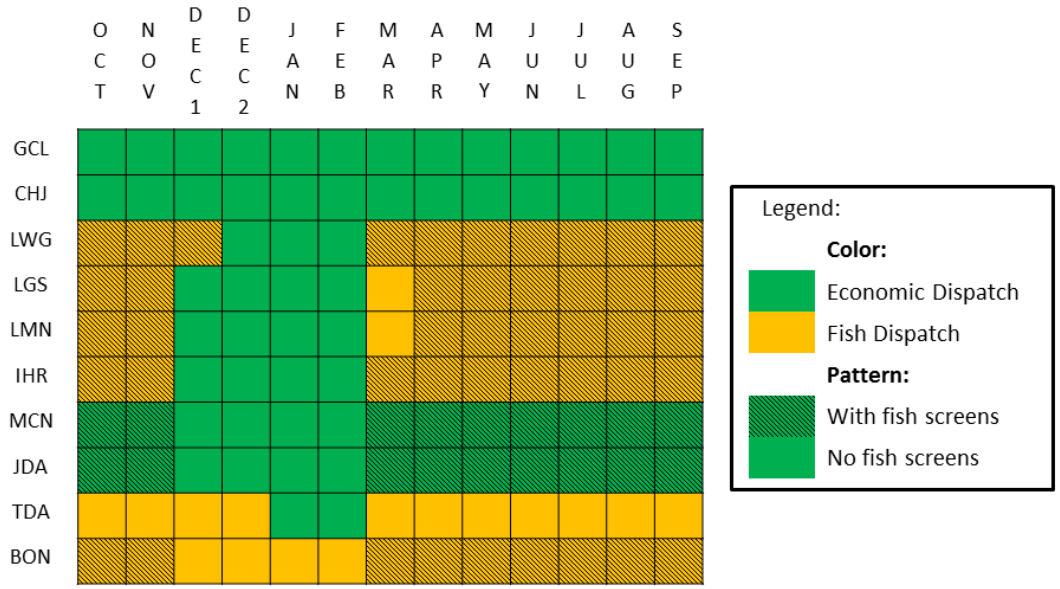

Figure 2-2: Powerhouse operations at the reservoirs (rows) for each month of the year (columns). Each reservoir is represented as a three-letter code. Economic Dispatch is when the turbine types are dispatched in order of the most efficient to the least efficient. Fish Dispatch follows a prescribed turbine order specified in the Fish Passage Plan.

2.4 Turbine operations and maximum Turbine Efficiency

When maximizing generation at a powerhouse that has several turbines, an optimal solution is to load each turbine at their most efficient operating point if possible (efficient turbine operation), and then vary the number of hours of operation at that release rate to pass the allocated volumes of water. This means that the turbine (or some turbines) may not operate all of the hours during a period. In the turbine overdrive case a turbine would be pushed beyond its efficient average

operating point (EAOP) and will operate at a higher flow rate for the entire period if more water is to be released than can be released at the most efficient operating point. An example with two turbine types will be discussed in later sections.

Turbines incur some power losses due to friction in the penstock, the turbine itself, the drive system and the generator. Thus, for a fixed head, the efficiency of a turbine is proportional to the average generation for a given flow, $\frac{GT(q)}{q}$. This can be written as Equation (2.1) .

$$efficiency = \frac{\text{Actual Generation}}{\text{Theoretical Maximum Generation}} \propto \frac{GT(q)}{q} \tag{2.1}$$

where $GT(q)$ is the energy generated with a release rate of q. The theoretical maximum generation would depend on the product of the head, the weight of water, and the flow rate q.

.

Analytical functions for actual hydropower turbine generation $GT(q)$ do not exist in general. Operators typically have tables of "observed" generation as a function of flow, defined here as $GT(\mathrm{q})$ for a fixed head shown as red open circles in Figure 2-3(a). We fit least-squares cubic splines to the turbine generation data, resulting in an approximation $\widehat{GT}(q)$, shown as the blue line through the circles in Figure 3(a).

Least squares cubic splines are developed in Chapra & Canale [2010]. Least squares splines are appropriate for cases such as the situation here where one has many data points that should be smoothed to obtain a reasonable approximation with a continuous second derivative. Cubic splines are defined by a set of knots, with cubic polynomials between knots. The

coefficients of the splines are selected to ensure that the spline has continuous first and second derivatives. A spline with k knots, has k-1 intervals with a different cubic polynomial defined over each of the (k-1) intervals. Those polynomials thus have 4(k-1) parameters, which are subject 3 constraints at each of (k-1) interior knots. Thus overall all there are k+2 free parameters that can be selected to fit the least squared spline to the available data [*Chapra and Canale,* 2010]. Figure 2-3(a) shows a fitted spline and the original data for a head of 182 feet at Chief Joseph dam.

The least squares cubic splines provide an approximation to the actual generation function provided by the BPA. Least-squares cubic splines allowed the development of a realistic smoothed representation of the available turbine operating data. Cubic splines are flexible while avoiding excessive oscillation, and are easy to evaluate. The residuals of the LS spline fit are shown in Figure 2-3(b). The ratio of the standard error to the average generation over the turbine range is 0.2% while the ratio of the maximum errors to the average generation is about 0.6%. This was thought to indicate a good fit overall. However, the smoothness in the residuals suggests that the turbine generation data we obtained from BPA experienced some smoothing itself.

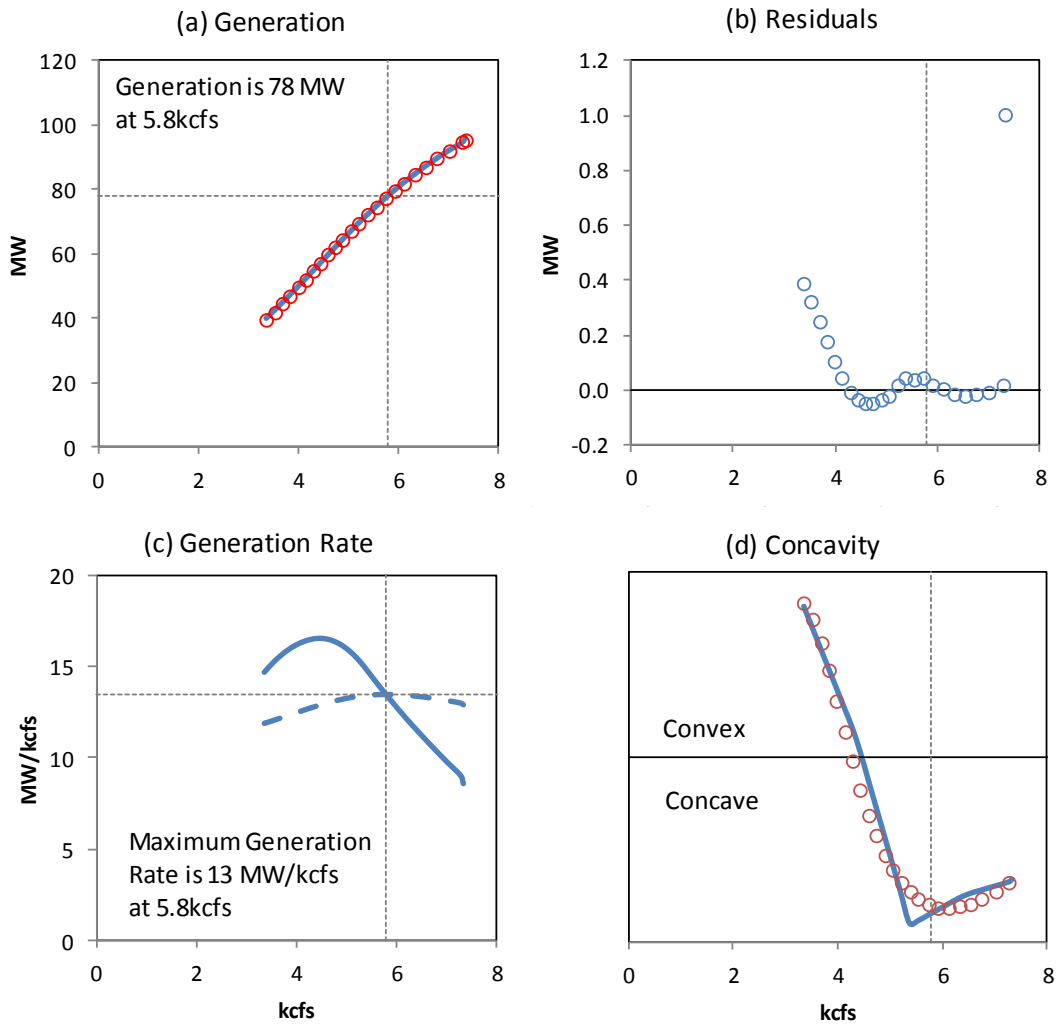

Figure 2-3: Turbine characteristic plots for Chief Joseph turbine type 1 at a head of 182 ft for different turbine flow values q. (a) shows the original generation data $GT(q)$ plotted as red open circles, with the spline approximation $\widehat{GT}(q)$ as a solid line. (b) shows the residual errors for different flow values q. (c) displays the first derivative of the spline approximation $\widehat{GT}'(q)$ as solid line and the average generation $GT(\mathrm{q})/\mathrm{q}$ as a dotted line . (d) shows the concavity for different flow values q, computed using the second derivative of the approximation function $\widehat{GT}''(q)$ (blue line) and the second derivative computed from the original turbine generation data (red circles).

We define the Efficient Average Operating Point (EAOP) as the flow q_{EAOP} at which the average generation rate $\frac{GT(q)}{q}$ in Equation (2.1) is maximized. To find the maximum of $\frac{GT(q)}{q}$,

we can set the derivative of this ratio with respect to q to zero. Thus we seek the $q = q_{EAOP}$ that solves Equation (2.2).

$$\frac{d}{dq}\left(\frac{GT(q)}{q}\right) = \frac{GT'(q)}{q} - \frac{GT(q)}{q^2} = 0 \tag{2.2}$$

Equation (2.2) yields the desired relationship to identify the most efficient operating point.

$$GT'(q_{EAOP}) = \frac{GT(q_{EAOP})}{q_{EAOP}} \tag{2.3}$$

The marginal generation per unit release, $GT'(q)$, and the average generation per unit flow through the turbine, $\frac{GT(q)}{q}$, describe the short and long-term generation rates per unit of flow release for each turbine type. Equation (2.3) states that at the most efficient operating point $q = q_{EAOP}$ the marginal generation per unit release $GT'(EAOP)$ equals the average generation rate $\frac{GT(q_{EAOP})}{q_{EAOP}}$. Figure 2-3c shows such a result. In this case, because flows less than 2 kcfs are relative inefficient, the maximum overall average generation $\frac{\widehat{GT}(q)}{q}$ occurs for a flow beyond the point where $\widehat{GT}'(q)$ has a maximum, which is where the last cfs of water released produced the maximum power possible.

The q_{EAOP} for the Chief Joseph type 1 turbine at a head of 182 feet is approximately 5.8 kcfs. The average and marginal generation per unit of flow at that point is approximately 14 MW/kcfs. The derivative of the turbine generation function shows that turbine generation is clearly a nonlinear function of the flow through the turbine. A linear approximation of the unit

generation function would result in errors in generation, especially when the turbine is operating towards the upper end of its generation capacity.

As a check, for the average generation per unit of flow $\frac{GT(q)}{q}$ to be a maximum, the second derivative of $GT(q)$should be negative; thus we ask if

$$\frac{d^2}{dq^2}\left(\frac{GT(q)}{q}\right)=\frac{GT''(q)}{q}-2\frac{GT'(q)}{q^2}+2\frac{GT(q)}{q^3}<0 \tag{2.4}$$

Substituting the flow $q = q_{EAOP}$ and Equation (2.3) into Equation (2.4) gives Equation(2.5).

$$\begin{aligned}\left.\frac{d^2}{dq^2}\left(\frac{GT(q)}{q}\right)\right|_{q=q_{EAOP}} &= \frac{GT''(q_{EAOP})}{q_{EAOP}}-2\frac{GT'(q_{EAOP})}{q_{EAOP}^{\ 2}}+2\frac{GT(q_{EAOP})}{q_{EAOP}^{\ 3}}\\ &= \frac{GT''(q_{EAOP})}{q_{EAOP}}-\frac{2}{q_{EAOP}^{\ 2}}\left(\frac{GT(q_{EAOP})}{q_{EAOP}}\right)+2\frac{GT(q_{EAOP})}{q_{EAOP}^{\ 3}}\\ &= \frac{GT''(q_{EAOP})}{q_{EAOP}}<0\end{aligned} \tag{2.5}$$

Equation (2.5) shows that in order for the flow $q = q_{EAOP}$ to maximize the average generation rate, the second derivative of the turbine generation function GTshould be less than zero: $GT''(q_{EAOP}) < 0$. This means that it is important that the turbine generation functions are concave downward, at least in the region where the turbine would be operating. The second derivative of the function should never go from negative to positive, indicating an inflection point. This would cause reservoir operation with multiple turbines to have local optima, which can cause convergence problems with quasi-Newtonian optimization algorithms and failure to fine the true optimum. Figure 2-3(d) shows that the second derivative of that turbine generation

function is indeed negative (i.e. the turbine generation function is concave) near the efficient average operating point q_{EAOP}.

2.5 Economic Dispatch Powerhouse Generation Functions

Consider now the efficient operation of a powerhouse which has several turbines of different types. For a given head and release, it must be resolved which turbines will run (dispatch) and with what release (loading). During the times when a hydropower project is not constrained for fish operations, the dispatch order of the turbines is unconstrained. Thus, the turbines can be dispatched in an order to maximize the generation at the powerhouse for a given powerhouse function flow rate r_{PH}. We refer to this type of dispatch as Economic Dispatch.

The derivation in Section 2.4 shows that for a single turbine, we cannot do better than releasing at the efficient average operating point q_{EAOP}. So if just k identical turbines are available, and we need to release at an average rate of r_{PH}, then for $k * q_{EAOP} \leq r_{PH}$, a best solution is to have all k turbines release at EAOP a fraction $r_{PH}/(k\ q_{EAOP})$ of the time. Alternatively, let $k_{need} = r_{PH}/(k\ q_{EAOP})$ and k_{min} be the value of k_{need} rounded down. Then we can run k_{min} turbines at q_{EAOP} for the whole period and one turbine for a fraction $(k_{need} - k_{min})$ of the time. Because every turbine that is operating is releasing at their most efficient operating point, no rescheduling of flows can result in generation of more power, if there are enough turbines. If all k identical turbines are dispatched, and $* q_{EAOP} \leq r_{PH}$, then water must be released at a higher rate or even spilled if necessary. Let q_{max} be the maximum power release for the k identical turbines. Then for $k * q_{max} > r_{PH}$, the optimal solution is to

let every turbine release at rate $q = r_{PH}/k$ so that they all have the same marginal generation rate; then for concave $GT(q)$, no reallocation of releases among turbine can increase the overall generation. For $k * q_{max} < r_{PH}$, then every turbine can release at q_{max} and the e xtra water must be spilled. That resolves how to operate a powerhouse with one type of turbine.

Now suppose a powerhouse has k Type 1 turbines and m Type 2 turbines, where the Type 1 turbines that are more efficient than the Type 2 turbines, i.e. $GT'(q_{EAOP,1}) > GT'(q_{EAOP,2})$. Following the logic above, the optimal powerhouse generation function as a function of powerhouse flow r_{PH}, starting at r_{PH} = 0, is to load each of the k Type 1 turbines of the most efficient turbine type sequentially at their most efficient operating point; as r_{PH} increases beyond $r_{PH} > k * q_{EAOP,1}$, the second most efficient turbines will be dispatched. But before bringing on the Type 2 turbines, there should be a transition period where the Type 1 turbines will be loaded beyond their EAOP until they operate at a marginal generation level $GT'(q_1)$ equal to that of the most efficient operating point of the Type 2 turbines $GT'(q_{EAOP,2})$, where $q_1 > q_{EAOP,1}$; for any given powerhouse flow r_{PH}, all turbines that are dispatched should have the same marginal generation rate GT'; were that not so, more energy could be generate by diverting some of the flow from turbines with smaller *GT'* values to turbines with larger *GT'*. This is the first-order condition for an optimum.

Following the algorithm above, we use the knowledge of the most efficient operating points q_{EAOP} and the turbine generation behaviors at flows beyond each q_{EAOP} from the turbine functions $\widehat{GT}(q)$ described in Section 2.4, for each turbine type, to construct the optimal powerhouse generation function $GH(r_{PH})$ as a function of the total powerhouse flow r_{PH}.

2.5.1 Assumption for Turbine Operation

In the construction of the powerhouse generation function, we assume that individual turbines of the same turbine type are identical. For example, consider a powerhouse that has turbines numbered 1-3 of type 1 and turbines numbered 4-6 of type 2. Then the order in which the individual units of type 1 are loaded does not matter (e.g. it can be 1,2,3 or 2,1,3). However, the dispatch order determines the number of units of each type that are dispatched in each time period.

Further, as discussed in Section 2.5, all turbines should be running at the same marginal generation rate when possible. This ensures that no reallocation of flows will result in a higher generation. Consider what happens as the total powerhouse flow r_{PH} increases starting at zero. The assumption is that a turbine is run with a release q_{EAOP} all or part of the time. If for a certain time period, the powerhouse release $r_{PH}$is greater than the number of turbines running at EAOP, i.e. $k * q_{EAOP}$, then the $k + 1$th unit of the same type can be brought on and the time it is operated increases until it is operating at q_{EAOP} for the entire period. Only the latest unit brought on would be run part of the time. This would continue until all units of the same types are running for the entire period. Before bringing on the next most efficient turbines, all turbines currently running will be pushed beyond their most efficient operating type to the efficiency of the next group of turbines brought online. The process continues until all turbines are dispatched.

The dispatch order of the unit types is determined by the efficiency of the generating unit. The most efficient unit types are run first, followed by the second most efficient unit types and so on. The convenient assumption that the last turbine loaded runs only part of the time results in

reasonable operation within each time period. Actually, the critical number is just the number of hours units of each type operate at their EAOP or another flow rate. The actual dispatch of turbines within each time period would be determined by a model with a smaller time step that might also consider within-period variations in load, needs for spinning reserve, and variation in generation across a region.

2.5.2 Algorithm for Construction of Economic Dispatch Powerhouse functions

For a powerhouse with *M* unit types and NT_m units in each type *m (m=1,…,M),* the powerhouse function will have $2M$ segments – odd numbered segments correspond to a linear segmentfor the dispatch of the units of type m at their most efficient operating point $q_{EAOP,m}$. Even numbered sections correspond to a nonlinear transition segment that describes what happens then all the unit types online are pushed beyond their q_{EAOP} to where their marginal generation equals that of the next unit type. At the very end, all turbines are simultaneously loaded at the same marginal generation except for units that have reached their respective capacities. Thus no reallocation of flows can result in generation of more power (assuming concave turbine generation functions $GT(q)$).

The algorithm for Economic Dispatch of units in a powerhouse with two unit types is described in the following paragraphs. This algorithm can be generalized to *M* unit types.

Step 1: For $0 \leq r_{PH} \leq NT_1 q_{EAOP,1}$

Sequentially load the most efficient turbines (type 1) at their EAOP with the assumption that the latest turbine brought online is run only part of the time period. Equation (2.6)

describes how the powerhouse flow rate, r_{PH} to the powerhouse generation given the head, $GH(r_{PH}|H)$.

$$GH(r_{PH} \mid H) = \frac{r_{PH}}{q_{EAOP,1}} GT_1(q_{EAOP,1} \mid \mathrm{H})$$
$$\text{where} \qquad (2.6)$$
$$0 \le r_{PH} \le NT_1 q_{EAOP,1}$$

In general, where n_1 is the number of turbines of type 1, and there are $n < NT_1$ turbines loaded, the ratio $\frac{r_{PH}}{q_{EAOP,1}}$ within the interval $(n-1, n)$, indicates that $n-1$ turbines could be running full time at their EAOP, while the n^{th} turbine runs at a fraction $\frac{r_{PH}}{q_{EAOP,1}}$ - $(n-1)$of the time period. Other allocations of the $\frac{r_{PH}}{q_{EAOP,1}}$ hours are possible.

Step 2:For $NT_1 q_{EAOP,1} \le r_{PH} \le NT_1 q_1$

Before bringing on the next most efficient units, all the most efficient (type 1) units are run beyond their most efficient operating point until the marginal generation for unit type 1, $\widehat{GT_1'}(q_1)$ is equal to the marginal generation for unit type 2 at its most efficient operating point, $\widehat{GT_2'}(q_{EAOP,2})$, or at its maximum flow, whichever comes first. Thus no reallocation of flows can generate more power, for concave $GT(q)$.

A cubic polynomial approximation (Equation (2.7)) was developed to describe GH over this transition section this transition section:

$$GH(r_{PH} \mid H) = GH_{0,2} + a_2(\mathrm{r}_{PH} - r_{0,2})^3 + b_2(\mathrm{r}_{PH} - r_{0,2})^2 + c_2(\mathrm{r}_{PH} - r_{0,2}) + d_2$$

where

$$GH_{0,2} = GH(r_{0,2} \mid H) \tag{2.7}$$

$$r_{0,2} = NT_1 q_{EAOP,1}$$

$$r_{0,2} \le r_{PH} \le NT_1 q_1$$

The parameters a_2, b_2, c_2 and d_2 are fit using the following information:

- the powerhouse generation at the point where all type 1 units are running full time at their EAOP, $GH\left(NT_1 q_{EAOP,1} \mid H\right)$;
- the slope of the powerhouse function at the point where all type 1 units are running full time at their EAOP, which is also the slope of the Type 1 turbine generation function at EAOP $\widehat{GT}_1'\left(q_{EAOP,1}\right)$;
- the powerhouse generation at the point where all type 1 units are running full time at the marginal generation of the next most efficient turbine or at its maximum flow, $GH(n_1 q_1 \mid H), where\ \widehat{GT}_1'(q_1) = \max\left(\widehat{GT}_2'\left(q_{EAOP,2}\right), \widehat{GT}_1'\left(q_{max,1}\right)\right)$;
- the slope of the powerhouse function at the point where all type 1 units are running full time at the marginal generation of the next most efficient (type 2) units, which is also the slope of the Type 2 turbine generation function at its EAOP $\widehat{GT}_2'(q_{EAOP,2})$.

Step 3: For $NT_1 q_1 \le r_{PH} \le NT_1 q_1 + NT_2 q_{EAOP,2}$

Load the next most efficient (Type 2) units at their most efficient operating point, with a similar assumption that latest turbine loaded can run part of the time period. Equation

(2.8) describes the linear relationship between powerhouse flow, r_{PH} and the powerhouse generation given the head, $GH(r_{PH}|H)$, across this section:

$$GH(r_{PH} \mid H) = GH_{0,3} + \frac{GT_2(q_{EAOP,2})}{q_{EAOP,2}}(\mathrm{r}_{PH} - r_{0,3})$$
where
$$GH_{0,3} = GH(r_{0,3} \mid H) \tag{2.8}$$
$$r_{0,3} = NT_1 q_1$$
$$r_{0,3} \le r_{PH} \le NT_1 q_1 + NT_2 q_{EAOP,2}$$

(2.9)

Step 4: For $NT_1 q_1 \le r_{PH} \le NT_1 q_1 + NT_2 q_{EAOP,2}$

At this point, all turbine types 1 and 2are loaded. As r_{PH} increases further all units are run at the same marginal generation until they reach their capacities.

A cubic polynomial (Equation (2.10)) approximates this last overdrive section.

$$GH(r_{PH} \mid H) = GH_{0,4} + a_4(\mathrm{r}_{PH} - r_{0,4})^3 + b_4(\mathrm{r}_{PH} - r_{0,4})^2 + c_4(\mathrm{r}_{PH} - r_{0,4}) + d_4$$
where
$$GH_{0,4} = GH(r_{0,4} \mid H) \tag{2.10}$$
$$r_{0,4} = NT_1 q_1 + NT_2 q_{EAOP,2}$$
$$r_{0,4} \le r_{PH} \le NT_1 q_{\max,1} + NT_2 q_{\max,2}$$

The parameters a_4, b_4, c_4 and d_4 are fit using the following information:

- the powerhouse generation at the point where all Type 2 units are running full time at their EAOP, $GH(n_1 q_1 + n_2 q_{EAOP,2}|H)$;
- the slope of the powerhouse function at the point where all type 2 units are running full time at their EAOP, which is also the slope of the Type 2 turbine generation function at its EAOP, $GT_2'(q_{EAOP,2})$;
- the powerhouse generation at the point where all type 2 and type 1 units are running full time at the marginal generation of the next most efficient turbine or at their respective capacities,

$$GH(NT_1 q_{max,1} + NT_2 q_{max,2}|H)$$

- the slope of the powerhouse function at the point where all units are running at maximum flow, which is determined by the smaller of the efficiency of the Type 1 turbine at its maximum flow rate, or the efficiency of the Type 2 turbine at its maximum flow, $\min(GT_1'(q_{max,1}), GT_2'(q_{max,2}))$.

It is important to note that the second derivative of the function approximating the overdrive section should be negative in the whole range, indicating a concave function. Transitions from negative to positive indicate a local optimum which is unrealistic and could slow down the sequential quadratic programming algorithm.

2.6 Fish Dispatch Powerhouse Generation Functions

Fish Dispatch differs from Economic Dispatch in that the dispatch order is not necessarily in the most efficient order. Each powerhouse will have its own specific dispatch order, as certain

turbines are prioritized to improve flow patterns in the vicinity of the dam, or to provide attraction flow for fish ladders in order to meet environmental legislation for protection of endangered fish species[*US Army Corps of Engineers*, 2012]. Typically, the Fish Dispatch algorithm is used when the efficiencies of the turbine are not in descending order (e.g. the more efficient turbines are not used first). The methodology discussed here is an improvement over the linear regression equation based on historical data used to approximate the powerhouse generation during the fish migration season discussed in Schwanenberg et al. [2014]. Similar to the Economic Dispatch algorithm, the turbines are loaded at their most efficient operating point, q_{EAOP}, and only the latest turbines brought on are allowed to operate for part of the time period.

2.6.1 Assumptions

The fish-dispatch loading patterns of the turbines for the 10 reservoirs fall into three categories:

A. There is no pre-specified turbine loading order for the fish season, or there is only one turbine type, and all units are assumed to have the same characteristics. Hence, the turbines can be loaded efficiently using economic dispatch, as described in Section 2.5. Type A reservoirs consist of Grand Coulee, Chief Joseph, McNary and John Day.

B. A dispatch order is specified that alternates between inefficient and efficient turbine units. Here, the inefficient and efficient turbines can be paired one-to-one and loaded together so as to achieve an average efficiency over their range of operation (i.e., each unit operates at their own EAOP, but for a fraction of the time). Type B reservoirs consist of Lower Granite and Lower Monumental.

C. The ratio of inefficient-to-efficient turbine units being loaded is higher in the first section than in the second. For example, the dispatch order for Ice Harbor is that 2 inefficient units are loaded first, followed by 1 efficient unit, then the remaining inefficient unit, and finally the remaining 2 efficient units. There are several ways in which these units can be grouped. Firstly, the third and fourth units can be loaded together, which would result in each group of two units having progressively increasing average efficiencies, which potentially creates alternative optima and trouble in the optimization step. Alternatively, the units can be loaded in groups of three, which would result in the first group having a lower average efficiency than the second. Either method of loading gives a non-concave curve, which would result in a slow convergence of the nonlinear optimization algorithm to a solution. Type C reservoirs consist of Ice Harbor, Little Goose, The Dalles and Bonneville.

For the reservoirs of Type B and Type C, we will describe two ways of developing non-economic powerhouse functions (that result from a dictated dispatch order): loading the turbines one at a time at their EAOP (single dispatch in Section 2.6.2.1), or loading the turbines in pairs or more (joint dispatch in Section 2.6.2.2). For non-economic dispatch powerhouse functions that result in nonconcave functions, an approximation of the nonconcave section is needed to allow the nonlinear optimization algorithm to converge quickly to a solution, described in 2.6.2.3.

The same assumptions are made for the Non-Economic Dispatch Powerhouse Generation functions as the Economic Dispatch Powerhouse functions:

1. While particular unit numbers may be specified in the dispatch order, only the unit type matters in the dispatch. For example, at Bonneville, Unit 8 has to be loaded before Unit 1. If Unit 1 and Unit 8 are Type 1 turbines, then the algorithm reads this as "two units of type 1 are loaded." If Unit 8 is Type 2 and Unit 1 is Type 1, then the algorithm reads this as "one unit of Type 2 is loaded first, followed by a unit of Type 1."

2. Each unit group brought online is loaded at its q_{EAOP} until all units are loaded. For the Non-Economic Single Dispatch, each unit group contains 1 turbine unit, while for Non-Economic Joint Dispatch, each unit group may contain multiple turbine units.

3. Only the latest turbine group brought online can be run for part of the time step (4, 8, or 24 hours).

An additional assumption is made for the approximation to the "best" dispatch which is that errors of approximation within 5MW is acceptable since the automatic generation control within the reservoir power plant can only adjust to within 5MW of precision. In the case of Bonneville, the errors are allowed to be higher because of tidal effects.

2.6.2 Algorithms for Construction of Fish Dispatch Powerhouse Functions

2.6.2.1 Fish Single Dispatch Algorithm

We first describe the Fish Single Dispatch algorithm, or simply the Fish Dispatch algorithm, by providing an example at Ice Harbor. The number of turbines of each type are $NT_1 = 3$ of Type 1, and $NT_2 = 3$ of Type 2, and Type 1 turbines are more efficient than the Type 2 turbines. The dispatch order for Ice Harbor for Fish passage season is: first load up to two Type 2 turbines, followed by a Type 1 turbine, then a Type 2 turbine, and finally two Type 1 turbines. Based on the dispatch order for Ice Harbor, this powerhouse function has 4 sections. The number of units to be loaded in each section are $n_1 = 2, n_2 = 1, n_3 = 1$ and $n_4 = 2$.

The algorithm is as follows:

Step 1: For $0 \le r_{PH} \le n_1 q_{EAOP,2}$

Sequentially load $n_1 = 2$ of the less efficient turbines (Type 2) at their EAOP with the assumption that the latest turbine brought online can run part of the time period. Equation (2.11) describes the relationship between powerhouse flow, r_{PH} to the powerhouse generation given the head, $GH(r_{PH}|H)$.

$$GH(r_{PH} \mid H) = \frac{GT_2(q_{EAOP,2} \mid \mathrm{H})}{q_{EAOP,2}} r_{PH}$$
$$\text{where} \qquad (2.11)$$
$$0 \le r_{PH} \le n_1 q_{EAOP,2}$$

Here, if n_1 is the number of turbines of type 1, and there are $n < n_1$ turbines loaded, the ratio $\frac{r_{PH}}{q_{EAOP,2}}$ within the interval $(n-1, n)$, indicates that $n-1$ turbines are running full

time at their EAOP, while the n^{th} turbine is running at a fraction $\frac{r_{PH}}{q_{EAOP,2}}$ - $(n-1)$ of the time period.

Step 2: For $n_1 q_{EAOP,2} \leq r_{PH} \leq n_1 q_{EAOP,2} + n_2 q_{EAOP,1}$

Load the $n_2 = 1$ of the more efficient (Type 1) units at their most efficient operating point, with a similar assumption that this turbine can run part of the time period. Equation (2.12) describes the relationship between powerhouse flow, r_{PH} to the powerhouse generation given the head, $GH(r_{PH}|H)$.

$$GH(r_{PH} \mid H) = GH_{0,2} + \frac{(r_{PH} - r_{0,2})}{q_{EAOP,1}} GT_1(q_{EAOP,1})$$

where

$$GH_{0,2} = GH(r_{0,2} \mid H) \qquad (2.12)$$

$$r_{0,2} = n_2 q_{EAOP,1}$$

$$r_{0,2} \leq r_{PH} \leq n_1 q_{EAOP,2} + n_2 q_{EAOP,1}$$

Step 3: For $n_1 q_{EAOP.2} + n_2 q_{EAOP,1} \leq r_{PH} \leq NT_2 q_{EAOP,2} + n_2 q_{EAOP,1}$

Load the $n_3 = 1$ of the less efficient (Type 2) units at their most efficient operating point, with a similar assumption that this turbine can run part of the time period. Equation (2.13) describes the relationship between powerhouse flow, r_{PH} to the powerhouse generation given the head, $GH(r_{PH}|H)$.

$$GH(r_{PH} \mid H) = GH_{0,3} + \frac{GT_2(q_{EAOP,2})}{q_{EAOP,2}}(\mathrm{r}_{PH} - r_{0,3})$$

where

$$GH_{0,3} = GH(r_{0,3} \mid H) \tag{2.13}$$

$$r_{0,3} = n_1 q_{EAOP,2} + n_2 q_{EAOP,1}$$

$$r_{0,3} \le r_{PH} \le (n_1 + n_3) * q_{EAOP,2} + n_2 q_{EAOP,1}$$

Step 4:For $NT_2 q_{EAOP,2} + n_2 q_{EAOP,1} \le r_{PH} \le NT_2 q_{EAOP,2} + NT_1 q_{EAOP,1}$

Load the $n_4 = 2$ of the more efficient (Type 1) units at their most efficient operating point, with a similar assumption that the latest turbine loaded can run part of the time period. Equation (2.14) describes the relationship between powerhouse flow, r_{PH} to the powerhouse generation given the head, $GH(r_{PH}|H)$.

$$GH(r_{PH} \mid H) = GH_{0,4} + \frac{GT_1(q_{EAOP,1})}{q_{EAOP,1}}(\mathrm{r}_{PH} - r_{0,4})$$

where

$$GH_{0,4} = GH(r_{0,4} \mid H) \tag{2.14}$$

$$r_{0,4} = (n_1 + n_3) * q_{EAOP,2} + n_2 q_{EAOP,1}$$

$$r_{0,4} \le r_{PH} \le (n_1 + n_3) * q_{EAOP,2} + (n_2 + n_4) * q_{EAOP,1}$$

Step 5:For $NT_2 q_{EAOP,2} + NT_1 q_{EAOP,1} \le r_{PH}$

$$\le NT_2 q_{EAOP,2} + NT_1 * \min(q_1, q_{max,1})$$

At this point, all turbine types 1 and 2 are loaded. Before pushing all the turbines to their limits, all the more efficient (Type 1) turbines are loaded at the same flow q_2 such that all units that are loaded are run at the same marginal generation (i.e. $GH_2'(q_1) = GH_2'(q_{EAOP,2})$) or at their respective capacities, whichever comes first.

A cubic polynomial (Equation (2.15)) approximates this transition section.

$$
\begin{aligned}
&GH(r_{PH} \mid H) = GH_{0,5} + a_5(\mathrm{r}_{PH} - r_{0,5})^3 + b_5(\mathrm{r}_{PH} - r_{0,5})^2 + c_5(\mathrm{r}_{PH} - r_{0,5}) + d_5 \\
&\text{where} \\
&GH_{0,5} = GH(r_{0,5} \mid H) \\
&r_{0,5} = (n_1 + n_3) * q_{EAOP,2} + (n_2 + n_4) * q_{EAOP,1} \\
&r_{0,5} \le r_{PH} \le (n_1 + n_3) * q_{EAOP,2} + (n_2 + n_4) * q_1 \\
&GT'_1(q_1) = \max(GT'_1(\mathrm{q}_{\max,1}), GT'_2(q_{EAOP,2}))
\end{aligned}
\tag{2.15}
$$

The parameters a_5, b_5, c_5 and d_5 are fit using the following information:

- the powerhouse generation at the point where all type 1 and 2 units are running full time at their EAOP, $GH\big((n_1 + n_3)q_{EAOP,2} + (n_2 + n_4)q_{EAOP,1} | H\big)$;
- the slope of the powerhouse function at the point where all type 1 units are running full time at their EAOP, which is also the slope of the Type 1 turbine generation function at EAOP, $GT_1'\big(q_{EAOP,1}\big)$;
- the powerhouse generation at the point where all Type 1 and Type 2 units are running full time at the marginal generation of the less efficient (Type 2) units,

$$GH\left((n_1 + n_3)q_{EAOP,2} + (n_2 + n_4)q_1 \middle| H\right)$$

$$where\ GT_1'(q_1) = \max\big(GT_1'\big(q_{max,1}\big), GT_2'(q_{EAOP,2})\big)$$

- the slope of the powerhouse function at the point where all units are running full time at the marginal generation of the less efficient (Type 2) units, which is determined by the larger of the efficiency of the Type 1 turbine at its maximum

flow rate, or the efficiency of the Type 2 turbine at its EAOP,

$\max\left(GT_1'\left(q_{max,1}\right), GT_2'(q_{EAOP,2})\right)$

Step 6: Repeat the same process as Section 4 in Section 2.5.2

2.6.2.2 Fish Joint Dispatch Algorithm

Recall that the dispatch order is 2 less efficient (Type 2) turbines are loaded first, followed by 1 more efficient (Type 1) unit, then the remaining less efficient turbine, and finally the remaining 2 efficient units. This creates non-concavity in the powerhouse generation function as the loading of less efficient turbines are followed by that of efficient turbines, which creates problems for the optimization.

This can be overcome partially using the joint dispatch approach, which is described below. The joint dispatch algorithm gives a realistic physical representation of the turbine loadings. Although BPA loads the turbines in an inefficient manner to facilitate the movement of fish through the fish passages, they usually load the turbines in sequence between separate powerhouses. Since each powerhouse separately houses the same type of turbines (i.e. one powerhouse will contain the less efficient turbines while the other contains the more efficient ones), the BPA is thus loading a less efficient and an efficient turbine simultaneously, but running them together for only a fraction of the time. This results in a powerhouse generation function that is a straight line until all the units are running, with an efficiency of release that is always the average of the turbines being loaded.

By using the joint dispatch approach, the unit groups for Ice Harbor thus consists of three turbines each. The first unit group contains 2 less efficient and 1 more efficient turbine, while the second unit group contains 1 less efficient and 2 more efficient turbines, in accordance with the dispatch order for Ice Harbor.

The joint dispatch turbine loading algorithm for Ice Harbor is as follows. This powerhouse function has 2 sections. The number of units to be loaded in each section is $N_1 = 3$ and $N_2 = 3$, where the number of turbines of each type are $NT_1 = 3$ of type 1 and $NT_2 = 3$ of type 2, as before.

Step 1:For $0 \leq r_{PH} \leq n_{1,2}q_{EAOP,2} + n_{1,1}q_{EAOP,1}$

Simultaneously load $N_1 = 3$ turbines at each turbine's individual EAOP with the assumption that all N_1 turbines brought online can be run for part of the time period. For Ice Harbor, the $N_1 = 3$ turbines consist of $n_{1,2} = 2$ of the less efficient (Type 2) turbines and $n_{1,1} = 1$ of the more efficient (Type 1) turbines, where $n_{i,j}$ refers to the number of Type j turbines being loaded in Section i, and $\sum_j n_{i,j} = N_i$. Equation (2.16) describes the relationship between the powerhouse flow, r_{PH} to the powerhouse generation given the head, $GH(r_{PH}|H)$.

$$GH(r_{PH} \mid H) = \frac{n_{1,1}GT_1(q_{EAOP,1} \mid H) + n_{1,2}GT_2(q_{EAOP,2} \mid H)}{n_{1,1}q_{EAOP,1} + n_{1,2}q_{EAOP,2}} r_{PH}$$

where (2.16)

$$0 \leq r_{PH} \leq n_{1,1}q_{EAOP,1} + n_{1,2}q_{EAOP,2}$$

The ratio $\frac{r_{PH}}{n_{1,1}q_{EAOP,1}+n_{1,2}q_{EAOP,2}}$ corresponds to our assumption that the latest turbine group brought online can be run part-time. In this first step, if N_1 is the number of turbines being loaded in step 1, and there are $n < N_1$ turbines loaded, then all N_1 turbines are only run for a fraction of the time period.

Step 2: For $n_{1,2}q_{EAOP,2} + n_{1,1}q_{EAOP,1} \leq r_{PH} \leq NT_2q_{EAOP,2} + NT_1q_{EAOP,1}$

Simultaneously load $N_2 = 3$ turbines at each turbine's individual EAOP with the assumption that all N_2 turbines brought online can be run for part of the time period. The $N_2 = 3$ turbines consist of $n_{2,2} = 1$ of the less efficient (Type 2) turbines and $n_{2,1} = 2$ of the more efficient (Type 1) turbines. Equation (2.17) describe the relationship between the powerhouse flow, r_{PH} to the powerhouse generation given the head, $GH(r_{PH}|H)$.

$$GH(r_{PH} \mid H) = GH_{0,2} + \frac{n_{2,1}GT_1(q_{EAOP,1} \mid H) + n_{2,2}GT_2(q_{EAOP,2} \mid \mathrm{H})}{n_{2,1}q_{EAOP,1} + n_{2,2}q_{EAOP,2}}(r_{PH} - r_{0,2})$$

where

$$GH_{0,2} = GH(r_{0,2} \mid H) \tag{2.17}$$

$$r_{0,2} = n_{1,1}q_{EAOP,1} + n_{1,2}q_{EAOP,2}$$

$$r_{0,2} \leq r_{PH} \leq (n_{1,1} + n_{2,1})q_{EAOP,1} + (n_{1,2} + n_{2,2})q_{EAOP,2}$$

Step 3: Follow steps 5 and 6 in Section 2.6.2.1

2.6.2.3 Function approximation

Since the Fish Dispatch order involves loading some less efficient turbines before the most efficient turbines, the resulting function from Section 1 through 4 in Section 2.6.2.1 is non-concave. The approximation for the non-concave (i.e. "sawtooth") part of the powerhouse

function curve results in a concave powerhouse function to be used in nonlinear optimization. This will enable the nonlinear program to converge to an optimal solution relatively quickly without being stuck at a particular section. The equation for the approximation is shown in Equation (2.18). Note that this function approximation is precisely the Fish joint dispatch algorithm for Type B reservoirs described in Section 2.6.1, thus giving a realistic physical representation of this approximation.

$$GH_{approx}(r_{PH} \mid H) = \begin{cases} \dfrac{\mathrm{GH}(\mathrm{r}_{0,5} \mid H)}{r_{0,5}0} r_{PH} & \text{for } 0 \le r_{PH} \le r_{0,5} \\ GH(r_{PH} \mid H) & \text{for } \mathrm{r}_{PH} \ge r_{0,5} \end{cases} \tag{2.18}$$

Where $r_{0,5} = NT_1 q_{EAOP,1} + NT_2 q_{EAOP,2}$ is the point where all turbines are running at their most efficient operating point, corresponding to the beginning of Step 5 of the Fish Single Dispatch algorithm in Section 2.6.2.1 or the beginning of Step 3 of the Fish Joint Dispatch algorithm in Section 2.6.2.2.

Note here that the approximation is only for the portion of the powerhouse function where the slope increases and decreases according to the turbine types that are loaded. When all the turbines are loaded and are pushed to their limits, the approximation and the "optimal" powerhouse function are the same. We will later show that the differences in solutions found between the approximation and the actual powerhouse function are very small compared to the total system generation.

2.7 Results

2.7.1 From Turbine Functions to Powerhouse Functions: An Example

In this section we show an example of the turbine characteristics, economic dispatch powerhouse function, and the fish dispatch powerhouse functions for the Ice Harbor (IHR) reservoir. The head is fixed to be 93 feet, which is the middle of the normal operating range for head at IHR. IHR was chosen because it has some of the most complicated Fish Dispatch operations in the 10-reservoir system.

Turbine generation functions $\widehat{GT}(q)$ were fitted to the empirical generation data provided by the BPA for the type 1 and type 2 units at IHR according to the methodology outlined in Section 2.4. Table 2-1 summarizes the turbine characteristics obtained from fitting $\widehat{GT}(q)$. Here the type 1 turbines are slightly more efficient and thus have a higher rate of generation than the type 2 turbines. Both turbines also have their most efficient operating points just past the middle of the operating range as shown by the ratio of the efficient average operating point to the maximum flow, $\frac{q_{EAOP}}{q_{max}}$. Meanwhile, the generation at the most efficient operating point is at about three quarters of the maximum generation of the turbine as shown by the ratio of the generation at the EAOP to the maximum generation of the turbine, $\frac{\widehat{\mathrm{GT}}(\mathrm{q_{EAOP}})}{\widehat{\mathrm{GT}}(\mathrm{q_{max}})}$.

Table 2-1: Characteristics of fitted turbine generation $\widehat{GT}(q)$ at the efficient average operating point q_{EAOP} for the type 1 and type 2 turbines at Ice Harbor at a head of 93 feet, in the middle of its normal operating range

	Type 1	**Type 2**
Peak efficiency	90%	88%
$\widehat{\boldsymbol{GT}}'(\boldsymbol{q_{EAOP}})$**, MW/kcfs**	7.1	6.9
$\frac{\mathbf{q_{EAOP}}}{\mathbf{q_{max}}}$	62%	65%
$\frac{\widehat{\mathbf{GT}}(\mathbf{q_{EAOP}})}{\widehat{\boldsymbol{GT}}(\mathbf{q_{max}})}$	75%	74%
$\frac{\textbf{Standard error of residuals}}{\textbf{generation midpoint}}$	< 0.1%	< 0.1%
$\frac{\textbf{Max(residual)}}{\textbf{generation midpoint}}$	1.6%	0.1%
$\widehat{\mathbf{GT}}"(\mathbf{q_{EAOP}})$	negative	negative
Number of times second derivative goes from negative to positive	0	0

The residuals of the function fit show a good fit of $\widehat{GT}(q)$ to the empirical data. The standard error normalized by the generation midpoint is less than 0.1% while the maximum errors normalized by the generation midpoint is less than 2%. Both turbine functions are concave downwards around the most efficient operating point, as shown by the second derivative of the powerhouse function with respect to flow $\widehat{GT}"(q_{EAOP})$. The second derivative never crosses from negative to positive, which means that the function is concave through the range considered for operation.

The turbine functions are then used to develop the powerhouse functions for each reservoir. Figure 2-4 shows the rate of generation of the Economic Dispatch Powerhouse function (algorithm described in Section 2.5.2) as a function of the powerhouse flow. The

marginal generation rate is shown here rather than the actual generation rate to highlight the nonlinearity of the powerhouse generation function. This powerhouse generation function is concave over the operating range of the powerhouse, as seen by the nonincreasing slope of the function. Observe that the marginal generation rate in the linear segment of the powerhouse function in Figure 2-4 is equal to the EAOP of the turbines being loaded sequentially in that section as shown in Table 2-1. Note also the relatively small nonlinear segment between 40 kcfs and 45 kcfs since the efficiencies of the two turbine types are so close to one another. Finally, observe the relatively long nonlinear segment at the end where all the turbines are being pushed to the top of their typical operating range. Recall from Table 2-1 that the EAOP is about 65% of the maximum flow, and the top of the typical operating range of the turbine may be lower than the flow maximum flow. A comparison of the linearity of the powerhouse functions at the different sites in the Federal Columbia River Power System is discussed in Section 2.7.2.

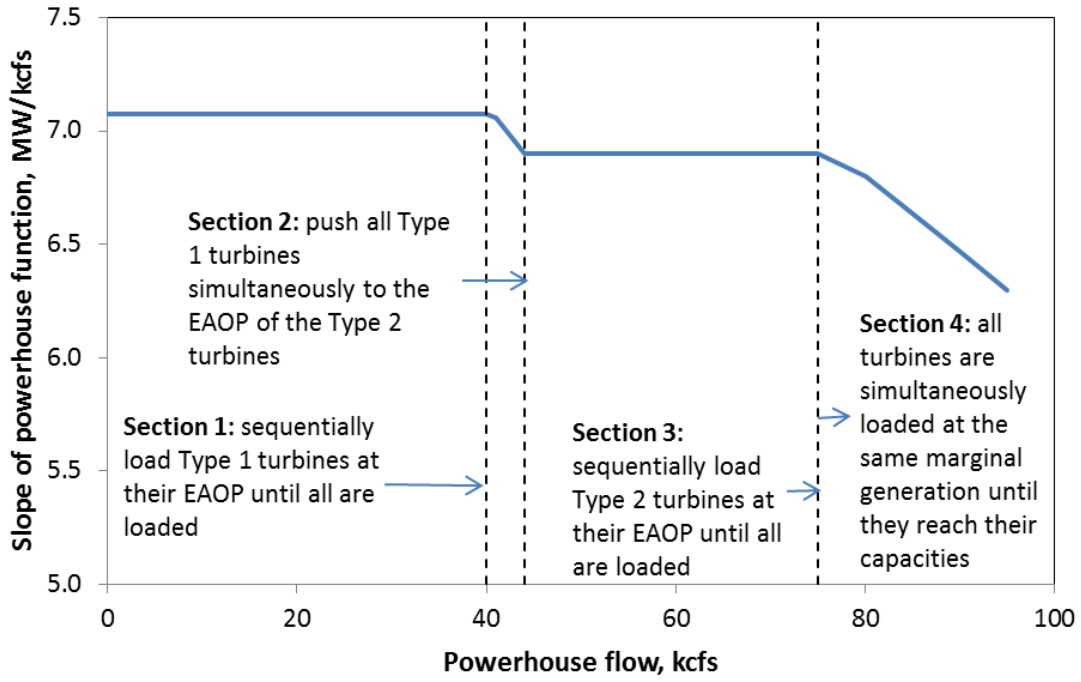

Figure 2-4: The Economic Dispatch algorithm from Section 2.5 shown as steps against a plot of the rate of generation as a function of total powerhouse flow at Ice Harbor for a head of 93 feet.

Figure 2-5 shows again the marginal generation rate now for the Fish Dispatch powerhouse generation functions derived using the algorithm in Section 2.6 for single unit dispatch and joint unit dispatch. These functions are now no longer concave, since the marginal generation rate is not nondecreasing over the powerhouse flow range. The differences are particularly problematic for the single dispatch powerhouse functions, shown by the solid blue line in Figure 2-5. A function like this would cause long convergence times for a nonlinear programming algorithm, potentially creating a need to use integer variables.

The joint dispatch powerhouse function, shown as the orange line in Figure 2-5, is another way that the powerhouse operator could choose to operate. Joint operation does not alleviate the non-concavity issue, but there is only one point where the marginal generation rate

increases, and that increase is much smaller than the jumps with single dispatch. Thus, our recommendation would be assume that the powerhouse could operate using single or joint dispatch, but to approximate either of the dispatches using the function approximation, shown as the dashed blue line in Figure 2-5 . We will show in Section 2.7.3 that the difference in total generation is less than 5 MW, a small value compared to the total system generation. In general the joint dispatch model describes feasible, reasonable, and relatively efficient operation.

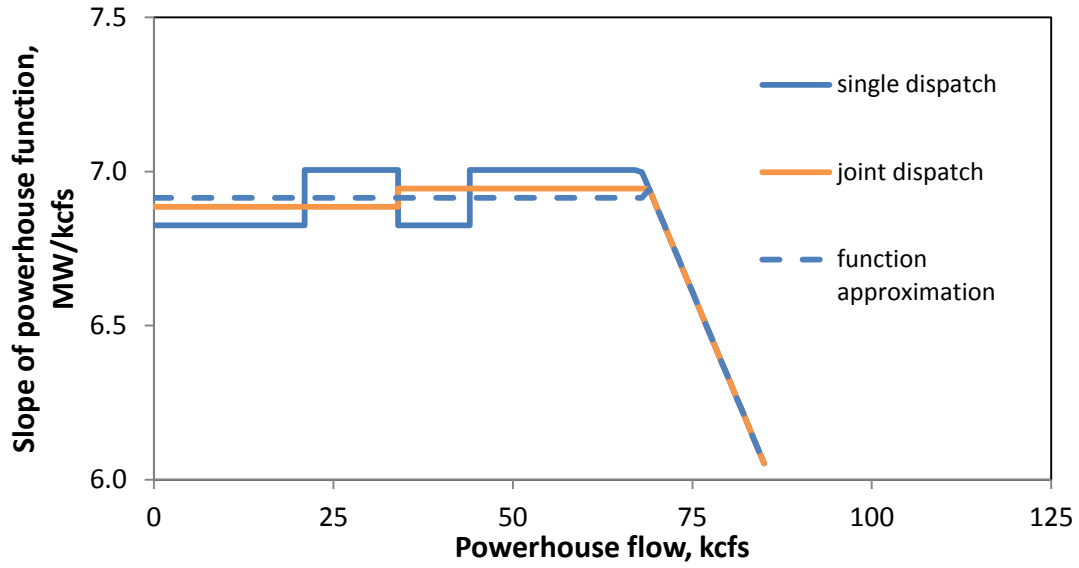

Figure 2-5: The slope of the Fish Dispatch powerhouse function for single and joint dispatch algorithms overlaid with the function approximation for Ice Harbor at a head of 93 feet. The algorithm is described in detail in Section 2.6.

2.7.2 Economic Dispatch Powerhouse functions at Columbia System Reservoirs

In this section, we summarize the results for all the Economic Dispatch powerhouse functions for all the reservoirs modeled in the BPA system. We show the relative linearity of the powerhouse functions, which depends on the differences in the marginal generation rate of the least and most efficient turbines at their EAOP. If the marginal generation rates of different turbine types are nearly the same, the powerhouse function will be made up of linear segments and transitions

with nearly the same slopes.

The Economic Dispatch powerhouse functions can be divided into two segments:

(1) The Efficient Loading segment where turbines are sequentially loaded at their most efficient operating point (EAOP) and there are still more turbines to load or which are not operating for the entire load. The Efficient Loading segment is described by Steps 1 through 3 in the algorithm described in this chapter's Section 2.5.2.

(2) The Overdrive segment where all the turbines are running at release rates greater than their EAOP. Overdrive segment is described by Step 4 in the algorithm described in this chapter's Section 2.5.2.

In both segments, all turbines should have the same marginal generation rate unless they are constrained by their maximum flow rate.

The Efficient Loading segment of the powerhouse curve starts with a slope corresponding to the efficiency of the most efficient turbine running at its EAOP. So in terms of Turbine Efficiency, the intial slope of the powerhouse function is the *Maximum Turbine Efficiency (MaxTE)* slope. MinTE is the largest marginal generation rate of the powerhouse function, which is also the marginal generation rate of the most efficient turbine type, i.e. $\max_i \left(GT_i'\left(q_{EAOP,i}\right)\right)$. This corresponds to the slope of the powerhouse function in Step 1 of the algorithm described in Section 2.5.2..

At the end of the Efficient Loading segment of the powerhouse curve, the least efficient turbine is being added at its EAOP. Here, the slope of the powerhouse curve reflects the

efficiency of the least efficient turbine, or the *Mininmum Turbine Efficiency (MinTE)*, i.e.$\min_i \left(GT_i'\left(q_{EAOP,i}\right)\right)$. This corresponds to the slope of the powerhouse function at the end of Step 3 of the algorithm described in Section 2.5.2.. Thus, MaxTE and MinTE describe the slope of the powerhouse function at the bounds of the Efficient Loading section of the Economic Dispatch powerhouse function. If these two values are very close, then the powerhouse function in this first segment is very close to a straight line.

In the Overdrive section, the powerhouse curve starts with a slope of MinTE, and when all turbines reach their maximum flow, has a slope we denote *Minimum Overdrive Efficiency (MinODE)* slope is the slope of the powerhouse function when all turbines are running at maximum flow q_{max}, which is also the minimum marginal generation rate at maximum flow over all turbines, i.e. $\min_i \left(GT_i'\left(q_{max,i}\right)\right)$. This corresponds to the slope of the powerhouse function at the end of Step 4 of the algorithm described in Section 2.5.2

In summary, the Efficient Loading and Overdrive sections are bounded by three different points each with different slopes, or marginal generation rates MaxTE, MinTE, and MinODE. Figure 2-6 shows each of these values at each of the 10 reservoirs modeled in the BPA system.

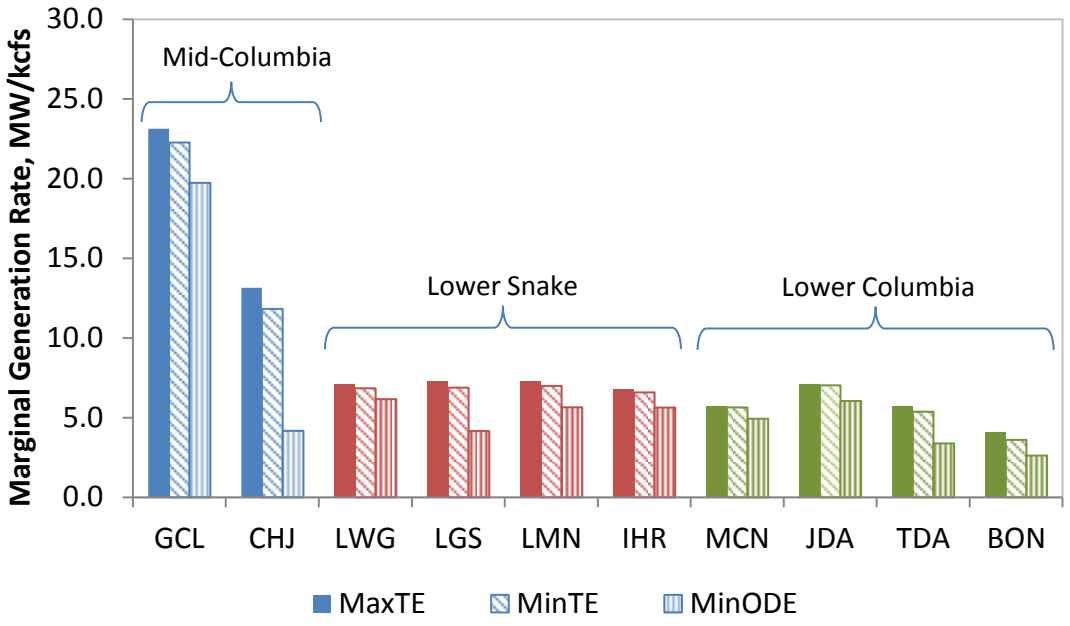

Figure 2-6: The marginal generation rates MaxTE, MinTE, MinODE, corresponding to slopes of the Economic Dispatch powerhouse functions for the 10 Federal Columbia River Power System reservoirs. The column chart shows the average values over all the head values at a particular reservoir in which generation data is available.

Observe from Figure 2-6 that Grand Coulee (GCL) and Chief Joseph (CHJ) have the highest marginal generation rates overall, meaning that the generation per unit of flow is highest at these reservoirs. This is because due to the much higher head at those reservoirs. Across the other reservoirs they have similar MaxTE values and MinTE values of megawatts generated per unit of flow because these reservoirs have very similar head values. Looking at the MinTE and MaxTE values Figure 2-6, when all turbines are operating above the marginal generation rate of MinTE, all of the powerhouse functions should be nearly linear because the two slopes are not very different. Note that McNary (MCN) and John Day (JDA) have only one turbine type, so the MaxTE is equal to the MinTE.

In the Overdrive section, as all the turbines in the powerhouse are being pushed to overdrive towards their maximum flow and the marginal generation rate approaches the MinODE, we expect the power curves to be nonlinear with a negative second derivative. At GCL and CHJ, these slopes can change a lot, whereas at other projects the possible drop in efficiency is relatively small (e.g. at the Lower Snake projects LWG, LMN, IHR, and MCN). Again, this depends upon the characteristics of the turbines installed at those projects.

Figure 2-7 shows the range of differences in efficiencies (i.e. MaxTE – MinTE) converted to percentage values over the entire operating range of head at each of the reservoirs. Note that MCN and JDA are not shown in this figure because there is only one turbine type in this reservoir. This figure shows how linear the Efficient Loading section of the Economic Dispatch powerhouse functions will be. Over the 8 reservoirs with multiple turbine types studied in this chapter, the MaxTE – MinTE values typically range between 1.5% and 2.5%. Smaller MaxTE – MinTE values indicate a relatively linear Efficient Loading section as compared to a larger value. Thus, it appears as though TDA will be relatively linear in its Efficient Loading section, while CHJ and BON will be more nonlinear in their Efficient Loading sections.

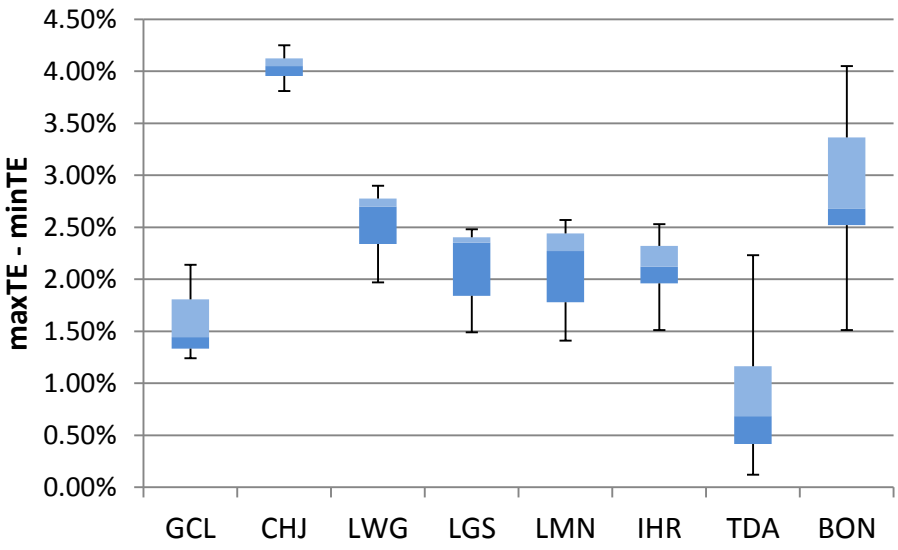

Figure 2-7: Box-and-whiskers plot showing the difference between the maximum and minimum turbine efficiencies converted to percentage values over the entire operating range of head at each project in the Federal Columbia River Power system. The whiskers show the min and max values. The boxes show the location of the 1st quartile, median, and 3rd quartile. MCN and JDA are not plotted here as there is only one turbine type.

The range of MaxTE – MinTE in Figure 2-7 shows how this difference can change with head. The ranges for most of these reservoirs are about 1%. CHJ powerhouse functions remain relatively unchanged with respect to head, while BON and TDA tend to have a large variation with head.

2.7.3 Comparison of Approximate and Exact Fish Dispatch Powerhouse Functions

The Fish Single Dispatch powerhouse functions described in Section 2.6.2.1 reflect required fish-dispatch constraints on turbine dispatch. This poses problems when the resulting powerhouse function is not concave, as occurs in the example shown in Figure 2-5**.** This could yield multiple local optima that might result in convergence problems with the nonlinear optimizer, and slow convergence to potentially local optima. In some cases joint fish-dispatch operations solved the problem, or at least made it much smaller. To address any problems, our fish-dispatch powerhouse functions in some cases were approximated by very similar linear and concave functions, as described in Section 2.6.2.3. A natural question is how different are the solutions in terms of estimated energy generation when approximate powerhouse functions are used in place of exact fish-dispatch powerhouse functions.

In order to test the difference in system generation found using approximate and exact powerhouse functions, a 5-day optimization for the 10-reservoir system was run for April under different drawdown requirements at Grand Coulee (GCL) and appropriate Fish Dispatch powerhouse functions where applicable. Each of the runs have the same objective, price, load, and inflow conditions. All reservoirs other than GCL have to be at least the same elevation level at the end of the optimization period as in the beginning of the optimization period. Recall that Figure 2-2 shows that in April, the Lower Snake reservoirs (LWG, LMN, LGS, and IHR), TDA, and BON are all operating under fish dispatch, rather than economic dispatch. GCL and CHJ never have fish operations.

Let $\boldsymbol{GH}_0^i$be the vector of power generated over all time periods with the approximate powerhouse function at powerhouse i. Let $\boldsymbol{GH}_1^i$ be the vector of power generated over all time periods with the exact single dispatch powerhouse function at powerhouse i. For each of the different drawdown constraints:

1) Run a system optimization using the approximate Fish Dispatch functions GH_0^i where applicable. Obtain optimal flow vector $\boldsymbol{r}_0^i$ and generation vector $\boldsymbol{GH}_0^i(\boldsymbol{r}_{PH,0}^i)$ at each powerhouse.
2) With the optimal flow vector $\boldsymbol{r}_0^i$ found in Step (1), calculate the generation vector with the exact Fish powerhouse functions described in Section 2.6.2.1. with flow policy $\boldsymbol{r}_0^i$, $\boldsymbol{GH}_1^i(\boldsymbol{r}_{PH,0}^i)$ and the difference vector

$$\boldsymbol{\Delta}_{00} = \boldsymbol{GH}_1^i\left(\boldsymbol{r}_{PH,0}^i\right) - \boldsymbol{GH}_0^i(\boldsymbol{r}_{PH,0}^i)$$

3) Rerun the optimization with $\boldsymbol{r}_0^i$ as the initial solution and use the exact Fish Single Dispatch functions GH_1^i. Obtain optimal flow policy $\boldsymbol{r}_1^i$ and generation vector at each powerhouse $\boldsymbol{GH}_1^i\left(\boldsymbol{r}_1^i\right)$.
4) Calculate

$$\boldsymbol{\Delta}_{10} = \boldsymbol{GH}_1^i\left(\boldsymbol{r}_1^i\right) - \boldsymbol{GH}_0^i(\boldsymbol{r}_0^i)$$

This is the resulting optimal generation schedule for Step (1) computed using the approximate Fish Dispatch powerhouse function to the optimal generation schedule from Step (3) using the exact Fish Dispatch powerhouse functions.

Table 2-2 shows the maximum difference over all time periods of the optimization for two optimization scenarios with different drawdown levels at GCL.

Table 2-2: The maximum difference in generation (in MW) over all time periods at each reservoir and for the total 10-reservoir system generation. The powerhouse generation is optimized for an 8-hour time step over a 5 day period in April under different drawdown constraints at GCL. $\Delta_{00} = GH_1^i(\boldsymbol{r}_0^i) - GH_0^i(\boldsymbol{r}_0^i)$, *and* $\Delta_{10} = GH_1^i(\boldsymbol{r}_1^i) - GH_0^i(\boldsymbol{r}_0^i)$. GH_0^i *is the energy generated with the approximate powerhouse function at powerhouse* i. GH_1^i *is the energy generated with the exact powerhouse function at project* i. $\boldsymbol{r}_0^i$ *is the optimal flow vector using the approximate Fish Dispatch functions where applicable.* $\boldsymbol{r}_1^i$ *is the optimal flow vector using the exact Fish Dispatch functions where applicable. Reservoirs in the greyed rows are reservoirs with no fish dispatch operations.*

	no change in GCL elevation		5 foot drawdown at GCL	
	max Δ_{00}	max Δ_{10}	max Δ_{00}	max Δ_{10}
GCL	0.0	2.1	0.0	3.2
CHJ	0.0	1.0	0.0	1.3
LWG	(0.2)	0.3	(0.6)	0.2
LGS	(0.9)	(0.6)	(1.4)	(0.9)
LMN	(1.0)	(0.7)	(1.5)	(1.0)
IHR	(0.8)	(0.6)	(2.0)	(1.5)
MCN	0.0	0.2	0.0	0.2
JDA	0.0	0.4	0.0	0.5
TDA	0.0	0.3	0.0	0.3
BON	(5.0)	(4.9)	(3.3)	(3.2)
Total System	**(5.3)**	**(0.0)**	**(7.5)**	**0.0**

Overall, the system can generate that power in several ways; GCL generally has great flexibility with CHJ acting as a very large reregulating reservoir. The average system generation is between 8,000 to 12,000 MW in each time period. The largest differences anywhere tends to occur at Bonneville. This is because of the relatively high nonlinearity of the powerhouse functions compared to the other projects as shown previously in Figure 2-7, as well as the Fish Dispatch operations at Bonneville, which dictate that all the less efficient turbines are loaded

before the most efficient turbines thus maximizing the possible error from using the approximate powerhouse functions [*US Army Corps of Engineers*, 2012].

When we compare the generation with the optimized flow vector found by optimizing using the approximate powerhouse function, $\boldsymbol{r}^i_{PH,0}$ in both the approximate fish dispatch function GH^i_0 and the exact powerhouse function, GH^i_1, the biggest difference Δ_{00} in all the time periods anywhere in the system between both drawdown scenarios is -5MW. The biggest difference Δ_{00} in total generation of the 10-reservoir system in any time period is only around -7.5MW at Bonneville (BON). This is equivalent to less than 1% of the generation at BON at any period of time.

When the optimal flow vector over all time periods is reoptimized for the exact powerhouse functions (Step 3 in the procedure detailed above), $\boldsymbol{r}^i_{PH,1}$, the resulting differences $\boldsymbol{\Delta}_{10} = \boldsymbol{GH}^i_1(\boldsymbol{r}^i_1) - \boldsymbol{GH}^i_0(\boldsymbol{r}^i_0)$ at any reservoir and any time period has a maximum of about -5MW at Bonneville. Note that the reoptimization causes a redistribution of the flows among the reservoirs so that the biggest difference Δ_{10} in total generation of the 10-reservoir system in any time period is nearly 0MW. Additionally, we have used a comparison of the Fish Single Dispatch powerhouse function to the approximate function. If we used a Fish Joint Dispatch powerhouse operation, the errors are likely to be smaller still. Thus non-concavity caused by required fish operations can be dealt with in the development of powerhouse functions.

2.8 Conclusions

In this chapter, we demonstrated how to generate precomputed optimized multi-turbine Powerhouse Generation Functions for each reservoir in the 10-reservoir Federal Columbia River Power System. Cubic splines are used to fit the turbine generation functions from available empirical generation data. This enables us to estimate the efficient average operating point (EAOP) of the turbine as well as the generation when turbines in overdrive, i.e. beyond their most efficient operating points. Turbines can be operating all or part of each of the time periods within the optimization horizon. We show that when we run multiple turbines at the same marginal generation rate throughout the reservoir operating range for flow, no reallocation of releases among turbine can increase the overall generation.

In times when there are no restrictions on the turbine dispatch and loading order, the powerhouse function describes the optimal generation at the powerhouse for a given flow through the powerhouse. For these Economic Dispatch powerhouse generation functions, the turbine types are loaded sequentially in order of decreasing efficiency resulting in the maximum possible generation by that project at that flow.

Fish Dispatch powerhouse generation functions are used primarily when there is a need to incorporate legally-required fish passage considerations. During these times, turbines may not be loaded in the economic dispatch order as certain turbines are prioritized to improve flow patterns in the vicinity of the dam, or to provide attraction flow for fish ladders. In this case, fish are the prioritiy, and economic efficiency is a secondary objective.

For Fish Dispatch powerhouse functions, we introduce three different patterns. First, Fish Single Dispatch loads the turbines one-by-one following the predetermined dispatch orders as detailed in the yearly Fish Passage Plans. Turbines are loaded sequentially at their EAOP in the Fish Dispatch order. This could result in powerhouse generation functions that are non-concave whenever a newly dispatched turbine is more efficient than the previously dispatched turbine, and both are load at their EAOP.

Second, Fish Joint Dispatch overcomes the non-concave problem for some reservoirs by assuming that inefficient and efficient turbines are loaded together. Joint dispatch is often the accurate representation of the actions of the operator, especially when considering time periods of 8 hours or more. By loading inefficient and efficient turbines together and running them for the same fraction of the time, the powerhouse generation function avoids the problem of non-concavity while also providing a physical representation of reasonable powerhouse operation.

Third, an approximation is used for powerhouses when even the joint dispatch will produce non-concave powerhouse generation functions, which produces a more concave function necessary for optimization. We showed that the difference in total system generation when we used actual and approximation Fish Dispatch powerhouse generation functions were in the 10s of MWs, which is very small compared to total generation of up to 12,000 MW in each time period. Generation differences at any powerhouse are around 5 MW in any period at any powerhouse, which is assumed to be acceptable since the automatic generation control within the reservoir power plant can only adjust to within 5MW of precision. The reoptimization step results in changes of less than 1% of generation at each reservoir in any time period. Thus, we

did not need to further improve the optimal solution found by the approximate Fish Dispatch powerhouse function H_0^i with a second iteration of the optimization.

The use of powerhouse generation functions eliminates the need for dynamic programming or a large number of integer decision variables to represent the number of each of the turbine types employed in the optimization model that is re-solved in each time period. Rather, piecewise polynomial powerhouse functions were produced that require only a single powerhouse flow decision (the total amount of water released from the reservoir) at each reservoir. Further, the use of such concave functions during Economic Dispatch periods will ensure a convergence of the sequential quadratic programming algorithm to a global maximum.

2.9 References

Barros, M. T. L., F. T. Tsai, S. Yang, J. E. G. Lopes, and W. W. Yeh (2003), Optimization of Large-Scale Hydropower System Operations, *J. Water Resour. Plan. Manag.*, *129*(3), 178–188.

Becker, L., and W. W.-G. Yeh (1974), Optimization of Real Time Operation of a Multiple-Reservoir System, *Water Resour. Res.*, *10*(6), 1107–1112.

Boggs, P. T., and J. W. Tolle (1995), Sequential Quadratic Programming, *Acta Numer.*, *4*(January 1995), 1, doi:10.1017/S0962492900002518.

Bonneville Power Administration, U.S. Bureau of Reclamation, and U.S. Army Corps of Engineers (2001), The Columbia River System: Inside Story, , 1–80.

Catalão, J. P. S., S. J. P. S. Mariano, V. M. F. Mendes, and L. A. F. M. Ferreira (2009), Scheduling of Head-Sensitive Cascaded Hydro Systems : A Nonlinear Approach, *IEEE*

Trans. Power Syst., *24*(1), 337–346.

Chang, G. W., M. Aganagic, J. G. Waight, J. Medina, T. Burton, S. Reeves, and M. Christoforidis (2001), Experiences with Mixed Interger Linear Programming Based Approaches on Short-Term Hydro Scheduling, *IEEE Trans. Power Syst.*, *16*(4), 743–749.

Chapra, S. C., and R. P. Canale (2010), *Numerical Methods for Engineers*, 6th ed., McGraw Hill Higher Education.

Digna, R. F., Y. A. Mohamed, P. van der Zaag, S. Uhlenbrook, and G. A. Corzo (2017), Nile River Basin modelling for water resources management - a literature review, *Int. J. River Basin Manag.*, *15*(1), 39–52, doi:10.1080/15715124.2016.1228656.

Hamann, A., G. Hug, and S. Rosinski (2017), Real-Time Optimization of the Mid-Columbia Hydropower System, *IEEE Trans. Power Syst.*, *32*(1), 157–165.

Jacobs, J., G. Freeman, J. Grygier, D. Morton, G. Schultz, K. Staschus, and J. R. Stedinger (1995), SOCRATES: A system for scheduling hydroelectric generation under uncertainty, *Annals*, *59*, 99–133.

Labadie, J. W. (2004), Optimal Operation of Multireservoir Systems : State-of-the-Art Review, *J. Water Resour. Plan. Manag.*, *130*(2), 93–111.

Li, C.-A., E. Hsu, A. J. Svoboda, C. Tseng, and R. B. Johnson (1997), Hydro Unit Commitment in Hydro-Thermal Optimization, *IEEE Trans. Power Syst.*, *12*(2), 764–769.

Li, F., C. A. Shoemaker, J. Wei, and X. Fu (2013a), Estimating Maximal Annual Energy Given Heterogeneous Hydropower Generating Units with Application to the Three Gorges System, *J. Water Resour. Plan. Manag.*, *139*(June), 265–276, doi:10.1061/(ASCE)WR.1943-5452.0000250.

Li, X., T. Li, J. Wei, G. Wang, and W. W.-G. Yeh (2013b), Hydro Unit Commitment via Mixed Integer Linear Programming : A Case Study of the Three Gorges Project , China, *IEEE Trans. Power Syst.*, 1–10.

Matevosyan, J., M. Olsson, and L. Söder (2009), Hydropower planning coordinated with wind power in areas with congestion problems for trading on the spot and the regulating market, *Electr. Power Syst. Res.*, *79*(1), 39–48, doi:10.1016/j.epsr.2008.05.019.

Pérez-Díaz, J. I., J. R. Wilhelmi, and J. Á. Sánchez-Fernández (2010), Short-term operation scheduling of a hydropower plant in the day-ahead electricity market, *Electr. Power Syst. Res.*, *80*(12), 1535–1542, doi:10.1016/j.epsr.2010.06.017.

Ponrajah, R. A., J. Witherspoon, and F. D. Galiana (1998), Systems to optimise conversion efficiencies at ontario hydro's hydroelectric plants, *IEEE Trans. Power Syst.*, *13*(3), 1044–1050, doi:10.1109/59.709097.

Schwanenberg, D., M. Xu, T. Ochterbeck, C. Allen, and D. Karimanzira (2014), Short-term management of hydropower assets of the Federal Columbia River Power System, *J. Appl. Water Eng. Res.*, *2*(1), 25–32, doi:10.1080/23249676.2014.912952.

Shawwash, Z. K., T. K. Siu, S. Member, and S. O. D. Russell (2000), The B . C . Hydro Short Term Hydro Scheduling Optimization Model, *IEEE Trans. Power Syst.*, *15*(3), 1125–1131.

Siu, T. K., G. A. Nash, and Z. K. Shawwash (2001), A Practical Hydro , Dynamic Unit Commitment and Loading Model, *IEEE Trans. Power Syst.*, *16*(2), 301–306.

US Army Corps of Engineers (2012), *Fish Passage Plan*.

Yeh, W. W.-G. (1985), Reservoir Management and Operations Models: A State-of-the-Art Review, *Water Resour. Res.*, *21*(12), 1797–1818.

CHAPTER 3

COMPUTATIONALLY EFFICIENT HYDROPOWER OPERATIONS OPTIMIZATION REFLECTING UTILITY MARKET POWER, FISH CONSTRAINTS, AND MULTI-TURBINE POWERHOUSE FUNCTIONS

3.1 Introduction

Operators of large cascaded hydropower system generally turn to models to inform daily operation. Some examples include models built to optimize the operations of the PG&E hydropower system in Northern California [*Jacobs et al.*, 1995], the BC Hydro system in British Columbia, Canada [*Shawwash et al.*, 2000], the Brazilian hydropower system [*Barros et al.*, 2003], the Federal Columbia River Power system in Washington and Oregon [*Schwanenberg et al.*, 2014], and the Ume River hydropower system in Sweden [*Matevosyan et al.*, 2009]. These models will be run frequently (at least daily), so computational efficiency is a key factor in the usability of such modeling systems if operators are to have the ability to look at many options and/or consider stochastic futures. The optimization of a system of reservoirs with hydropower generation can be broken down into three temporal - spatial levels: (1) the overall system level addresses the quantity and timing of the flows between individual reservoirs and total system energy generation in different periods that result from those releases, (2) the power plant level, where the quantity and timing of the flows among different turbines each with their own generation characteristics are optimized given a total reservoir releases, and (3) the turbine level, where turbine generation as a function of head and flow through the turbine is characterized to enable optimization of power plant operations. In Chapter 2 we discussed the optimization of the powerhouse and turbine level operations.

This chapter addresses the system level optimization. We develop a computationally efficient deterministic optimization model for the operation of a cascaded large multi-reservoir system. The model provides optimized hydropower system operations by maximizing the hydropower production value given streamflow forecasts, hydropower plant unit availability, utility system loads, electricity market prices and depths. The model is unique in that it uses precomputed powerhouse functions to describe economically efficient turbine dispatch and loading, and when applicable allows for special seasonal constraints for flow released from specified turbines for various fish operations. Additionally, this model accounts for the market power of a large hydropower utility. Large hydropower systems that have a significant amount of generation capacity are typically operated and run by government-run entities: systems such as the Brazilian hydropower system [*Barros et al.*, 2003], Nile River system [*Digna et al.*, 2017], the B.C. hydro system [*Shawwash et al.*, 2000], and the Federal Columbia River Power System (FCRPS) [*Schwanenberg et al.*, 2014]. The capabilities of the model are demonstrated using ten reservoirs in the Federal Columbia River Power System (FCRPS) operated by the Bonneville Power Administration (BPA), a part of the U.S. federal government.

A variety of methods have been used for reservoir operations optimization, ranging from traditional methods like linear programming, dynamic programming, and network modeling [*Yeh*, 1985; *Labadie*, 2004], to newer methods including heuristic optimization and artificial neural networks [*Ahmad et al.*, 2014; *Nazari-Heris et al.*, 2017].

While linear programming can solve large network problems efficiently [*Shawwash et al.*, 2000; *Zagona et al.*, 2001; *Schwanenberg et al.*, 2014], the linearization of the power

generation function results in approximations that may be unacceptable for planning operations with a short time step (i.e. when the turbines are run beyond their most efficient operating point, and when head effects have to be taken into account) [*Catalão et al.*, 2009]. Moreover, if piecewise-linear functions are used that take into account head effects and turbine losses for generation rates beyond their most efficient operating point [*Chang et al.*, 2001; *Li et al.*, 2013b], the addition of a large number of integer variables from these piecewise-linear functions can render the problem solution too slow for usefulness in operations. This is certainly the case for the large-scale hydropower system modeled in this chapter, which includes 10 active storage reservoirs, each of which has many turbine types in one of more powerhouses.

Dynamic programming can incorporate nonlinear power generation functions that are realistic descriptions of system characteristics [*Yi et al.*, 2003], but the exponential increase of state variables with each additional reservoir limits its functionality . Sequential linear programming solves a sequence of localized linear programs based on a first order approximation of the nonlinear objective function [*Grygier and Stedinger*, 1985; *Barros et al.*, 2003; *Labadie*, 2004].Still, the solution is still an approximation to the actual solution that can be found using a full nonlinear programming formulation.

Nonlinear programming has been shown to be a practical method to provide more exact operating policies and estimations of value for real-time operations compared to linear programming and sequential linear programming [*Arnold et al.*, 1994; *Barros et al.*, 2003]. It has been applied to large scale, cascaded reservoir systems in Brazil [*Barros et al.*, 2003], Portugal [*Catalão et al.*, 2009], and in California [*Tejada-Guibert et al.*, 1990]. A weakness of nonlinear

programming methods is that convergence to a global optimum is not guaranteed if the problem is not convex. To overcome this hurdle, we can generally develop concave generation functions for each project that take account for the characteristics of different units. The value of hydropower generation (to be maximized) is also a concave function with respect to the decision variables. Therefore, in most cases case the nonlinear program should converge to a globally optimum solution.

The remainder of the chapter is laid out as follows: first, Section 3.2 provides a brief overview of the features of the hydropower system optimization Model developed in this paper. Section 3.3 develops the fundamental model. Section 3.4 reports results runs that illustrate the features of the optimization model. Finally, Section 3.5 provides conclusions.

3.2 Deterministic Optimization Model Features

The model developed in this chapter has four important characteristics: (1) it accounts for a large hydropower system's market power in the wholesale electricity market, , (2) it employs precomputed optimized powerhouse functions, (3) it models special operations for maintaining compliance with federally set operations for to protect fish populations, and (4) it allows the user to specify a combination of 8 and 24-hour time steps for flow routing through the system.

We introduce a value function that enables the user to model the effect of a large power system on market prices. This is explained in Section 3.3.1. We account for the fact that a hydro utility has an option to satisfy its load obligations by purchasing power on the whole market. Additionally, the hydro utility is also able to sell power on the wholesale market, earning some value from the generation while balancing system needs and future opportunity costs. We

provide an improvement over the combined hydropower production and marketing value function employed by Perez-Diaz et al [2010] and Schwanenberg et al [2014] by incorporating the market power effect that a large hydropower system has on the market prices in the surrounding area. Other optimization algorithms assume that their hydropower system is a price taker or that the hydropower system is only deployed to meet load and therefore simply seek to meet system loads by minimizing flow [*Hamann et al.*, 2017]. We explain in Section 3.3.1 why maximizing revenue will lead to monopolization behavior by a utility with a large share of the generation in a particular area; a formulation for maximizing the societal benefit is presented as an alternative for utilities that have a large capacity and could move the market significantly. By adding the wholesale market to the optimization function, we can more closely mimic what would be done in day-to-day operations in the planning horizon.

Precomputed powerhouse functions are also employed to decrease the nonlinear programming runtime. The powerhouse function describes the optimal generation of the multiple turbines as a function of total flow through the project within a particular project. The powerhouse function created has four important characteristics: (1) reduction of many turbine-level decision variables to one function for a multi-reservoir optimization model, (2) precomputation of the plant-level function in (1), (3) incorporation of operational constraints and turbine availability, and (4) continuity and convexity of the powerhouse generation function. The fourth feature of the powerhouse function is to ensure that the nonlinear optimization model presented here can converge quickly to a global optimal solution. Chapter 2 provides detail on the development of the powerhouse functions.

The Fish Operations mandated by Federal and state laws to protect endangered fish populations in the case study river are also accounted for in this chapter. For the Federal Columbia River Power System, the Fish Passage Plan [*US Army Corps of Engineers*, 2012] describes the constraints under which the hydropower system must operate. These Fish Operations are defined in several ways: turbine loading order (dispatch), spill constraints, and the prescribed total volume of release from the powerhouse. Previous studies have modeled these issues as penalty functions [*Schwanenberg et al.*, 2014]. We explicitly model such requirements in our powerhouse generation functions: the turbine loading order is described in Chapter 2, while spill constraints and the total volume released from the reservoir is modeled either as total flow constraints in the optimization or constraints requiring spill as a proportion of the total reservoir flow, described in more detail in Section 3.3.3.

The user-defined time step feature of the model should provide computational savings when detailed flow routing is not needed to describe system. In general, most forecasts for streamflow, load, and market data can be quite accurate in the first few days after the forecast is made, but becomes less accurate the further out in the forecast period we go, which diminishes the motivation for detailed hydrodynamic descriptions. Thus, a longer 24-hour time step can be used further out in the model horizon. This cuts down drastically the number of decision variables in the model and therefore the required time for the optimization algorithm. Section 3.3.1 describes how the model accounts for the travel time between the reservoirs based on the time step granularity. Additionally, we incorporate a feature that enables the flows to be routed on a 24-hour time step, but generation decisions to be made separately for the off-peak and on-

peak hours with associated prices. This ensures we still are able to capture and take advantage of the diurnal load and price patterns in the 24-hour model as well as we do in the 8-hour time step model.

3.3 Hydropower System Optimization Model Description

This section introduces the reservoir operations optimization model, with details provided in the following sections. We model a 10-project subsystem of the federal projects in the Federal Columbia River Power System (FCRPS). The FCRPS is jointly operated and managed by the Bonneville Power Administration, the U.S. Army Corps of Engineers, and the Bureau of Reclamation. The total generation capacity for the 10-project system is about 20 GW, which is more than half of the region's hydroelectric generating capacity [*U.S. Army Corps of Engineers et al.*, 2003]. A schematic of the system with average travel times is shown in Figure 3-1. The optimization prescribes release decisions at all 10 individual projects for every period (8 to 24 hours per period) in the model.

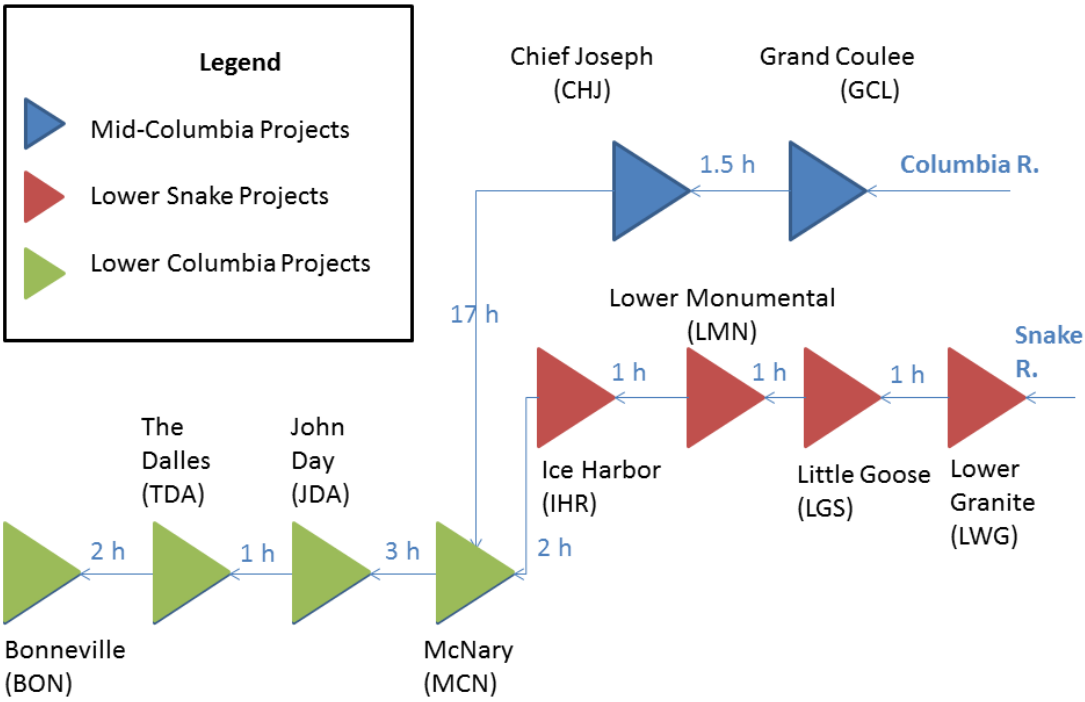

Figure 3-1: Schematic of the 10-reservoir system. The direction of flows follows the in the schematic follows the east to west flow of the Columbia and Snake Rivers. The system is divided into three smaller subsystems: The Mid-Columbia subsystem (in blue) on the upper reach of the Columbia River is made up of the Grand Coulee and Chief Joseph projects. The Lower Snake projects (in red) are Lower Granite, Little Goose, Lower Monumental, and Ice Harbor. Finally, the Lower Columbia projects (in green) are McNary, John Day, The Dalles, and Bonneville.

The goal of the optimization model is to maximize the social value of hydropower generation over the planning horizon. The objective can be written as Equation (3.1)

$$\max\left\{J = \sum_{t} F_t(E_t)\right\} \tag{3.1}$$

where the function $F_t(\cdot)$ is a function that simulates energy market behavior; it is a nonlinear, concave function. Section 3.3.1 discusses the development of the function F_t for each time period t. E_t is the energy to be sold or purchased in the day-ahead wholesale energy market, after considering the load in the utility's balancing area, as shown in Equation (3.2).

$$E_t = \left(\sum_i GH_t^i \right) * t_{length} - Load_t \quad (3.2)$$

A positive E_t indicates that energy is being sold in the wholesale energy market, while a negative E_t indicates that energy is being purchased in the wholesale energy market to meet loads. In Equation (3.2), $Load_t$ is the energy BPA serves within its balancing area to its rate-paying customers.

The powerhouse generation function from project *i* at time *t*, GH_t^i is calculated using the precomputed powerhouse functions described in Section 3.3.2. GH_t^i is the power, or rate of energy generation, and is multiplied by the time period length $t_{length}$to compute the energy generated during time period t. GH_t^i is a function of the powerhouse function releases r_{PH}^i, and net head H_t^i.The net head H_t^i is a function of the reservoir storage levels S_t^i and the total releases from the powerhouse, the sum of powerhouse function releases $r_{PH,t}^i$ and spills $r_{spill,t}^i$. At certain times of the year, the total powerhouse releases will be prescribed by Fish Operations, described in more detail in Section 3.3.3.

The decision variables are $r_{t,PH}^i$, the flow through the powerhouses at project *i* at time *t*, $r_{t,spill}^i$, the flow through the spillway at project *i* at time *t*, and S_t^i, the storage at project *i* and time *t*.

Optimization of Equation (3.1) is subject to the following constraints:

1. Conservation of mass is to be observed at all times and need to reflect the travel times between BPA projects. The storage continuity equation is expressed as Equation (3.3)

$$S_t^i = S_{t-1}^i + \sum_\tau C_\tau^i * (\vec{r}_{PH,t-\tau} + \vec{r}_{spill,t-\tau}) + I_t^i \qquad \forall i,t \tag{3.3}$$

where S_t^i is the storage in reservoir *i* for the tth time period. τ is the lag (in time periods) of flow between reservoirs. C_τ^i is the *i*th row in the lag τ routing coefficient matrix C_τ corresponding to *i*th reservoir. This is a row vector represents the fraction of the flows from lag τ that arrive at project *i* from all other projects upstream from it at time *t*. $I_{,t}^i$ is the incremental flow into project *i* at time *t*. The system dynamics equation, the lagged routing coefficient matrix C_τ, and calculation of the routing coefficients is discussed in more detail in Section 3.3.4.

2. Reservoir storage S_t^i should be within its bounds at all times *t* and at all projects *i* (Equation (3.4)):

$$S_{\min}^i \le S_t^i \le S_{\max}^i \qquad \forall i,t \tag{3.4}$$

3. The storages at the end of the horizon S_T^i should exceed the target storage S_{target}^i (Equation (3.5)):

$$S_T^i \ge S_{\text{target}}^i \qquad \forall i \tag{3.5}$$

4. Flows through the powerhouse are bounded by minimum powerhouse flow requirements and powerhouse maximum flow capacity (Equation (3.6)):

$$r^{i}_{PH\min} \le r^{i}_{t,PH} \le r^{i}_{PH\max} \qquad \forall i,t \tag{3.6}$$

Power generation at a project is typically a function of releases through the powerhouse as well as the net head, or the difference in elevation between the forebay and tailwater elevations. Generally, the tailwater elevation for project *i* at time *t* also depends on the total outflows of the project. The project tailwater elevation-discharge relationship has been found to be reasonably approximated using simple linear relationships, and is discussed in further detail in Appendix A.

5. Flows through the spillway are bounded by the minimum spillway flow required for fish passage in some periods, and the spillway flow cap for total dissolved gas (Equation (3.7)) if possible.

$$r^{i}_{\text{spill}\min} \le r^{i}_{t,spill} \le r^{i}_{spill\max} \qquad \forall i,t \tag{3.7}$$

3.3.1 Economic modelling

We model the impact of the hydropower system on the day-ahead energy market. Wholesale day-ahead energy prices are affected by streamflow levels in the region, by the availability of thermal generation, and by tie-line capacities limiting export out of the BPA balancing area to

British Columbia and California. The 31 hydropower projects in the FCRPS are jointly operated by the U.S. Army Corps of Engineers, the Bureau of Reclamation, and Bonneville Power Administration (BPA). They provide about 60% of the total hydropower generation in the Pacific Northwest [*U.S. Army Corps of Engineers et al.*, 2003]. The 10 hydropower projects we model in our generation model make up about 91% of the generation from the FCRPS. Thus, the marketing of power generated by the hydropower system by BPA affects market prices and such shifts should be anticipated in the analysis of the value of hydropower generation[*Howe*, 1971].

The value assigned to hydropower produced by the hydropower system can be valued simply by BPA total system revenue, or by its social value described by the willingness-to-pay of other entities that purchase BPA's power to meet their load. Willingness-to-pay then reflects the total cost of other energy displaced by BPA production [*Russell*, 2001]. In this case existing index price data, which is an average price reported by market participants in the bilateral market in which BPA transacts, cannot be taken as a simple measure of the value the energy sold by BPA; this is because the output of energy from the hydropower system is so large compared to the output from other utilities in the market that it affects the market price for electricity.

3.3.1.1 Modeling a Utility with Market Power

We model BPA as having market power rather than as a price taker. Stoft [2002] defines market power as the ability to profitably maintain prices above competitive levels for a significant period of time. The demand function $D_t(E_t)$ gives the market clearing price at which BPA can buy ($E_t < 0$) or sell ($E_t > 0$) excess energy after meeting its own load. The excess production is different for each time step t , as was shown in Equation **Error! Reference source not found.**.

The buyers in the day-ahead wholesale energy market are other utilities that can either purchase energy generated by BPA or generate power using their own sources. Those who would be buying energy from BPA might benefit by not having to turn on their own expensive thermal units on to meet load, or would need to buy power from more expensive sources, or use their own hydropower capacity which has its own opportunity cost. The critical function here is the demand function D(E). It describes the price in the energy market that results when BPA sells energy E. That price should be the buyers' marginal cost of production (MC) or their cost to get energy from other sources. Here we assume other utilities are "price-takers" who make their decisions based upon the market price, which they cannot affect.

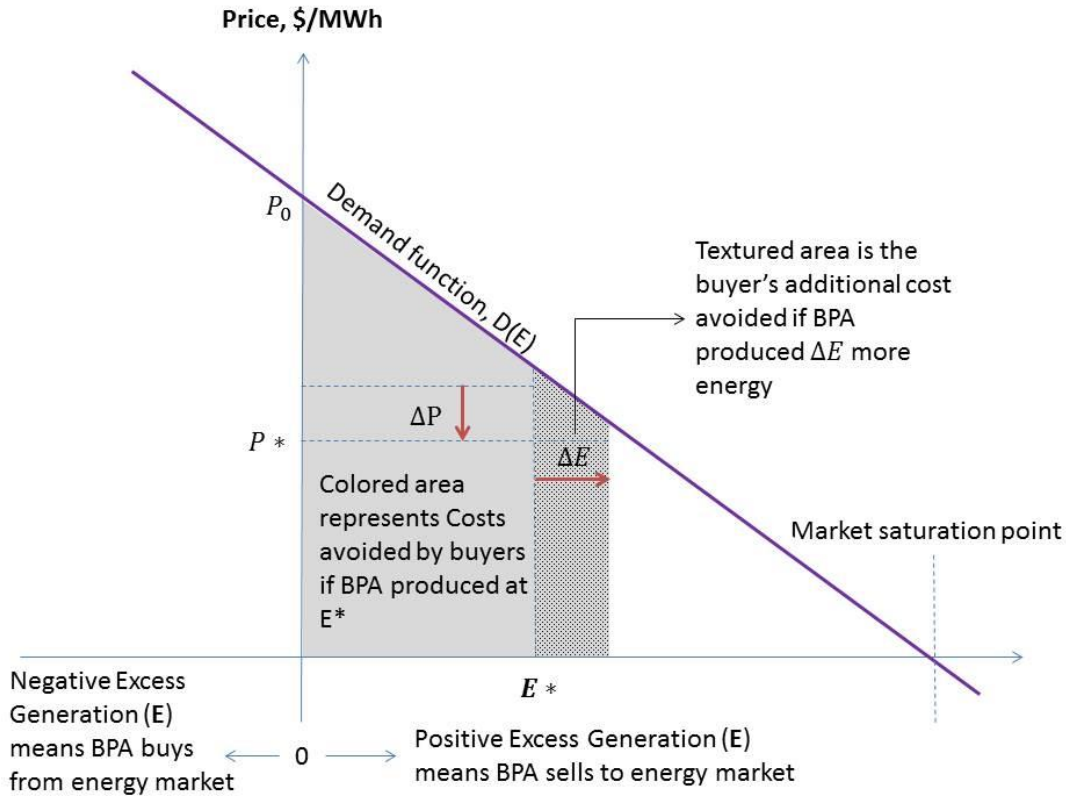

Figure 3-2: Illustrative demand function, or energy prices as a function of E, the excess energy sold by BPA. The net generation for each time step E is the total system generation minus the system load. The demand function has parameters P_0, which is the index price of energy for the Mid-C trading hub, and a market saturation point determined by the time of day (on-peak or off-peak).

We model the demand function as linear. Figure 3-2 provides an example. What will be critical is to know the cost savings to utilities purchasing a significant amount of additional energy ΔE from BPA. If initially BPA is selling energy E* resulting in a price P*, one could assume the value of the additional energy ΔE was P* times ΔE, if BPA did not have market power. However, the demand function shown in Figure 3-2 shows that a change in energy generation ΔE will result in a decrease in the wholesale energy price of ΔP. Over the range E* to $(E^* + \Delta E)$, not every unit of energy has the same value. Specifically, the last unit on the margin had marginal value $(P^* - \Delta P)$. The correct calculation of the costs avoided by other

utilities integrates the demand function (which represents the buyers marginal cost of production) over the interval E* to $(E^* + \Delta E)$ to obtain *the costs avoided* by other utilities who are buying from BPA in period t as a result of BPA selling additional energy ΔE_t, as shown in Equation (3.8).

$$C(E_t + \Delta E_t) - C(E_t) = \int_{E_t}^{E_t + \Delta E_t} D(e)de \tag{3.8}$$

This equation and the assumption that the demand function is linear allows construction of the regional costs of production avoided when BPA sells energy E. Because the demand function is linear, the reduction in regional cost of generation can be computed using Equation (3.9)

$$C(E_t + \Delta E_t) - C(E_t) = \frac{1}{2}\Delta E_t[C(E_t + \Delta E_t) + C(E_t)] \tag{3.9}$$

At some point (called the *market saturation point* in this chapter), the other utilities no longer have any capacity to receive any additional energy (because, for example, transmission lines are at capacity, all the other utilities' balancing area loads are met, they have no more generators to shut down, etc.) and cannot absorb more energy. Then the price of energy drops to zero. Beyond that point, BPA may have to pay other utilities to take their energy or in some extreme cases curtail some of their ratepayers'$Load_t$. A negative price in a wholesale electricity market indicates that there is a supply inflexibility (e.g. when water must run through the turbines for fish operations) [*U.S. Energy Information Administration*, 2012]. Generally, BPA would rather spill (if constraints permit) than to participate in a negative market.

In this chapter, we adopt linear demand functions for every period t. Some periods will be on-peak hours, while others are off-peak hours. Depending on the length of a period, all on-

peak or off-peak periods may be assigned the same demand function. Index price data for the Mid-C trading hub was used to develop the demand functions adopted. Equation (3.10) displays the form of the demand function.

$$D_t(E_t) = P_{0,t} - \frac{P_{0,t}}{E_{\max,t}} E_t \tag{3.10}$$

where

E_t is the energy sold in time step t, as described in Equation (3.2)

$P_{0,t}$ is the implied wholesale price when $E_t = 0$ in time step t

$E_{max,t}$is the market saturation point

3.3.1.2 Revenue and Avoided Cost Objective Functions

There are several ways in which we can quantify the value of hydropower generation. In this chapter, we describe two such functions: revenue and avoided cost. We provide formulas for their evaluation based on the linear demand function developed above

The revenue received by the hydro utility from selling some amount of power on the market E_t for each time period t is given in Equation (3.11)

$$R_t(E_t) = E_t * D(E_t) = \frac{P_{0,t}}{E_{0,t} - E_{\max,t}} E_t^2 - P_{0,t} \frac{E_{\max,t}}{E_{0,t} - E_{\max,t}} E_t \tag{3.11}$$

In this case, the revenue function is a quadratic function of E, the excess generation or energy sold in the wholesale energy market, with a peak that occurs at a point before the market saturation point $E_{max,t}$, as shown in Figure 3-3.

As discussed in Section 3.3.1.1, the socially efficient solution would be to maximize A_t, the avoided cost of energy generation in the region, or the area under the demand function as shown in Equation (3.12).

$$A_t = \int_{E_0}^{E_t} D(e)de = \frac{1}{2}\frac{P_{0,t}}{E_{0,t} - E_{\max,t}} E_t^2 - P_{0,t}\frac{E_{\max,t}}{E_{0,t} - E_{\max,t}} E_t \tag{3.12}$$

Given our linear demand function, the avoided cost function A_t would be a quadratic function at each time step, with a maximum at the market saturation point $E_{max,t}$, as seen in Figure 3-3.

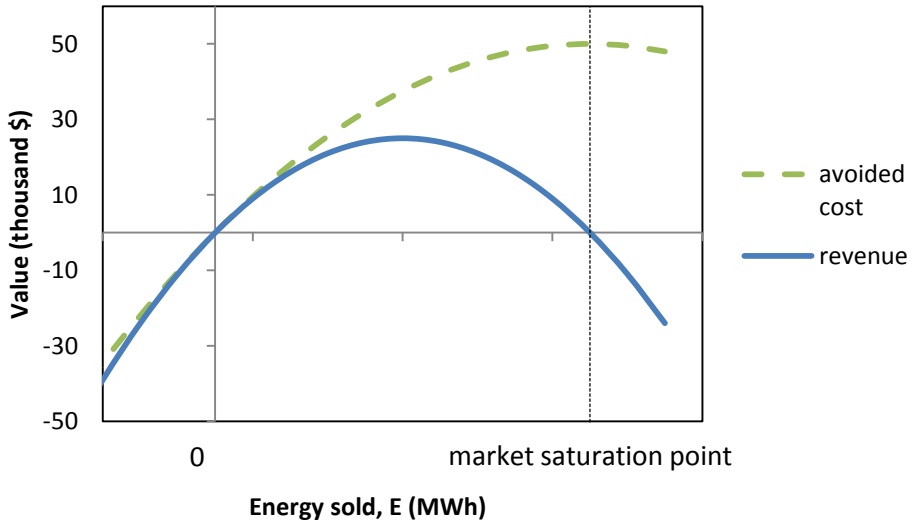

Figure 3-3: An illustrative comparison of revenue and avoided cost functions

To understand the implications of efforts to maximize BPA's total revenue, consider the formulation of the situation of revenue maximization in Equation (3.13).

$$\max_{E_t} \sum_t R_t = \max_{E_t} \sum_t (a_t E_t^2 + b E_t) \tag{3.13}$$

where

$$\sum_t E_t = E_{total} \tag{3.14}$$

Here all the real details of the operation of the reservoirs, powerhouses, and turbines have been summarized by Equation (3.14), which indicates how much energy BPA can generate over the planning period. Clearly this is a major simplification, but it is adequate to understand the implications of revenue maximization.

In the optimal solution to the maximization of revenue in Equation (3.13), the marginal revenue in period t is simply the first derivative of the objective function with respect to the energy bought or sold on the wholesale market (E_t) in period t. The market price is the revenue divided by the total energy sold (i.e. $R(E_t)/E_t$); that is the actual price which BPA is paid or must pay for each MWh produced or purchased. Thus the optimization problem in Equation (3.13) will attempt to generate energy in the periods with the highest marginal revenue (and less in periods with lowest marginal revenue). This would continue shifting energy generation until the marginal revenue is the same over all time periods, assuming the constraints allow these conditions to be reached and head effects are ignored.

First-order conditions for optimality of the optimization of Equation (3.13) can be obtained with the simple model that ignores all of the complex system constraints. If we maximize the revenue expressed by Equation (3.13), with the resource constraints in Equation (3.14) appended with a Lagrange multipler -λ, the first order conditions become Equation (3.15):

$$\frac{\partial}{\partial E_t}\{\mathrm{R}_t(\mathrm{E}_t)\} - \lambda = \frac{\partial}{\partial E_t}\{\mathrm{E}_t * \mathrm{D}(\mathrm{E}_t)\} - \lambda = D_t(E_t) + E_t \frac{\partial D(E_t)}{\partial E_t} - \lambda = 0$$
$$\Rightarrow \lambda = D_t(E_t) + E_t \frac{\partial D_t(E_t)}{\partial E_t} \tag{3.15}$$

At the revenue maximizing optimum, the marginal revenue in each period should be equal. However, in Equation (3.15) the marginal revenue is not the market price λ; marginal revenue has an additional term which describes the sensitivity of the price described by the demand function $Dt(Et)$ to the energy suppliedEt. Thus the utility will withhold production when selling to get a higher market price on the energy sold on the market. They may even dump water so as to avoid generating electricity in some periods if doing so sufficiently increases the price. They would never want to generate electricity to the point the price dropped to zero, because they would then get zero revenue.

Thus, we show above that for a very large hydropower producer such as BPA in the wholesale market with market power, the revenue objective function will result in monopolistic behavior. However as a federal agency, BPA should be looking out for the public good. In a competitive energy market when no participant can affect the price, the solution to Equation (3.13) for the simple model would be for the price to be the same in every period; that is, energy supply is targeted to the periods where costs of production by other utilities are the largest, and this would continue until the price was the same in every period, if possible. This is the socially efficient solution.

Now consider the case where we are maximizing system avoided costs in Equation (3.16).

$$\max_{E_t} \sum_t A_t = \max_{E_t} \sum_t (\frac{a}{2}_t E_t^2 + bE_t) \tag{3.16}$$

If we solve for the first-order conditions for optimality of Equation (3.16), for the simple model with Equation (3.14) appended with a Lagrange multipler -λ, the first order conditions end up as Equation (3.17):

$$\lambda = D_t(E_t) \tag{3.17}$$

Thus, if BPA operates to minimize the total avoided cost in the region, the simple model says they will attempt to make the price for electric energy the same in every period. In practice, there are head effects and constraints on operations. However, attempting to maximize avoided-costs will result in the greatest reduction in regional energy generation costs, which may be a desired outcome for a hydropower system that is operated by a governmental organization.

3.3.2 Optimized Multi-Turbine Powerhouse Functions

In Chapter 2, we demonstrated how to precompute optimized multi-turbine Powerhouse Generation Functions for each reservoir in the 10-reservoir hydropower system. We make use of the fact that operators prefer to operate turbines at their efficient average operating point (EAOP) because it is the flow that maximizes the generation. In times when there are no such restrictions, the powerhouse function describe the optimal generation at the powerhouse for a given flow through the powerhouse. For these Economic Dispatch powerhouse generation functions, the

turbine types are loaded sequentially in order of decreasing efficiency resulting in the best possible generation of the powerhouse.

Fish Dispatch powerhouse generation functions are used primarily when there is a need to incorporate fish passage considerations. During the spring and summer months (April – August), the FCRPS is operated in accordance to project-specific criteria so as to support fish facilities and protect and enhance anadromous and resident fish species listed as endangered or threatened under the Endangered Species Act [*US Army Corps of Engineers et al.*, 2011; *US Army Corps of Engineers*, 2012]. These operations include specific turbine dispatch priorities, which were accounted for in the predetermined powerhouse generation functions (see Chapter 2 of this thesis), as well as minimum spill requirements.

Powerhouse operations for the Federal Columbia River Power system are different for each project and for each monthly period. This is summarized in Figure . The green shaded cells show times where there are no dispatch restrictions, and so the project operates under economic dispatch when the different turbine types are dispatched in decreasing order of efficiency. In times when there are no dispatch restrictions, the powerhouse function describes the optimal generation at the powerhouse for a given release from the project. The yellow shaded areas describe project operations in which certain turbines are prioritized to improve flow patterns in the vicinity of the dam, or to provide attraction flow for fish ladders. Note also that fish screens are installed in certain times of the year, further complicating the representation of system operations.

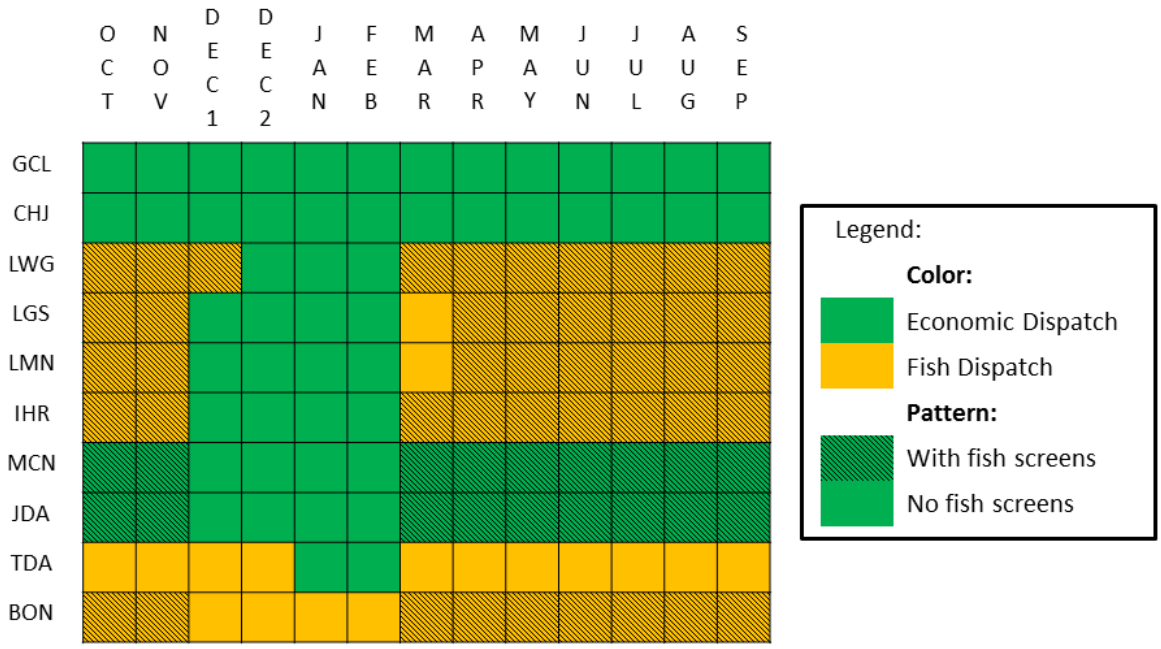

Figure 3-4: Powerhouse operations at the projects (rows) for each month of the year (columns). A single month can have different operation rules, as illustrated in the Dec1 and Dec 2 columns. Each project is represented as a three-letter code corresponding to Figure 3-1. Economic Dispatch is when the turbine types are dispatched in order of the most efficient to the least efficient. Fish Dispatch follows a prescribed turbine type order specified in the Fish Passage Plan.

For Fish Dispatch powerhouse functions, we introduce different algorithms for creating the powerhouse functions reflecting two possible implementations of the fish turbine dispatch priorities, plus a third addressing the desire to have a concave powerhouse function even if some approximation must be accepted.

Algorithm 1 (Fish Dispatch): turbines dispatch follows the predetermined dispatch orders as detailed in the yearly Fish Passage Plans – turbines are loaded sequentially in the Fish Dispatch order, and each is loaded until it operates at its most efficient release for the entire

period. This is the fish-dispatch rule. This rule can result in powerhouse generation functions that are non-concave.

Algorithm 2 (Joint dispatch): suppose fish dispatch requires that one first load a less efficient turbine of type 2, and then can load a more efficient turbine of type 1. Our "joint operation" rule prescribes that the two turbines both be run at the same time, for part of or all of the time step; that way the turbine of type 1 is only run when the less efficient type 2 turbine is running. The joint rule is both feasible and realistic, and results in as much or more energy generation than the fish-dispatch rule, while always satisfying the fish passage regulations. For 4- and 8-hour time periods, this may reflect the operation that is preferred by the operator. It is still possible for the joint rule to have non-concave sections, though it is less frequent; for those few cases.

Algorithm 3 (Approximation): a third rule is to compute the average generation rate if all turbines were operated at the maximum efficiency of the least efficient turbines (its EAOP defined in Chatper 2). This is the point on the fish-dispatch powerhouse function where the total release has just reached the point that all available turbines are running for the entire period. The rule then assumes that energy will be generated at that average rate for all releases less than or equal to the total release corresponding to that loading rate schedule; beyond that release point, all three rules go into "overdrive", where the release rate for all turbines are increased so as to retain the same marginal value for power production at each. The approximate rule always produces a concave function as is desirable for the optimization.

We found that the difference in generation between the Fish Dispatch rule and approximation powerhouse generation functions is generally so small as to be negligible in most case. The difference between the fish dispatch and the joint rule is even smaller; so if the joint rule yields a concave powerhouse function, there is no need to use the approximate rule. The largest generation differences are equivalent to less than 1% of the generation at each powerhouse at any given time period. The largest difference tends to occur at Bonneville, where the operations dictate that all the inefficient turbines have to be loaded before the efficient turbines.

The use of powerhouse generation functions developed in Chapter 2 eliminates the need to use mixed-integer linear programming to maintain the nonlinear relationship between powerhouse generation and flow through the powerhouse. Rather, concave, piecewise polynomial powerhouse functions were produced that require only a single powerhouse flow decision at each project. Further, the use of concave approximations to the fish-priority powerhouse functions that result from required fish-dispatch ensured a convergence of the sequential quadratic programming algorithm to a global maximum.

3.3.3 Reservoir Operation with Fish Spill Constraints

Minimum spill requirements for fish change by project and time of year, as described in Table 3-1. Note that these spill requirements take effect after the minimum powerhouse flow requirements have been met, which requires that at low flow, a single turbine unit is run at a certain flow. Spill requirements are set as a minimum spill or are described as a percentage of the total releases from the reservoir.

The spill at each project also has to be capped to meet the Total Dissolved Gas (TDG) limits at each project. TDG limits also vary by project and time of year. When the spill requirements in Table 3-1 are introduced into the model as constraints, the algorithm can fail to identify a feasible solution. This occurs because in order for the spill requirements constraints to be met, the system often needed to exceed its TDG limit. These TDG saturation levels are monitored at the forebay and tailrace of each mainstream project during the fish passage season. The limits exist because high concentrations of TDG as fish enter the tailrace will cause Gas Bubble Disease, which increases fish mortality. This occurs during periods of high inflow, such as in April, when the system has to balance between routing the water through the system meeting to meet mandates spill while avoiding large spills over the top of the dam that result in exceeding the TDG limit.

Table 3-1: Minimum spill requirements at each project during fish passage season, as described in the 2012 Fish Passage Plan [*US Army Corps of Engineers*, 2012]

Project	SEP - MAR	APR	MAY	JUN	JUL	AUG
GCL	no minimum spill requirements					
CHJ	spills to meet constraints at Priest Rapids Dam					
LWG	No min spill	20 kcfs			18 kcfs	
LGS	No min spill	spill ≥ 30% of total discharge				
LMN	No min spill	spill cap			17 kcfs	
IHR	No min spill	45 kcfs			alternate between spilling ≥ 30% of total discharge vs. 45 kcfs day and spill cap night	
MCN	No min spill	spill ≥ 40% of total discharge			spill ≥ 50% of total discharge	
JDA	No min spill	alternate between spilling 30% of total discharge and 40% of total discharge over 4-day blocks				
TDA	No min spill	spill ≥ 40% of total discharge				
BON	No min spill	100 kcfs			alternate between spilling 85 kcfs day and 121 kcfs night vs. 95 kcfs	

To overcome this problem, "project release functions" were generated for use during the spring and summer months (April – August) to guarantee the minimum water released over the spillway. These functions account for the minimum generation and spill requirements in accordance to the project priorities set by the BPA. The minimum generation levels must be met first, followed by the spill requirement up to its TDG limit; then all the turbines are run at capacity before allowing the rest of the spill to exceed the TDG limit, resulting in uncontrolled or forced spill. The project release functions thus take as input the total release flowing through the project, and returns the amount of flow that is being passed through the turbines according to the pre-established spill requirements. Powerhouse functions compute the resultant power generation. Figure 3-5 shows an example of a project release function which describes how the

total project release is divided between the turbine and spillway releases, in accordance to the spill requirements and a desire to generate as much power as possible.

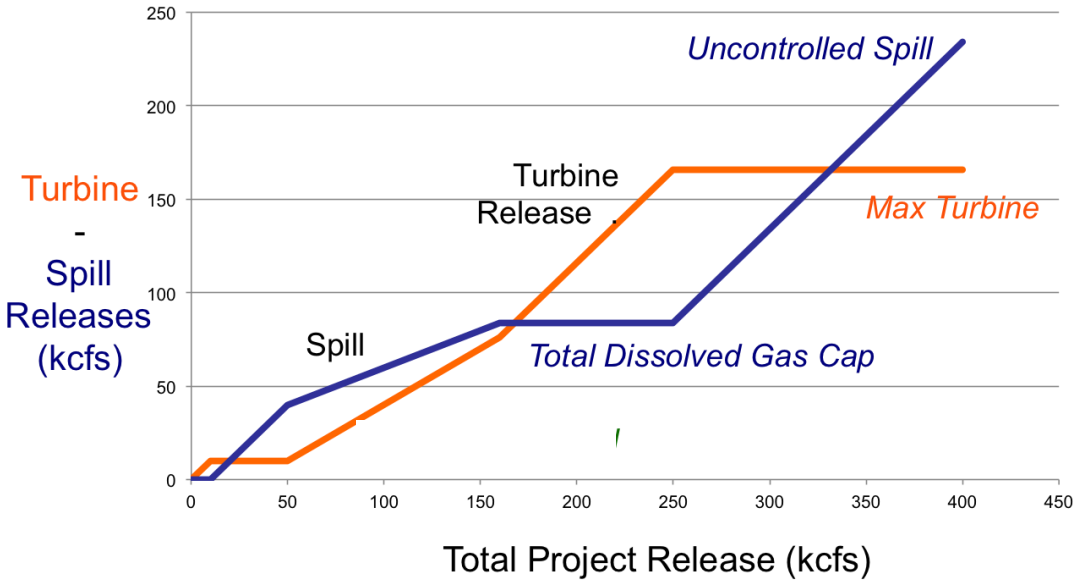

Figure 3-5: An example of a project release function which details how total project release is divided into the turbine and spillway releases. The project release function takes as input the total project release and returns the turbine release.

By using the project release functions, we are able to overcome the problems of infeasibility. Since the Columbia/Snake mathematical programming model would not have to explicitly decide how the release from these critical projects is divided between powerhouse releases and spills, we avoid having a set of nonlinear constraints that would cause infeasibility for some time periods due to inability to accurately account for the spill priorities and allocations. The nonlinearities still show up in the objective function, where the optimization model can deal with them. However, this means that the global optimum is no longer guaranteed because of the nonconvexity of the project functions.

A post processer can generate a time series of the flow through the turbines, and over the spillway. The model would also generate the power (energy) generated with each project following the fish rules using the flow through the turbines for any total release.

3.3.4 Flow routing

The reservoir system dynamics are based on the conservation of mass. In order to ensure that water that flows through the system is neither gained nor lost in the routing process, the mass balance constraint Equation (3.3) must be satisfied at all reservoirs and at all time steps. The flow routing in the deterministic optimization model considers the travel times between the 10 reservoirs through the use of the lagged-routing coefficient matrix C_τ that appears in Equation (3.3). The routing coefficients are calculated based on the length of each period, and the travel times in Figure 3-1,which represent the average travel times between the reservoirs [*Labadie*, 2004].

The reservoir system dynamic equations depend on the time=step or time-period length considered. We consider combinations of 4-, 8-, and 24-hour time steps, where time steps can be longer during later periods. Coarser time steps can significantly reduce run times. However, a coarse 24-hour time step would fail to capture time-of-day energy values, and the flexibility and reserve-requirements hydropower provides. A simple solution that we employ here with the 24-hour time step system representation is to optimize with on- and off-peak releases in the generation decisions and economic computations within the 24-hour period, but then route these releases using the routing matrix computed for the 24-hour routing.

An example of the computation of the lag coefficients and subsequently the flow between reservoirs follows. First, assume that the outflows from each reservoir are constant each time step with no time lags in between. The system dynamics equation for all reservoirs in each time period t, $\vec{S}_t$ with powerhouse release vector $\vec{r}_{PH,t}$, spill release vector $\vec{r}_{spill,t}$, inflow vector $\vec{I}_t$ and the routing coefficient matrix C for the BPA system shown Equation (3.3) is Equation (3.18). In the matrix C, the columns correspond to the upstream project and the rows correspond to the downstream project. Since there are no time lags considered between when the upstream project releases water and when the downstream project receives the water, the coefficients are either 0 or 1 conditional on there being a flow path between one reservoir to another. The outflows from each reservoir at time *t* are represented as -1 down the main diagonal of the matrix.

$$\vec{S}_{t+1} = \vec{S}_t + C * \left(\vec{r}_{PH,t} + \vec{r}_{spill,t}\right) + \vec{I}_t$$

where $C =$

GCL	*CHJ*	*LWG*	*LGS*	*LMN*	*IHR*	*MCN*	*JDA*	*TDA*	*BON*
–1	0	…	…	…	…	…	…	…	0
1	–1	⋱							⋮
0	0	–1	⋱						⋮
⋮	⋱	1	–1	⋱					⋮
⋮		⋱	1	–1	⋱				⋮
⋮			⋱	1	–1	⋱			⋮
0	1	0	…	0	1	–1	0	…	0
⋮					⋱	1	–1	⋱	⋮
⋮						⋱	1	–1	0
0	…	…	…	…	…	…	0	1	–1

(3.18)

When the lag times are considered for each of the different projects, the resulting system dynamics equation and lagged routing coefficient matrixes C_τ for the BPA system are more

complicated. In particular, flow released by one reservoir uniformly during time step t may show up partially in time step t, t+1, or even later at the next downstream reservoir. For a 24-hour time step, there are two lagged routing coefficient matrices C_0 and C_1 corresponding to flows arriving at time step t and time step $t+1$. The resulting system dynamics equation for all reservoirs in each time period t, $\vec{S}_t$ with powerhouse release vector $\vec{r}_{PH,t}$, spill release vector $\vec{r}_{spill,t}$, inflow vector $\vec{I}_t$ and lagged routing coefficient matrices C_τ for a 24-hour time step is shown in Equation (3.19).

$$\vec{S}_{t+1} = \vec{S}_t + \sum_{\tau=0} \boldsymbol{C}_\tau * \left(\vec{r}_{PH,t-\tau} + \vec{r}_{spill,t-\tau}\right) + \vec{I}_t$$

where $C_0 =$

GCL	*CHJ*	*LWG*	*LGS*	*LMN*	*IHR*	*MCN*	*JDA*	*TDA*	*BON*
–1	0	…	…	…	…	…	…	…	0
0.938	–1	⋱							⋮
0	0	–1	⋱						⋮
⋮	⋱	0.958	–1	⋱					⋮
⋮		⋱	0.958	–1	⋱				⋮
⋮			⋱	0.958	–1	⋱			⋮
0	0.292	0	…	0	0.917	–1	0	…	0
⋮					⋱	0.875	–1	⋱	⋮
⋮						⋱	0.958	–1	0
0	…	…	…	…	…	…	0	0.917	–1

(3.19)

$C_1 =$

GCL	*CHJ*	*LWG*	*LGS*	*LMN*	*IHR*	*MCN*	*JDA*	*TDA*	*BON*
0	0	…	…	…	…	…	…	…	0
0.063	0	⋱							⋮
0	0	0	⋱						⋮
⋮	⋱	0.042	0	⋱					⋮
⋮		⋱	0.042	0	⋱				⋮
⋮			⋱	0.042	0	⋱			⋮
0	0.708	0	…	0	0.083	0	0	…	0
⋮					⋱	0.125	0	⋱	⋮
⋮						⋱	0.042	0	0
0	…	…	…	…	…	…	0	0.917	0

In the C_τ matrices in Equation (3.19), the off diagonal elements are no longer 1, but are numbers between 0 and 1 that describes the proportion of flows from the upstream project that arrive at the downstream project at time lag τ. Note also that the elements on the main diagonal of matrix C_1 are 0.

To illustrate how these lagged coefficients are calculated, consider the 17-hour travel time between the Chief Joseph (CHJ) and McNary (MCN) projects with 24-hour time steps. In

this model, we assume that the releases are constant over the 24-hour period. As this wave of water travels down the reach, with a 24 hours time step not all the water released in time step *t* shows up at MCN in that time step. The proportion of CHJ outflow that MCN receives in time step *t* is the ratio of the difference between the time step length and the travel time dived by the time step length, or $\frac{(24-17)}{24} = 0.292$. The remainder, $1 - 0.292 = 0.708$, shows up at the next time step. Thus at time *t*, only about 30% of the water that shows up at MCN from CHJ is from the current time step. Finer time steps provide greater resolution.

When considering different time step lengths, we also have to consider the number of C matrices that will capture all the flows going through the system. For our system, the number of matrices needed for the 24-hour time step is two. The number of lags considered for the 8-hour and 4-hour time steps are 4 and 6 given the 17 hour lag CHJ to MCN.

3.4 Illustrative Runs

This section illustrates the capabilities of the model through a number of illustrative runs. The illustrative runs show operations in December and April for different planning horizons, economic objectives, fish constraint operations, and routing time steps.

Figure 3-6 shows the historical average monthly reservoir storage levels for water year 2012 as a percentage of the reservoir capacity. In December, the system operates in a drawdown period in preparation for the increased inflow into the system during the wet season [*Bonneville Power Administration*, 1992]. Thus, Grand Coulee (GCL) which is at the most upstream point of

the Mid-Columbia subsystem is at 86% of its capacity. In contrast for April, the system is in a refill period, storing the spring runoff for summer generation. Here we see that the starting storage at Grand Coulee is only at 33% of its capacity. The remaining reservoirs tend to operate between 80% and 100% of capacity year round. Thus the entire system depends on Grand Coulee for flow regulation. An exception is John Day dam (JDA), which operates within a 1.5 ft range of the minimum level that provides irrigation pumping between April and September to reduce juvenile salmon travel time [*US Army Corps of Engineers et al.*, 2011].

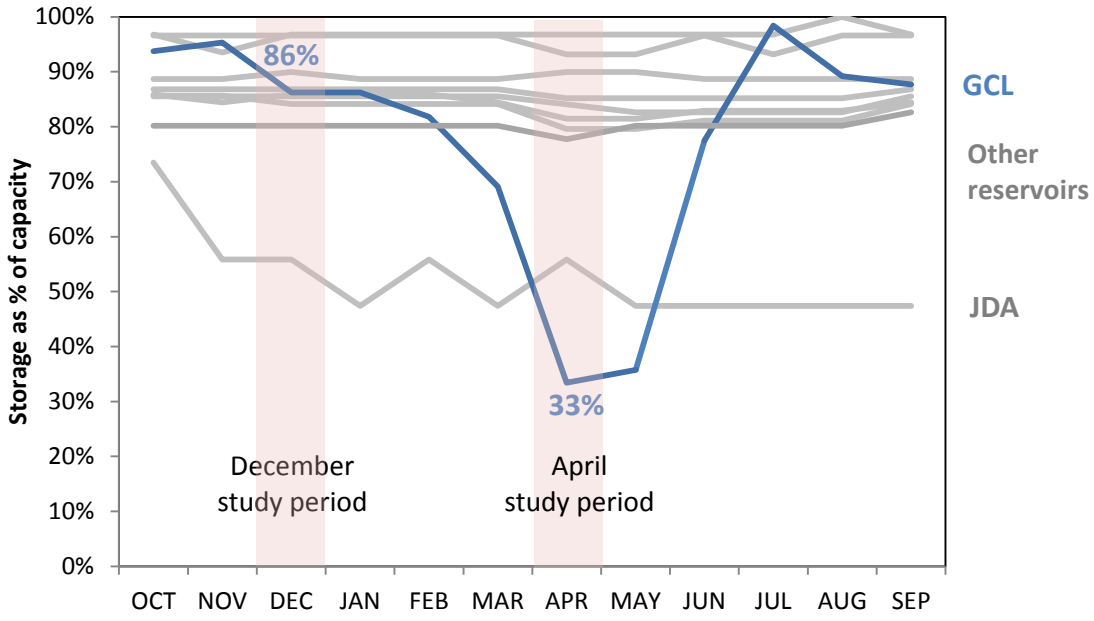

Figure 3-6: Reservoir average monthly storage levels for water year 2012 as percentage of their capacities.

Table 3-2 shows the historical average inflows, prices, and loads over the investigated 21-day period for December and April. Inflows into GCL and Lower Granite (LWG) tend to be higher in April than in December. Prices tend to be higher in December than in April even though loads are generally lower in December as compared to April. This is because with spring

runoff, cheap hydro generation is abundant (even with the refill requirement) which in turn depresses market prices even though the load is high.

Table 3-2: Inflows, prices, and loads for December and April. Prices shown are the inferred price at the point where system generation equals the load, resulting in price P_0 for $E_t = 0$ in Equation (3.10)*. Inflows and loads are the average over the entire period. The price data is set based on index price data for the Mid-C trading hub.*

	Average Inflow (kcfs)		**P_0 ($/MWh)**		**Average Load (MW)**	
	GCL	**LWG**	**On- peak**	**Off-peak**	**On- peak**	**Off-peak**
December	93	24	$42	$13	7,458	7,249
April	142	120	$21	$6	9,025	9,009

3.4.1 Operations to meet different market objectives

This section illustrates the operations of the hydropower system when operating to maximize in: revenue versus maximizing avoided energy production costs in the region, as described in Section 3.3.1.2. Fish Operations are enforced in April. Table 3-3 summarizes the results for two test cases run in December and April. GCL is allowed to drawdown by 6 feet over an 8-day period in the December runs, and is constrained to refill by 3 feet over an 8-day period in April. As expected, the total revenues after optimization are higher when optimizing under the revenue objective in December and April, while the total avoided costs are higher when optimizing under the avoided cost objective in both December and April.

Table 3-3: Summary of the operations of the 10 reservoir system for two 8-day periods in December and April. The total load over the 8-day periods in December and April is 1517 GWh and 1683 GWh respectively. The different operational constraints between the December and April are described in Sections 3.3.2 and 3.3.3

	Dec		April	
	revenue objective	**avoided cost objective**	**revenue objective**	**avoided cost objective**
Total revenue ($M)	3.5	2.9	1.7	1.1
Total avoided cost ($M)	5.3	6.1	2.9	3.5
Total Generation (GWh)	1,701	1,733	1,679	1,678
Total On-peak sales (GWh)	160	219	36	75
Total Off-peak sales (GWh)	24	-3	-41	-80
Min on-peak price	$21.21	$13.30	$17.55	$15.00
Max on-peak price	$21.22	$13.60	$18.80	$16.76
Min off-peak price	$6.36	$13.28	$10.54	$14.97
Max off-peak price	$6.37	$13.58	$12.19	$17.83
Total Spill (ksfd)	75	0	3798	3781

What is striking is the large differences between the values of revenue and avoided cost that result from maximizing the two objectives, and the differences in energy market prices. The choice of objective is important. The total generation levels are not very different for both the revenue and avoided cost . This is because both models have the same storage minimum level constraints at the end of the horizon. In April, the solutions are very similar because the system is further constrained to be operating under the Fish Operations that dictate the spill and total project flow through the reservoirs, as described in Section 3.3.3

The prices show how the model tries to distribute the energy in the on-peak hours compared to the off-peak hours. For the avoided cost function, the optimization algorithm will try its best (constraints willing) to get the prices to be the same in all periods. For the revenue maximizing solution, the optimization solution has very different prices in the two periods, which results in greater revenue for BPA, as Table 3-3 shows.

3.4.2 System Operation With and Without Fish Operations

This section demonstrates the model operations during a period in Fish Passage season with and without Fish Operations in the Federal Columbia River Power System. We demonstrate the ability to quantify the change in value of hydropower generation when Fish Passage constraints are enforced. Table 3-4 summarizes the results for a 21-day horizon in April, with a combination of 4-, 8- and 24-hour time steps. The model objective is to maximize avoided cost, and Grand Coulee is constrained to fill to at least 20 feet through the planning horizon.

Table 3-4: Results for a 21-day run in April with a combination of 8- and 24-hour time steps maximizing avoided cost with GCL required to fill 20 feet, with and without Fish Operations. The total load to be served by the hydro utility is 4,564 GWh.

	With Fish Constraints	**Without Fish Constraints**
Avoided Cost ($M)	-1.3	9.1
Total Generation (GWh)	4,375	5,510
Total Peak sales (GWh)	37	799
Total Off peak sales (GWh)	-228	149
Min on-peak price	$17.40	($0.25)
Max on-peak price	$21.34	$0.38
Min off-peak price	$17.59	($0.32)
Max off-peak price	$20.14	$0.85
Total Spill (ksfd)	9855	9909

The avoided cost optimization results show that under the current assumptions, having to operate under Fish Operations results in a decrease in avoided costs to other utilities of $10.4 million. This amount is the opportunity cost to the system due to the Fish Operations being in effect. When there are no Fish Operations required, the system can generate and sell more energy on the wholesale market. In fact, the amount of power sold almost saturates the market,

as evidenced by the on- and off-peak prices being close to zero. This in turn results in an increase in spill during that time due to the system trying to avoid going into the negative prices.

*Table 3-5: Changes in storage, total spill and total powerhouse flow in ksfd at the 10 reservoirs **with** Fish Operations or **without** Fish Operations when maximizing the avoided cost function. The **difference**s in the change in storage, total spill and total powerhouse flow from the two operation types are also shown; the color scale indicates how high (more saturated) or low (less saturated) the differences are.*

volume, ksfd	Change in Storage		Powerhouse flow		Spill	
	with	**without**	**with**	**without**	**with**	**without**
GCL	707	707	1,959	1,932	0	27
CHJ	0	0	1,973	1,936	0	37
LWG	11	12	1,838	1,841	425	421
LGS	0	19	1,572	1,560	600	592
LMN	0	5	1,761	1,728	529	537
IHR	0	3	1,091	1,042	1,247	1,268
MCN	0	4	2,703	2,684	1,802	1,790
JDA	0	8	3,327	3,285	1,392	1,394
TDA	0	3	2,683	2,654	1,783	1,768
BON	0	27	2,850	2,782	2,077	2,076

Table 3-5 shows more detail on the total volumetric changes in the system. When the system is operating with Fish Operations, GCL fulfills its refill obligation, while LWG also refills. Recall that the target storages at the end of the horizon are minimum storage levels, so reservoirs can end up filling by the end of the optimization. When the system is operating without Fish Operations, most of the reservoirs tend to increase their storage levels. The reason is so that the increase in head would allow for an increased efficiency in generation, i.e. less flow will produce more power. This results in fewer spills at most of the projects that have a higher generation level.

3.4.3 24-hour Routing with On- and Off-Peak Generation

A feature of the model developed for the BPA system is that it allows for the combination of time steps of 8- and 24-hours. Shorter time steps are very attractive for near-term planning when more detailed schedules are needed. An interesting issue is if 8 hour steps are needed to evaluate the value of water a week or two hence. In these experiments the deterministic model was run for an 8-day and 21-day planning period in December. Consider 24-hour routing with separate on- and off- peak power generation releases, as opposed to a 24-hour time step model that assumes the selected release rate was maintained for all 24 hours. Model M8 uses 8-hour time steps, model M24-2 uses 24-hour time steps for routing with "on-peak" and "off-peak" powerhouse releases, and M8-24-2 combines the M8 model for the first 3 days and the M24-2 model for the remaining 5 days. Off-peak hours are between 10 p.m. to 6 a.m., while on-peak hours are between 6 a.m. to 10 p.m. Grand Coulee is allowed to draw down at its maximum rate of 1.5 ft/day, which provides the system the maximum flexibility of operations for this month [*US Army Corps of Engineers*, 2012].

Table 3-6: Results from 3 models with avoided cost optimization for a 8-day time horizon in December with 10 feet of allowable drawdown at Grand Coulee. The total load to be met over that time period is 1517 GWh. The models compared are the 8-hour time step model (M8), the 24-hour time step model with on- and off-peak releases (M24-2) and the combination between the 8-hour and 24-hour models (M8-24-2).

	M8	**M24-2**	**M8-24-2**
Avoided cost ($M)	7.1	7.1	7.1
% difference in value from M8		*0%*	*0%*
Run time (s)	686	146	233
speedup from M8		*4.7*	*2.9*
Total Generation (GWh)	1,883	1,885	1,885
Total on-peak sales (GWh)	319	320	320
Total off-peak sales (GWh)	47	48	48
Min on-peak price	$0.14	$0.00	($0.00)
Max on-peak price	$0.21	$0.00	$0.00
Min off-peak price	$0.13	($0.00)	($0.00)
Max off-peak price	$0.15	$0.00	$0.00
Total Spill (ksfd)	0.0	0.0	6.0

Table 3-6 shows the results of the 8-day model run. The choice of different time step lengths in the models all result in the same value, $7.1 million. The computational speedup due to the choice of the time step of the model is significant: about 5 times if the 24-hour with on- and off-peak releases is used for the entire horizon, and 3 times with the combination of 8-hour and 24-hour time steps.

The differences between the three model solutions is very small, in part because the market price is driven essentially to zero in all three models. Due to the ability of the model to draw down the GCL reservoir levels by its maximum rate of 1.5 ft/day, and the market depth assumptions made, the utility is able to saturate the energy market and drive the market energy prices down to $0 for both the on- and off-peak periods.

Table 3-7: Results from 3 models with avoided cost optimization for a 21-day time horizon with 6 feet of allowable drawdown in December. The total load for this 21-day period is 3815GWh. The models compared are the 8-hour time step model (M8), the 24-hour time step model with on- and off-peak releases (M24-2) and the combination between the 8-hour and 24-hour models (M8-24-2).

	M8	**M24-2**	**M8-24-2**
Avoided cost ($M)	8.7	9.3	8.8
% difference in value from M8		7%	1%
Run time (s)	12575	1491	2058
speedup from M8		8.4	6.1
Total Generation (GWh)	4,014	4,038	4,015
Total on-peak sales (GWh)	328	345	327
Total off-peak sales (GWh)	-128	-121	-129
Min on-peak price ($/MWh)	$25.12	$24.14	$24.92
Max on-peak price ($/MWh)	$26.86	$25.94	$26.82
Min off-peak price ($/MWh)	$24.86	$24.11	$24.92
Max off-peak price ($/MWh)	$26.63	$25.82	$26.59
Total Spill (ksfd)	0.0	0.0	0.0

Table 3-7 shows the results for the 21-day model run in December. Here, the model is more constrained in allowing GCL to drawdown only 6 feet over the whole 21-day horizon. We say more constrained because the optimal solution to maximize the avoided cost from hydropower generation is to generate as much power as it can, but it is unable to drive the prices to zero. Restricting the drawdown at GCL decreases the total amount of generation that the system can produce. Because the model is more constrained, there are differences in the values obtained with the three models.

Observe also that for a longer time horizon, the runtime advantage of having 24-hour time steps is greater, in excess of a factor of 8. The M24-2 model is able to find an optimal solution with higher value than the M8 model, since the routing constraints are averaged over the 24-hour time steps but one still has on- and off-peak releases. The 24-hour model is able to find

an optimal solution 8 times faster than the 8-hour time step model a 7% difference in value. The combination model M8-24-2 finds an optimal value that is only 1% higher than the 8-hour time step model.

In terms of energy and prices, M8-24-2 matches the M8 model very well. Here, the optimal price is at around $25/MWh. In order to maximize the avoided cost, the utility with market power would buy in the off-peak (thus the negative sales values) and sell in the on-peak hours. The M24-2 model has a better value because the 24-hour routing constraints allow for less energy bought to serve the load during off-peak hours and more energy sales during the on-peak. Though the prices are very similar between the M24-2 and the M-8 models, this appears to be enough to cause the 7% difference in value.

3.5 Conclusions

This chapter demonstrates the features of a computationally efficient deterministic optimization model for multi-reservoir system operation that incorporates expected stream inflow, hydropower plant operation, contracted energy loads, electricity power markets and when applicable also includes special seasonal constraints for fish on location and volume of flow released from specified turbines or reservoirs. The fast convergence times enables this model to serve as the basis for a stochastic model which includes realistic routing, operational constraints, and market behavior. It also uses pre-computed powerhouse functions that provide the hydroelectric power that can be generated by different projects for a given flow when turbines at that site are dispatched and loaded efficiently.

The model includes user-specified time steps that provide significant computational savings by allowing the combination of different time steps in modeling the operation of the system. An 8-hour routing model would capture the hydrology and load better, but take longer to solve than a 24-hour routing model with on- and off-peak generation. Combining both allows the optimization model to find a solution that in the near future has an 8-hour time step useful for guiding turbine and project-level decisions, while using a 24-hour time step to reflect the value of power over the next two to three weeks.

Our objective function takes into account the hydro utility's opportunities as a large player in the hydropower markets and thus participation in the day-ahead wholesale energy markets to minimize the regional cost of energy generation. The parameters for the objective function are the price forecast for a particular volume of power transacted in the market. We showed that for an entity with market power, maximizing revenue will result in prices that are not balanced across periods, which would be the economically efficient solution. By maximizing avoided cost, the entity generates such that the cost of energy is lowered for all.

Finally, we also implement the model to accommodate fish passage constraints during the months when these are in effect. Fish passage constraints affect operations by imposing minimum spill levels on the projects, thus potentially forcing generation to be lower than would otherwise occur without these additional constraints. The model clearly demonstrates the opportunity cost to the system by having to operate under Fish Operations.

3.6 References

Ahmad, A., A. El-Shafie, S. F. Mohd Razali, and Z. S. Mohamad (2014), Reservoir optimization in water resources: A review, *Water Resour. Manag.*, *28*(11), 3391–3405, doi:10.1007/s11269-014-0700-5.

Arnold, E., P. Tatjewski, and P. Wolschowicz (1994), Two Methods for Large-Scale Nonlinear Optimization and Their Comparison on a Case Study of Hydropower Optimization, *J. Optim. Theory Appl.*, *81*(2), 221–248.

Barros, M. T. L., F. T. Tsai, S. Yang, J. E. G. Lopes, and W. W. Yeh (2003), Optimization of Large-Scale Hydropower System Operations, *J. Water Resour. Plan. Manag.*, *129*(3), 178–188.

Bonneville Power Administration (1992), *Modelling the System: How computers are used in Columbia River Planning*.

Catalão, J. P. S., S. J. P. S. Mariano, V. M. F. Mendes, and L. A. F. M. Ferreira (2009), Scheduling of Head-Sensitive Cascaded Hydro Systems : A Nonlinear Approach, *IEEE Trans. Power Syst.*, *24*(1), 337–346.

Chang, G. W., M. Aganagic, J. G. Waight, J. Medina, T. Burton, S. Reeves, and M. Christoforidis (2001), Experiences with Mixed Interger Linear Programming Based Approaches on Short-Term Hydro Scheduling, *IEEE Trans. Power Syst.*, *16*(4), 743–749.

Digna, R. F., Y. A. Mohamed, P. van der Zaag, S. Uhlenbrook, and G. A. Corzo (2017), Nile River Basin modelling for water resources management - a literature review, *Int. J. River Basin Manag.*, *15*(1), 39–52, doi:10.1080/15715124.2016.1228656.

Grygier, J. C., and J. R. Stedinger (1985), Algorithms for Optimizing Hydropower System Operation, *Water Resour. Res.*, *21*(1), 1–10.

Hamann, A., G. Hug, and S. Rosinski (2017), Real-Time Optimization of the Mid-Columbia Hydropower System, *IEEE Trans. Power Syst.*, *32*(1), 157–165.

Howe, C. W. (1971), *Benefit-Cost Analysis for Water System Planning*, 4th reprin., American Geophysical Union, Washington, DC.

Jacobs, J., G. Freeman, J. Grygier, D. Morton, G. Schultz, K. Staschus, and J. R. Stedinger (1995), SOCRATES: A system for scheduling hydroelectric generation under uncertainty, *Annals*, *59*, 99–133.

Labadie, J. W. (2004), Optimal Operation of Multireservoir Systems : State-of-the-Art Review, *J. Water Resour. Plan. Manag.*, *130*(2), 93–111.

Li, X., T. Li, J. Wei, G. Wang, and W. W.-G. Yeh (2013), Hydro Unit Commitment via Mixed Integer Linear Programming : A Case Study of the Three Gorges Project , China, *IEEE Trans. Power Syst.*, 1–10.

Matevosyan, J., M. Olsson, and L. Söder (2009), Hydropower planning coordinated with wind power in areas with congestion problems for trading on the spot and the regulating market, *Electr. Power Syst. Res.*, *79*(1), 39–48, doi:10.1016/j.epsr.2008.05.019.

Nazari-Heris, M., B. Mohammadi-Ivatloo, and G. B. Gharehpetian (2017), Short-term scheduling of hydro-based power plants considering application of heuristic algorithms: A comprehensive review, *Renew. Sustain. Energy Rev.*, *74*(February), 116–129, doi:10.1016/j.rser.2017.02.043.

Pérez-Díaz, J. I., J. R. Wilhelmi, and J. Á. Sánchez-Fernández (2010), Short-term operation scheduling of a hydropower plant in the day-ahead electricity market, *Electr. Power Syst. Res.*, *80*(12), 1535–1542, doi:10.1016/j.epsr.2010.06.017.

Russell, C. S. (2001), *Applying Economics to the Environment*, Oxford University Press, Oxford, England.

Schwanenberg, D., M. Xu, T. Ochterbeck, C. Allen, and D. Karimanzira (2014), Short-term management of hydropower assets of the Federal Columbia River Power System, *J. Appl. Water Eng. Res.*, *2*(1), 25–32, doi:10.1080/23249676.2014.912952.

Shawwash, Z. K., T. K. Siu, S. Member, and S. O. D. Russell (2000), The B . C . Hydro Short Term Hydro Scheduling Optimization Model, *IEEE Trans. Power Syst.*, *15*(3), 1125–1131.

Steven Stoft (2002), *Power System Economics*, IEEE Press.

Tejada-Guibert, J. A., J. R. Stedinger, and K. Staschus (1990), Optimization of Value of CVP's Hydropower Production, *J. Water Resour. Plan. Manag.*, *116*(1), 52–70, doi:10.1061/(ASCE)0733-9496(1990)116:1(52).

U.S. Army Corps of Engineers, U.S. Bureau of Reclamation, and Bonneville Power Administration (2003), *Federal Columbia River Power System*.

U.S. Energy Information Administration (2012), Negative prices in wholesale electricity markets indicate supply inflexibilities, *Today in Energy*. Available from: http://www.eia.gov/todayinenergy/detail.cfm?id=5110# (Accessed 4 January 2014)

US Army Corps of Engineers (2012), *Fish Passage Plan*.

US Army Corps of Engineers, Bonneville Power Administration, and U.S. Bureau of Reclamation (2011), *2012 WATER MANAGEMENT PLAN*.

Yeh, W. W.-G. (1985), Reservoir Management and Operations Models: A State-of-the-Art Review, *Water Resour. Res.*, *21*(12), 1797–1818.

Yi, J., J. W. Labadie, and S. Stitt (2003), Dynamic Optimal Unit Commitment and Loading in Hydropower Systems, *J. Water Resour. Plan. Manag.*, *129*, 388–398.

Zagona, E. A., T. J. Fulp, R. Shane, T. Magee, and H. Morgan (2001), RiverWare: A Generalized Tool for Complex Reservoir System Modeling, *J. Am. Water Resour. Assoc.*, *37*(4), 913–29.

CHAPTER 4

A STOCHASTIC DYNAMIC PROGRAMMING APPROACH TO OPTIMIZING HYDROPOWER OPERATIONS WITH UNCERTAIN WIND GENERATION

4.1 Introduction

As part of a portfolio of solutions to combat climate change, many U.S. states have begun to adopt increasingly stringent renewable portfolio standards, which set targets for a certain percentage of generation from renewable resources by a prescribed date. According to the 2016 Annual Status Report of the U.S. Renewables Portfolio Standard (RPS) by the Lawrence Berkeley National Laboratory [*Barbose*, 2016], RPS policies collectively apply to 55% of total U.S. retail electricity sales. The same report also states that most of the 29 states that have set their RPS goals are on their way to meeting roughly 95% of their interim RPS targets in recent years.

The inherent unpredictability in renewable energy sources such as wind and solar can wreak havoc on a fragile electric grid that was built to run best on constant levels of supply and demand [*Bakke*, 2016]. As of 2016 California had about 10% of its energy served by wind and about 7% of its energy served by solar. At these penetration levels, the stochastic nature of wind becomes a significant issue, requiring a large amount of reserves to prevent sags in supply when there is no wind available [*Tuohy et al.*, 2009]. The forecast errors as a fraction of the wind power plant capacity usually average about 5 percent on an hour-ahead basis, and between 15 to 25 percent on a day-ahead basis [*Acker*, 2011]. Additionally, large amounts of solar generation

have caused negative energy prices to occur in the middle of the day, indicative of supply-side inflexibilities. This is the so-called duck curve [*St. John*, 2016].

4.1.1 Literature Review

While some grid-scale energy storage technologies like batteries are still in their early stages of development, existing hydropower systems with large storage capabilities can provide load following of wind generation at a relatively low environmental and economic cost [*Matevosyan et al.*, 2009; *Abreu et al.*, 2012]. The reservoir of a hydropower plant acts as energy storage and provides load following services on an hourly time scale; this can be accomplished by backing off the hydro generation during times when wind generation exceeds the forecast, and vice versa. Hamann and Hug [2016] attempt to characterize the hydropower system like a battery – by introducing deterministic methods for estimating the power capacity, energy storage capacity, and efficiency of the 5-reservoir cascaded Mid-Columbia hydropower system, also used as a basis for the hydropower system in this chapter. A caveat to this is that careful consideration must be made so that environmental constraints are not violated, as these can carry legal ramifications for the utility [*Fernandez et al.*, 2012; *Howard and Stedinger*, 2012].

Coordination of the wind and hydropower production can be mutually beneficial to both hydropower and wind power producers. However, a coordinated bidding strategy may only be acceptable to hydropower producers if there is a shared profit scheme between the hydro and wind power producers [*Zima-Bockarjova et al.*, 2010], or if the hydro and wind are both owned by the same utility [*Angarita and Usaola*, 2007; *Wangdee et al.*, 2010; *Abreu et al.*, 2012]. In this chapter we consider the coordination of hydropower production and wind power production

as two situations: (1) where the wind generation resource is part of the utility's generation mix, and (2) where the hydro utility provides load following services to an external entity that owns and operates the wind farm. The algorithm developed in this chapter will enable the hydro utility to better value its load following systems

Much of the previous research on wind and hydropower coordination has focused on using mixed-integer linear programming as their method of planning for hydropower production [*Angarita and Usaola*, 2007; *Matevosyan et al.*, 2009; *Abreu et al.*, 2012]. Mixed-integer linear programming allows for a piecewise linear approximation of the nonlinear power generation functions of the various units in a hydropower plant. Miranda et al [2014] use a hybrid neural network/genetic algorithm approach to solve a deterministic medium-term wind-hydro planning problem.

The difficulties experienced in forecasting wind in the near-term necessitates a stochastic approach to the optimization of hydropower production. Stochastic programming finds the optimal hydropower system operation by solving a large linear program that includes many different scenarios. Ideally, to fully capture the uncertainty in wind generation and its effect on hydropower system operations, a scenario tree with multiple branching points and multiple values at each branching point could be used. However, the addition of more branching points has the result of increasing computational time exponentially in stochastic programming. To reduce the computational time needed to converge to an optimal solution, previous research on hydropower operations with wind generation uncertainty employ Monte Carlo simulation to generate scenario trees that accurately characterize the uncertainty outside of the optimization

[*Abreu et al.*, 2012] and/or scenario reduction schemes [*Matevosyan et al.*, 2009]. Even so, a stochastic programming approach to mixed-integer linear programming models can result in intractable run times as a result of having to solve for many integer variables over many scenarios.

In contrast, the increase in computational time for stochastic dynamic programming (SDP) only increases linearly with each uncertain branch. SDP breaks down the large nonlinear and stochastic multi-day hydropower system operation problem into a series of smaller subproblems that are solved recursively. In this case, the optimal day-to-day operation of the hydropower system is solved in daily *stages* using a backwards recursion that maximizes both the present and future benefit. The future benefit of being at a particular storage and wind generation *state* is described by the future value function, solved for recursively by starting from an end state assumption and stepping back to the decision at the first time step. The different *states* of uncertain wind generation and resulting reservoir storage further generates scenarios that can be solved in parallel, saving computational time. SDP that employs the best forecast of future conditions can provide an optimal policy that maximizes the current and expected future benefits [*Stedinger et al.*, 1984; *Trezos and Yeh*, 1987]..

An issue that plagues the use of SDP in optimizing the operation of multi-reservoir systems is the so-called "curse of dimensionality", which means that the computational effort increases quickly as the dimension of the state variable increases. There exist many methods to counter this problem, including aggregation/disaggregation methods [*Turgeon*, 1980], approximate dynamic programming, i.e. using splines and response surfaces that require fewer

points to approximate the future value function over the entire state space [*Johnson et al.*, 1993; *Chen et al.*, 1999], and time-decomposition methods [*Becker and Yeh*, 1974]. In this chapter we employ an approximate dynamic programming model that uses radial basis functions [*Regis and Shoemaker*, 2007] to approximate the future value function over the many *states* of reservoir storage and wind generation levels, coupled with a modified formulation of Becker and Yeh's [1974] time decomposition technique.

4.1.2 Stochastic Dynamic Programming – Nonlinear Programming

This chapter describes a novel methodology for the optimization of the daily operation of a realistic multi-reservoir system in a deregulated electricity market setting when there is a stochastic wind forcing in the system. Section 4.2 describes the time-decomposition Stochastic Dynamic Programming – Nonlinear Programming (SDP-NLP) approach. The decision time frame is decomposed according to transactions in two wholesale electricity markets, the day-ahead and hour-ahead wholesale electricity markets. SDP simulates the sequential decision making process that occurs during the day-ahead planning process, while NLP is used to adapt and optimize for the best decisions on an hourly timescale. Our approach is from the perspective of a hydro utility that controls a hydropower system and is trying to operate under wind generation uncertainty, described in Section 4.3. The day-ahead wind forecast is modeled as a Markov process, while the forecast deviations are modeled as a conditional distribution to the forecast, described in Section 4.3.2. The economic environment of the hydro utility is described in Section 4.3.3. The day-ahead and hour-ahead markets are also used as ways to mitigate the financial burden on the hydro utility. Unlike the studies discussed previously, we consider the hydro utility to have market power, i.e. its participation in the wholesale electricity markets will

affect the energy prices. Moreover, the wind generation level can also have an effect on the wholesale price of energy. Section 4.4 describes the optimal policies for several marketing conditions and uncertainty scenarios, and shows how the day-ahead and hourly wholesale electricity markets can be used as a hedging tool for stochastic wind generation in the system.

4.2 System Optimization Problem Formulation

The Stochastic Dynamic Programming - Nonlinear Programming (SDP-NLP) framework described in this section decomposes the optimization horizon into two time scales.

On the daily timescale, Stochastic Dynamic Programming (SDP) is used to evaluate the consequences of a decision on commitments to the day-ahead wholesale electricity market, as described in detail in Section 4.2.1. The state variables in the SDP are the storages at reservoirs where release decisions are being made, and the wind forecast for that day. The wind forecasts can be modeled as stochastic in this paper. The decision variable for the SDP is what to commit to the day-ahead wholesale electricity market. The value of being at each particular state is calculated using a backwards recursion, starting from the end of the horizon (one week) and working backwards to the present, a common numerical method for solving the SDP problem.

On an hourly time scale, the benefit function corresponding to a particular SDP day-ahead commitment is calculated using a nonlinear programming (NLP) formulation. The NLP optimizes the hourly reservoir release decisions to maximize the value of hydropower generation, given the day-ahead commitment (the SDP decision variable) and wind power generation. The benefit function calculation is described in more detail in section 4.2.2.

4.2.1 Stochastic Dynamic Programming Formulation

Stochastic Dynamic Programming (SDP) is used for daily time steps, out to the specified time horizon. It models the day-to-day decisions made by the hydro utility. The objective at each stage t (i.e. at each day) is to maximize the present and future benefits by changing the daily power commitment to the day-ahead wholesale electricity market. The Bellman equation is shown in Equation (4.1). Appendix A.1 contains a short list of symbols used throughout this chapter.

$$V_t(S_t) = V_t(\vec{s}_t, \hat{w}_t) = \max_{\Gamma_t} \left\{ \mathop{\mathbb{E}}_{\Delta w_t} \left[B\left(\vec{s}_t, \vec{\Gamma}_t, \hat{w}_t, \Delta w_t\right) + \mathop{\mathbb{E}}_{\Delta w_t} \left(V_{t+1}(\vec{s}_{t+1}, \hat{w}_{t+1}) \right) \right] \right\} \tag{4.1}$$

Where

The two-dimensional state vector contains $S_t = (\vec{s}_t, \hat{w}_t)$, the vector of storages at each of the reservoirs where release decisions are being made $\vec{s}_t$ and the wind power production forecast $\hat{w}_t$.

$\vec{s}_t = [s_{1,t}, \dots, s_{i,t}, \dots]'$ is the vector of storages for each of the reservoirs *i* on day t,

$\hat{w}_t$ is the day-ahead wind power production forecast for day t,

Δw_t is the deviation from the wind power production forecast for day t, and the actual wind generation on day *t* is described in Equation (4.16).

B(·) is the benefit function (explained in more detail in Section4.2.2), and

Γ_t is the scalar average day ahead commitment over 24 hours for day t, the decision variable for SDP.

The decision variable for the SDP module is the day-ahead power commitment Γ_t. A positive value for Γ_t indicates that the power is to be sold in the day-ahead wholesale electricity market on day *t*, while a negative value for Γ_t indicates that the power is to be bought from the day-ahead wholesale electricity market. The power production by the hydropower system (and subsequently, the releases from each reservoir) is decided based on the power commitment, the occurrence of stochastic wind generation, customer loads, and contracted loads out of the system. Here, we assume that the inflows into the hydropower system are known.

The benefit function $B(\cdot)$, described in more detail in Section 4.2.2, calculates the within-day benefits received from participating in the day-ahead and hourly wholesale electricity markets. The allocation of the day-ahead energy commitment Γ_t to hourly values is done such that it maximizes the value of the day-ahead energy according to the different on-peak and off-peak hour prices. This is described in more detail in Section 4.2.2 and Section 4.3.3. The hourly decisions (releases and storage) in the reservoir system are calculated in $B(\cdot)$ using nonlinear programming to maximize the value of generation sold on the hour-ahead wholesale electricity market.

The SDP hydro storage state transition and the wind state transition come from two different modeling assumptions. The storage state $\vec{s}_t$ transition from day t to day $t+1$ is an output from $B(\cdot)$. The wind forecast for day t is modeled as a Markov chain. Note that the transition in storage depends on the independent deviation wind Δw_t while the transition in wind forecast $\widehat{w}_t$ does not. This is explained in more detail in Section 4.3.2.

Since our problem is made up of continuous state spaces and decision variables, an interpolation method is needed to interpolate between the future value functions $V_{t+1}(S_{t+1})$ at the discrete state variables. Johnson et al. [1993] shows that tensor-product cubic splines were more efficient than linear interpolants, and Chen et al. [1999] demonstrates that orthogonal arrays with multivariate adaptive regression splines were faster than tensor-product cubic splines with problems of six dimensions or more.

Our optimization framework uses a cubic radial basis function (RBF) to provide a continuous surface that interpolates between the discrete state values for which the future value function $V_{t+1}(S_{t+1})$ are known. Appendix A2 describes in detail how the RBF is fit. Unlike splines, radial basis functions are particularly suited to data sets that are large and are scattered in their domain, i.e. they do not form a uniform grid [*Buhmann*, 2003]. This allows us to be flexible particularly when decisions have to be made on a multi-dimensional scale. We are not aware that an RBF interpolant has ever been used for dynamic programming previously. RBF has been used in global optimization, as in Regis and Shoemaker [2007, 2009].

The SDP problem is solved using a backwards recursion with a terminal value function $V_{T+1}(\vec{s}_{T+1,k})$ at K discrete storage states$\{\vec{s}_{i,T+1,1}, \dots, \vec{s}_{i,T+1,K}\}$. Note that the value of water at the end of the horizon V_{T+1} are the same across the wind states $\widehat{w}_t$. The value of the terminal function is generally user-defined by the hydro utility. For the numerical examples considered here we used the function given below in Equation (4.2).

$$V_{T+1}(\vec{s}_{T+1,k}) = \begin{cases} a*(b-(\vec{s}_{T+1,k}-\vec{s}_{\text{target}})^{\delta}) & \text{if } \vec{s}_{T+1,k} \le \vec{s}_{\text{target}} \\ a*b & \text{otherwise} \end{cases} \quad k = 1,\ldots,K \tag{4.2}$$

Where

$\vec{s}_{T+1,k}$ is a vector of storages for a particular discrete storage state k,

δ, b, a are parameters of the equation, and

$\vec{s}_{target}$ is a vector of target storage level for each of the reservoirs, which is determined by the operations for the particular season that the reservoir is in.

The parameters δ, b, a are set such that the terminal value function $V_{T+1}(\vec{s}_{T+1,k})$ is a monotonically increasing concave nonlinear function with respect to the *k* discrete storage points. It has a higher marginal value at lower storage levels and levels out as it approaches the target storage. Thus, at lower storage levels the algorithm would like to conserve water, while at higher storage levels, the algorithm would be more willing to release more water, up to a certain point.

4.2.2 Benefit Function

The benefit function $B(\cdot)$ shown below in Equation (4.3) calculates the within-day benefits for a particular day t from participating in the day-ahead $F_t^{DA}(\Gamma_t)$ and hourly $F_t^{HA}(\vec{s}_t, \Gamma_t, \widehat{w}_t, \Delta w_t)$ wholesale electricity markets. The functions $F_t^{DA}(\cdot)$ and $F_h^{HA}(\cdot)$ in Equation (4.3) are concave, nonlinear functions for the value of the day-ahead and hour-ahead wholesale electricity market commitments respectively, discussed in further detail in Section 4.3.3.

$$B(\vec{s}_t, \Gamma_t, \hat{w}_t, \Delta w_t) = F_t^{DA}(\Gamma_t) + F_t^{HA}(\vec{s}_t, \Gamma_t, \hat{w}_t, \Delta w_t) \tag{4.3}$$

The inputs from the SDP are the average day-ahead commitment over 24 hours in day *t*, Γ_t (the scalar decision variable), and the state variable $S_t = (\vec{s}_t, \hat{w}_t)$. The random deviations from the forecast Δw_t are proportional to the forecasted wind for that day. More detail on the wind generation modeling is discussed in Section 4.3.2.

The first part of benefit function in Equation (4.3), $F_t^{DA}(\Gamma_t)$, describes the deterministic daily value of the SDP decision variable, Γ_t as a result of participating in the day-ahead wholesale electricity market. To reduce the number of decision variables for the SDP and greatly simplifie the optimization problem, the scalar variable Γ_t is optimally allocated to one fixed commitment during all on-peak hours Γ_t^{Hi} and another fixed commitment for all off-peak hours Γ_t^{Lo}.

To perform the optimal allocation, we adopt a common utility assumption that the day-ahead commitment is traded in 2 blocks: a 16-hour on-peak period, and an 8-hour off-peak period, . The equality in Equation (4.4) shows the relationship between the average daily commitment Γ_t and its "hourly" components Γ_t^{Hi} and Γ_t^{Lo}.

$$\begin{aligned} 24*\Gamma_t &= 8*\Gamma_t^{Lo} + 16*\Gamma_t^{Hi} \\ \Rightarrow \Gamma_t &= \frac{1}{3}*\Gamma_t^{Lo} + \frac{2}{3}*\Gamma_t^{Hi} \end{aligned} \tag{4.4}$$

The resulting daily value for the allocation of Γ_t(in MW) to its "hourly" components Γ_t^{Hi} and Γ_t^{Lo} (also in MW) is shown in Equation(4.5).

$$F_t^{DA}(\Gamma_t) = 8*F_t^{DA,\mathrm{Lo}}(\Gamma_t^{Lo}) + 16*F_t^{DA,\mathrm{Hi}}(\Gamma_t^{Hi}) \tag{4.5}$$

The optimal allocation to Γ_t^{Hi} and Γ_t^{Lo} that maximizes Equation (4.5) occurs when the derivative of Equation (4.5) is equal to zero (Equation (4.6)).

$$\frac{dF_t^{DA}}{d\Gamma_t} = 8 * \frac{dF_t^{DA}(\Gamma_t^{Lo})}{d\Gamma_t^{Lo}} \cdot \frac{\partial \Gamma_t^{Lo}}{\partial \Gamma_t} + 16 * \frac{dF_t^{DA}(\Gamma_t^{Hi})}{d\Gamma_t^{Hi}} \cdot \frac{\partial \Gamma_t^{Hi}}{\partial \Gamma_t} = 0 \tag{4.6}$$

Rearranging and solving for the partial derivatives in Equation (4.6) using Equation (4.4) results in Equation (4.7).

$$\frac{dF_t^{DA,Hi}}{d\Gamma_t^{Hi}} + \frac{dF_t^{DA,\mathrm{Lo}}}{d\Gamma_t^{Lo}} = 0 \tag{4.7}$$

Thus, solving equations (4.4) and (4.7) simultaneously will result in an optimal allocation of Γ_t to the commitment in the off-peak hours Γ_t^{Lo} and the commitment in the on-peak hours Γ_t^{Hi}.

The second part of benefit function in Equation(4.3), $F_t^H(\vec{s}_t, \Gamma_t, \widehat{w}_t, \Delta \mathrm{w_t})$, describes the benefit from participating on the hourly wholesale electricity market, shown in Equation (4.8). The nonlinear programming (NLP) environment optimizes the hourly releases and storages as determined by the actual wind generation (a function of the forecasted wind generation and its deviation, as explained in Section 4.3.2) and commitment to the day-ahead wholesale electricity market on an hourly basis. The deterministic non-linear program is solved for each deviation from the forecast, Δw_t given the day-ahead commitment decision from the SDP, Γ_t and the forecasted wind scenario, $\widehat{w}_t$.

$$F_t^{HA}(\vec{\mathrm{s}}_t, \Gamma_t, \hat{w}_t, \Delta w_t) = \max_{r_{\mathrm{i,t,}PH}^h, r_{\mathrm{i,t,spill}}^h, s_{i,t}^h} \left\{ \sum_h F_h^{HA} \left(\sum_i G_i^h(r_{\mathrm{i,t}PH}^h, \mathrm{s}_{i,t}^h) - L_t^h(\Gamma_t \, \mathrm{U}_t^h, \hat{w}_t, \Delta w_t) \right) \right\} \tag{4.8}$$

Where

$r_{i,t,PH}^h$ is the flow through the powerhouse at reservoir i at hour h and day t,

$r_{i,t,spill}^{h}$ is the spill out of reservoir i at hour h and day t,

$s_{i,t}^{h}$ is the storage level at reservoir i at hour h and day t,

$F_h^{HA}(\cdot)$ is the value of the hour-ahead commitment, described in Section 4.3.2,

$G_i^h(\cdot)$ is a concave generation function with respect to powerhouse releases $r_{h,PH}^{i}$ and storage s_h^i at reservoir i and hour h, described in Chapter 2,

$L_t^h(\cdot)$ is the load at hour h, which is explained in more detail in Section 4.3.3.2, and

U_t^h is the hydro utility's customer load for hour h in day t, an input into the model.

The optimization is subject to the following constraints:

1. Conservation of mass

$$\vec{s}_t^{\,h+1} = \vec{s}_t^{\,h} + \sum_{\tau=1}^{n_{lags}} C_\tau \vec{R}_t^{\,h-\tau} + \vec{Q}_t^{\,h} \tag{4.9}$$

Where

$\vec{s}_t^{\,h} = \left[s_{1,t}^h, \ldots, s_{n,t}^h\right]'$ is the vector of storages at reservoirs 1,..,n at hour h,

C_τ is the routing coefficient matrix described in Section 4.3.1,

τ is the time lag,

n_{lags} is the maximum number of discrete time steps it takes in the n reservoir system for the all the volume of water released from an upstream reservoir during hour h to arrive at the downstream reservoir,

$\vec{R}_t^{\,h} = \left[r_{1,t,PH}^h + r_{1,t,spill}^h, \ldots, r_{n,t,PH}^h + r_{n,t,spill}^h\right]'$ is the vector of total releases at reservoir $1, \ldots, n$ at hour h, and

$\vec{Q}_t^{\,h} = \left[Q_{1,t}^h, \ldots, Q_{n,t}^h\right]'$ is the vector of natural inflows into the reservoir at hour h

2. Reservoir storage should be within bounds at all times

$$s_{\mathrm{i,min}} \le s_{i,t}^{h} \le s_{\mathrm{i,max}} \qquad \forall i = 1,...,n; h = 1,..,24 \tag{4.10}$$

3. The storages at the end of the 24-hour period should at least be at the target storage

$$s_{i,t}^{24} \ge s_{\mathrm{i,target}}^{24} \qquad \forall i = 1,..,n \tag{4.11}$$

4. The flows through the powerhouse are bounded by minimum powerhouse flow requirements and powerhouse flow capacity

$$r_{i,PH\,\mathrm{min}} \le r_{\mathrm{i,t},PH}^{h} \le r_{i,PH\,\mathrm{max}}^{h} \qquad \forall i = 1,..,n; \mathrm{h} = 1,..,24 \tag{4.12}$$

5. Flows through the spillway are bounded by the minimum and maximum spillway flows

$$r_{i,spill\,\mathrm{min}} \le r_{\mathrm{i,t},spill}^{h} \le r_{i,spill\,\mathrm{max}} \qquad \forall i = 1,..,n; h = 1,..,24 \tag{4.13}$$

After calculating the day-ahead and hourly benefits for a particular SDP decision value Γ_t, the benefit function then returns to the SDP algorithm the value of the benefit function in Equation (4.1) and the resulting storage states at the reservoirs in the next time step, $\vec{s}_{t+1}(\Gamma_t, \widehat{w}_t, \Delta w_t)$.

4.3 Application to a Hypothetical System

We model the operations of a hypothetical hydro utility that owns a 2-reservoir system with characteristics that are similar to the Grand Coulee (GCL) and Chief Joseph (CHJ) dams in the Federal Columbia River Power System in Washington State, the largest and third largest reservoirs in the United States. The schematic of the system is shown in Figure 4-1. Generation characteristics for these two projects were based on publicly available information from the

Bureau of Reclamation for GCL for the Upper Reservoir and the Army Corps of Engineers for CHJ for the Lower Reservoir [*U.S. Army Corps of Engineers*, n.d.]. The combined cascaded system has a generation capacity of over 9300 MW, with about three quarters of the capacity coming from the Upper Reservoir. The travel time between the two reservoirs is 1.5 hours. It is assumed that only the hydro system is used to mitigate the uncertainty from forecasted wind power generation. The hydrologic modeling for this system is explained in more detail in Section 4.3.1.

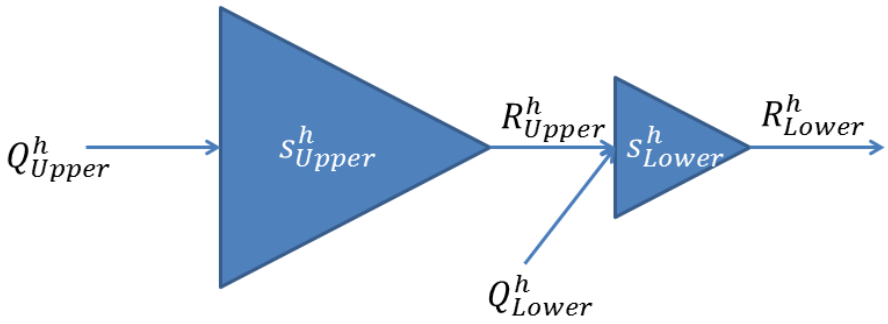

Figure 4- 1: Schematic of the modeled hydropower system

The wind generation capacity is 4782MW [*Bonneville Power Administration*, 2014], or about 50% of the generation capacity of the hydro system described above. Under the assumption that this hydropower system serves as the only balance for the wind generation, the wind generation has a high potential to be disruptive to the operation of the hydro system, particularly when the forecasted wind generation is large. The actual wind power generation and wind power generation forecast was based on publically available data provided by the Bonneville Power Administration [*Bonneville Power Administration*, n.d.]. The details of the wind modeling is explained in more detail in Section 4.3.2.

We model a *Marketing Wind* case where the hydro utility is able to sell the wind power generation on the wholesale electricity market and a *Wind Following* case where the hydro utility is responsible only for balancing the deviations from the wind forecast. The system is modeled as a price maker on the wholesale electricity market. The transactions occur on the day-ahead and hourly markets. The details of the economic modeling are explained in Section 4.3.3.

4.3.1 Hydrologic Modeling

The reservoir system dynamics are based on the conservation of mass. In order to ensure that water that flows through the system is neither gained nor lost in the routing process, the mass balance constraint must be satisfied at all reservoirs for all time steps. The flow routing in the nonlinear programming model described in Section 4.2.2 considers the travel times between the two reservoirs through the use of the lagged routing coefficient matrix C_τ n Equation (4.9).

If the outflows from one reservoir are constant over the whole time step with no travel time considered between the reservoirs, the resulting system dynamics equation and routing coefficient matrix C for the cascaded two-reservoir system is Equation (4.14).

$$\vec{S}_t^{\,h+1} = \vec{S}_t^{\,h} + C\vec{R}_t^{\,h} + \vec{Q}_t^{\,h} \qquad (4.14)$$

$$\text{where } C = \begin{bmatrix} -1 & 0 \\ 1 & -1 \end{bmatrix}$$

In the 2 x 2 matrix C in Equation (4.14), the columns denote the origin of the flows, while the row denote the destination of the flows. The first row or column corresponds to the Upper

Reservoir and the second row or column corresponds to the Lower Reservoir. The flow between the Upper Reservoir and the Lower Reservoir is represented as a 1 in the second row of the first column, that is, on the off-diagonal element. The outflows from each reservoir at time *h* are represented as -1 down the main diagonal of the matrix. In general this matrix as it is defined will be a lower triangular matrix.

When the travel times between projects are considered, Labadie [2004] suggests replacing the off diagonal elements with fractions corresponding to the lag and attenuation of flow from one reservoir to another. The lag τ is the number time steps between the current time step being considered and a previous time step, e.g if t is the current time step, then lag 1 or $\tau = 1$ is time step $t - 1$. The resulting system dynamics equation for a travel time of 1.5 hours between the Upper and Lower Reservoir is shown Equation (4.15) when the time step is one hour.

$$\vec{s}_t^{\,h+1} = \vec{s}_t^{\,h} + \sum_{\tau=0}^{2} C_\tau \vec{R}_t^{\,h-\tau} + \vec{Q}_t^{\,h}$$

$$\text{where } C_0 = \begin{bmatrix} -1 & 0 \\ 0 & -1 \end{bmatrix} \tag{4.15}$$

$$C_1 = \begin{bmatrix} 0 & 0 \\ 0.5 & 0 \end{bmatrix}$$

$$C_2 = \begin{bmatrix} 0 & 0 \\ 0.5 & 0 \end{bmatrix}$$

In the C_τ matrices in Equation (4.15), the off diagonal elements are no longer 0 or 1, but are numbers between 0 and 1 that describes the proportion of flows from the upstream project that

arrive at the downstream project at time lag τ. Note also that the elements on the main diagonal of matrix C_1 and C_2 are 0, since the lag 1 and 2 outflows are no longer considered in the routing at time h.

Chapter 2 discusses the general equation to obtain the values of the off-diagonal elements. For a travel time between reservoirs of 1.5 hours, the zero-lag coefficient matrix C_0 in Equation (4.15) states that in hour h, no water from the Upper Reservoir released in hour h has arrived at the Lower Reservoir, since it takes at least 1.5 hours for the first releases from the Upper Reservoir to arrive at the Lower Reservoir's forebay. However, in the same hour h, 50% of the volume of water from hour $h-1$, and 50% of the flow from Upper Reservoir in hour $h-2$ has arrived at The Lower Reservoir in hour h.

4.3.2 Wind Generation Modeling

The hourly wind power production w_t^h is calculated given the day-ahead wind power production forecast $\widehat{w}_t$ and daily deviation from the forecast Δw_t, shown in Equation (4.16)

$$w_t^h = \hat{w}_t * \psi^h * (1 + \Delta w_t) \tag{4.16}$$

where ψ^h is the fraction of total daily wind that is expected to occur in hour h, or the shape factor for hour h. The candidate values of wind generation forecast and the daily deviation from the forecast are obtained from historical generation data in the Bonneville Power Administration's balancing area.

Discrete wind states and the wind state transition probabilities are calculated from publically available historical aggregated wind generation data from the Bonneville Power Administration [*Bonneville Power Administration*, n.d.]. The historical daily average wind generation forecast is sorted into one of *W* intervals. The discrete wind state $\widehat{w}_t$ is obtained by taking the center of each of those intervals. To incorporate correlation of wind from one day to the next, the daily wind forecast $\widehat{w}_t$ is modeled as a Markov process. Given that $\widehat{w}_t$ is in state j, it transitions to another state k in the next time period with some probability $\mathbb{P}_{jk} = \Pr(\widehat{w}_{t+1} = k|\widehat{w}_t = j)$. The Markov transition matrix is $\mathbb{P} = \{\mathbb{P}_{jk}\}$.

The set of hourly shape factors $\{\psi^h|h = 1, \dots 24\}$ is obtained from historical hourly wind generation data by calculating the wind generation for each hour as a percentage of the total daily wind power generation, then taking the average percentage over each hour. An example wind generation profile showing the diurnal pattern of wind generation is shown in Figure 4-2.

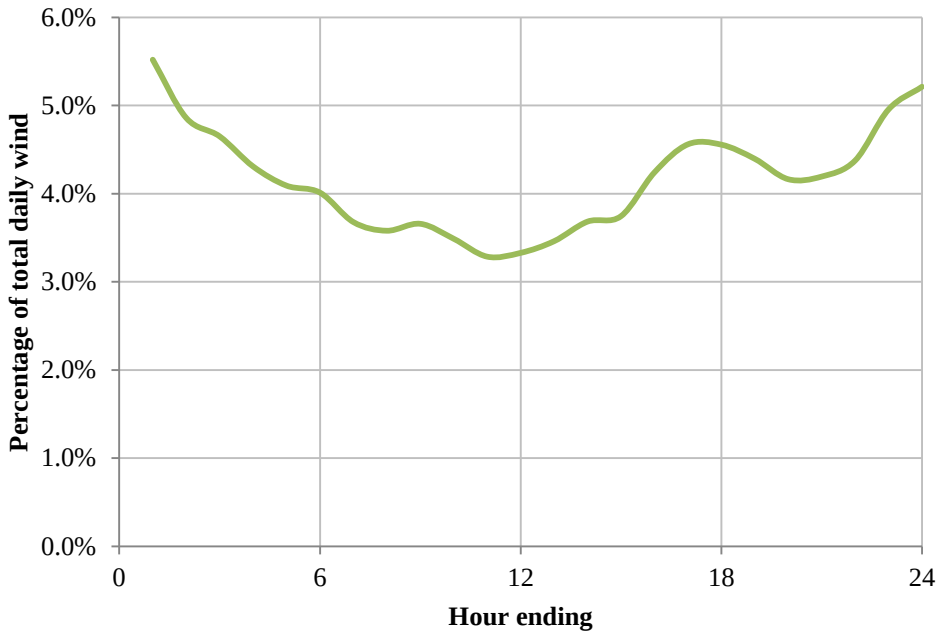

Figure 4- 2: The average hourly wind generation profile for the month of December, obtained using data provided by the BPA from the period 2008-2012. The vertical axis gives the fraction of total daily wind production for each hour in a day.

The distribution of the deviations from forecast $\Delta w_t = \frac{w_t - \widehat{w}_t}{\widehat{w}_t}$ in Equation (4.16) is estimated from the historical hourly day-ahead forecasted and actual wind power production. We assume no seasonal effects on the deviation . The deviations Δw_t are proportional to the wind power production forecast $\widehat{w}_t$; thus, the higher the forecasted wind, the more variable the wind is.

4.3.3 Economic Modelling

The Stochastic Dynamic Programming/ Nonlinear programming (SDP-NLP) formulation in Equations (4.1) and (4.3) models transactions made by the hydro utility in the wholesale day-ahead and real-time (hourly) electricity markets. The planning horizon is out to 7 days. By

modeling both day-ahead and hourly electricity markets, the hedging activity between the two markets can be modeled.

In the day-ahead wholesale electricity market, energy is committed on a day-ahead basis and paid the day-ahead forward price for energy. As mentioned earlier, the SDP is used to determine the optimal commitment to the day-ahead market. There are two possible drivers of the day-ahead energy price: (1) the commitment to the day-ahead electricity market Γ_t (since we model a hydro utility with market power), and (2) the level of wind generation in the system. These effects are described in more detail in Section 4.3.3.1.

The hydro utility is then committed to meeting this day-ahead energy during the actual day addition to meeting the customer load (e.g. residential, commercial, and industrial energy usage). Depending on the contract structure between the wind generator and the hydro utility, wind power generation may or may not help to meet this customer load and deviation. The within-day deviations from the forecasted wind power production can either be made up by adjusting the generation from the hydro system, or from buying or selling on the hour-ahead wholesale electricity market. This dynamic creates a tradeoff between the value of water and the value obtained by buying or selling on the hour-ahead market. As mentioned earlier, the NLP formulation optimizes this dynamic and is described in more detail in Section 4.3.3.2.

4.3.3.1 Day-ahead economic modeling

The first part of benefit function $F_t^{DA}(\cdot)$ in Equation (4.3) in Section 4.2.2 describes the deterministic value of the SDP decision variable, Γ_t as a result of participating in the day-ahead

wholesale electricity market. Recall that we assume the energy is assumed to be traded in two blocks: an 8-hour off-peak block and a 16-hour on-peak block; to maintain the generality of the equations however, the functions in this section could change hourly, and are denoted with a superscript *h*.

We model two drivers of the day-ahead energy price –the actions of the utility with a large hydro generation system, and wind. Index price data for the Mid-C trading hub and expert assumptions on the market depth were used to generate the price functions used in this section.

We model a hydro utility with some market power, i.e. it has the ability to affect the wholesale price of generation. This is true if the hydro utility has a flexible hydro generation fleet that has a comparable generation capacity to dams like Grand Coulee and Chief Joseph, which has a combined generation capacity of more than 9GW. The effect of the hydro utility's actions on the day-ahead price is modeled as a linear function that decreases as the hydro utility attempts to sell more on the day-ahead wholesale electricity market. The linearly decreasing function can be interpreted as the decreasing cost of generation of the system as a result of the hydro utility increasing its generation, analogous to a demand function. An example of the price function is shown in Figure 4-3.

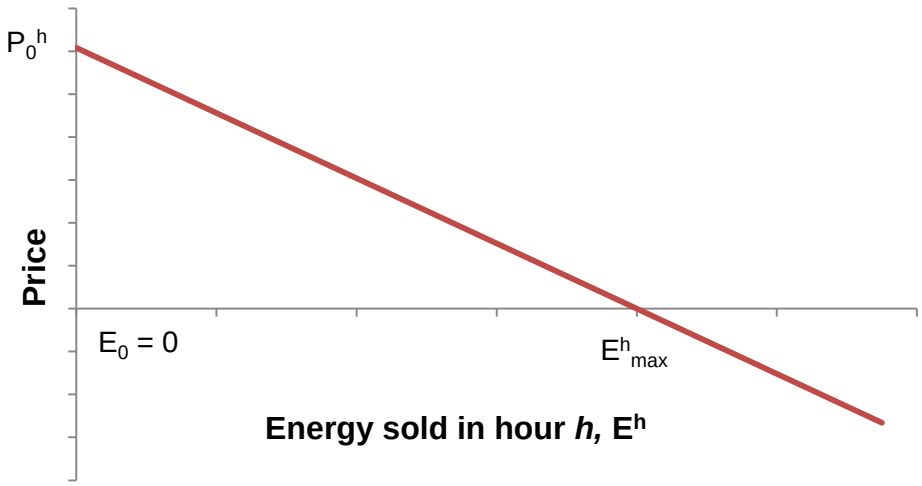

Figure 4- 3: Example of a price function $D^h(E^h)$ for a fixed time period t

The linear price function in Figure 4-3 has the functional form in Equation (4.17) and.

$$D^h(E^h) = \beta + mE^h = -P_0 \frac{E^h{}_{\max}}{E_0 - E^h{}_{\max}} + \frac{P_0}{E_0 - E^h_{\max}} E^h \tag{4.17}$$

Where

E^h is the energy commitment in hour h

P_0 is the wholesale price of energy at the hydro utility's wholesale electricity market commitment of E_0 (in most cases, E_0 is assumed to be 0, but could be nonzero depending on the data available)

E^h_{max} is the market saturation point where the wholesale price of electricity goes to zero

Beyond the market saturation point E^h_{max}, there may be negative prices. A negative price in a wholesale electricity market indicates that there is a supply inflexibility [*U.S. Energy Information Administration*, 2012] and the energy producer must pay other market participants to

accept the energy, or curtail renewable generation. Clearly, the hydro utility will try to avoid selling above E^h_{max}.

The revenue received by the hydro utility from selling that amount of power on the wholesale electricity market for each time period is shown in Equation (4.18).

$$F^h(E^h) = E^h * D^h(E^h) = \frac{P_0}{E_0 - E^h_{\max}}(E^h)^2 - P_0 \frac{E^h_{\max}}{E_0 - E^h_{\max}} E^h \tag{4.18}$$

In this case, the revenue function is a quadratic function, with a peak that occurs at the market saturation point E^h_{max}.

When modeling wind as a driver of the day-ahead energy price, we model higher day-ahead prices on days in which forecasted wind power generation is low, and conversely lower day-ahead prices on days in which the forecasted wind power generation is high. The assumption here is that an abundance of free energy from wind drives down the overall cost of generation in the system. The day-ahead price when the utility is not buying or selling, $P^h_{0,DA}(\hat{w}_t)$ is then a function of $\hat{w}_t$, the wind power production forecast for that day, shown in Equation (4.19). The superscript *h* indicates that the prices could be different in the on-peak hours or in the off-peak hours.

$$P^h_{0,DA}(\hat{w}^h_t) = (1 + \varepsilon(\hat{w}^h_t)) * P^h_{0,DA}\left(E^h_0, \bar{w}^h\right) \tag{4.19}$$

where

$\hat{w}^h_t = \hat{w}_t * \psi^h$ is the day-ahead forecast of wind power generation for hour h,

ψ^h is the hourly wind generation shape factor described in Section 4.3.2

$\varepsilon(\hat{w}_t^h)$ is wind effect on the day-ahead price and can be positive or negative, and

$P_{0,DA}^h(E_0^h, \bar{w}^h)$ is the day-ahead price at E_0^h at the historical average daily wind power generation $\bar{w}^h$ for hour h .

We assume that the wind effect function $\varepsilon(\hat{w}_t^h)$ is a linear function that is zero when the wind generation is at the average generation, i.e. $\hat{w}_t^h = \bar{w}^h$. The wind effect function is also tied to the wind generation capacity w_{max} as a proportion of the total hydro system capacity, $\sum_i G_{i,max}$. It is at its maximum when there is no wind, and at its minimum when the wind generation is at capacity. The minimum and maximum wind effect values, ε_{min} and ε_{max}, are calculated in Equations (4.20) and (4.21).

$$\varepsilon_{\min} = \omega \frac{w_{\max} - \bar{w}^h}{\sum_i G_{\mathrm{i,max}}} \tag{4.20}$$

$$\varepsilon_{\max} = \omega \frac{\bar{w}^h}{\sum_i G_{i,\max}} \tag{4.21}$$

Where ω is a user-defined factor that intensifies the wind effect. The wind effect $\varepsilon(\hat{w}_t^h)$ is calculated using a linear interpolation, shown in Equation(4.22).

$$\varepsilon(\hat{w}_t^h) = \varepsilon_{\min} + \frac{w_{\max} - \hat{w}_t^h}{w_{\max}} (\varepsilon_{\max} - \varepsilon_{\min}) \tag{4.22}$$

Figure 4-4 shows the modeled effect of the day-ahead wind forecast on the day-ahead on-peak and off-peak prices for a particular day in December. These prices would be the same across the 8-hour off peak block and the 16-hour on-peak blocks respectively.

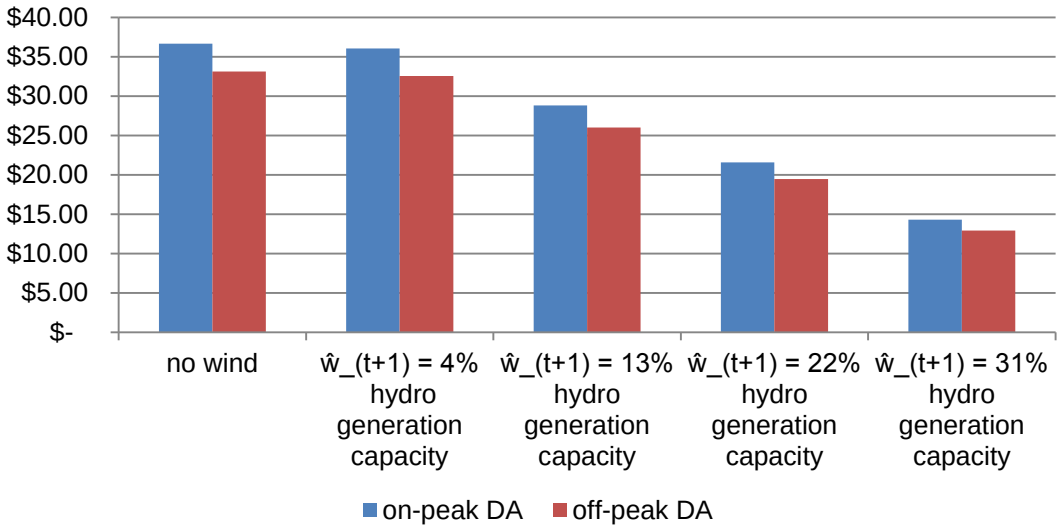

Figure 4- 4: The effect of the day-ahead wind forecast on day-ahead prices during on and off peak periods as calculated by Equation (4.22)

4.3.3.2 Hour-ahead economic modeling

The second part of the benefit function $F_h^{HA}(\cdot)$ in Equation (4.3) is the stochastic benefit from participating in the hour-ahead wholesale electricity market. As mentioned in Section 4.2.2, once the day-ahead commitment Γ_t is made, it becomes part of the load served by the hydro utility for each hour of the day $\left[\Gamma_t^{Lo}, \Gamma_t^{Hi}\right]$ designated according to Equations (4.4) and (4.7). The optimal releases from and the storages at each of the reservoirs that maximize the Equation (4.8) are calculated using the nonlinear programming formulation described in Section 4.2.2 and the nonlinear programming algorithm optimizes the hourly releases and storages for the hydro system for a particular day t.

The hydro utility also has to serve its customers in the area a service area load (MWh) of $\{U_t^h \big| h = 1, \ldots 24\}$. This customer load U_t^h is assumed to be known for the optimization horizon. An example of a customer load profile is shown in Figure 4- 5. Note that the peak customer load

near hour-ending 18 tends to coincide with the period when wind power production is starting to ramp up, as shown in Figure 4-2.

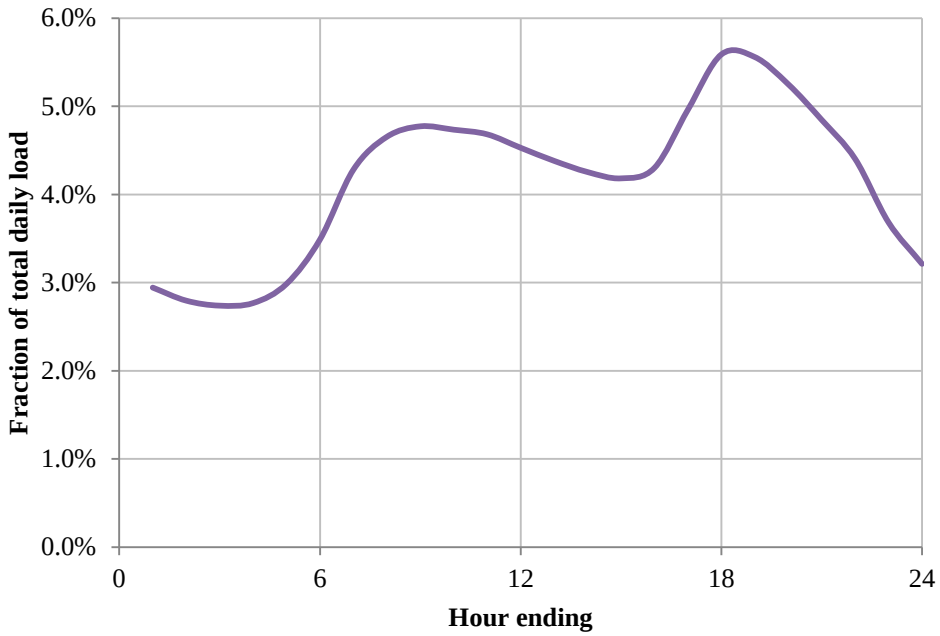

Figure 4- 5: The average hourly customer load profile for the month of December, obtained using data provided by the BPA from the period 2008-2012. The vertical axis gives the fraction of total daily customer load for each hour in a day.

We model two different contract structures between the wind generator and the hydro utility. In the *Marketing Wind* case, the hydro utility also owns the wind generation, and can market the wind energy. Thus, the wind serves as part of the generation mix that will meet the day-ahead commitment and customer load. The resulting load L_t^h (in MWh) to be served in each hour *h* on day *t* for this case is described in Equation (4.23).

Marketing Wind: $$L_t^h(\Gamma_t, U_t^h, \hat{w}_t, \Delta w_t) = \mathrm{U}_t^h + \Gamma_t^h(\Gamma_t) - w_t^h(\hat{w}_t, \Delta w_t) \quad (4.23)$$

Where $\Gamma_t^h(\Gamma_t)$ is allocated using the relationship in Equation (4.7), and $w_t^h(\widehat{w}_t, \Delta w_t)$ the wind energy produced and utilized in hour h, calculated using Equation (4.16). This is a typical case for an organization that owns both the hydropower and wind generation facilities.

In the *Wind Following* case, the hydro utility does not own the wind generation. Instead, the hydro utility provides load following services for the wind generator that has contracted to deliver energy outside of the hydro utility's service area. In this case, the contract states that the hydro utility shall deliver the power that would be generated by the day-ahead forecasted wind, $\widehat{w}_t$. The payments to or payments by the wind generator for deviations from the forecasted wind Δw_t is settled outside of the wholesale electricity market and thus is not considered in this formulation. However, the algorithm does provide an idea of what the compensation to the hydro utility should be for providing the load following services. This *Wind Following* case is based on the current situation for the Bonneville Power Administration. The resulting load L_t^h (in MWh) to be served in each hour *h* on day *t* for this case is described in Equation (4.24).

$$\textit{Wind Following: } L_t^h(\Gamma_t, U_t^h, \hat{w}_t, \Delta w_t) = U_h^t + \Gamma_t^h(\Gamma_t) + \hat{w}_t^h(\hat{w}_t) - w_t^h(\hat{w}_t, \Delta w_t) \tag{4.24}$$

Where $\widehat{w}_t^h(\widehat{w}_t) = \widehat{w}_t * \psi^h$ is the forecasted wind generation in MWh for hour h and day t.

The hydro utility can also take advantage of the hourly wholesale electricity market to help serve its load. The hourly generation $G_i^h(r_{i,PH}^h, s_i^h)$ is the amount of power produced at reservoir i as a function of the powerhouse releases $r_{i,PH}^h$ and storage s_i^h. The hourly load L_t^h is a function of the day-ahead commitment Γ_t, customer load U_t^h, day-ahead wind forecast $\widehat{w}_t$, and deviation from the day-ahead wind forecast Δw_t. Then the amount of energy sold or bought on

the hourly wholesale electricity market is the difference between the generation and load, E_t^h as defined in Equation (4.25).

$$E_t^h = \left(\sum_i G_i^h (r_{i,PH}^h, s_i^h) - L_t^h (\Gamma_t U_t^h, \hat{w}_t, \Delta w_t) \right) \tag{4.25}$$

Here, a positive value of E_t^h indicates that power is sold on the hourly wholesale electricity market while a negative value of E_t^h indicates that power is bought on the hourly wholesale electricity market. We again model the hydro utility as a price maker on the hourly market. Thus, the value of the hydropower generation on the hour-ahead markets is calculated using Equation (4.26) assuming the price is $P_{0,HA}^h$ at $E = E_0^h$. Unlike the day-ahead prices $P_{DA}^{h,}$ there is no wind-effect modeled for hour-ahead prices P_{HA}^h, which are used in Equation (4.26).

$$F_h^{HA}\left(E^h\right) = -\frac{P_{0,HA}^h}{E_{\max}^h} * (E^h)^2 + P_{0,HA}^h E^h \tag{4.26}$$

4.4 Optimal Policies for Various Scenarios Modeling Uncertainty and Treatment of Wind

We show how the optimal day-ahead power commitment in the first stage, Γ_1, can change given different scenarios. First, we establish a baseline scenario described in Section4.4.1, *Scenario 0*, to which each *Scenario (x, y, z)* are to be compared against. Each *Scenario (x, y, z)* is defined by three inputs: (1) how uncertainty is modeled (x), (2) marketing cases (y), i.e. Marketing Wind (Equation (4.23)) or Wind Following (Equation (4.24)), and (3) influence of wind on the day-ahead base price (z).

Table 4-1: List of symbols describing a particular Scenario (x, y, z). The Scenarios(x, y, z) are compared to a baseline scenario with no wind, called Scenario 0. These symbols are used in text, tables, and figures to follow.

Input type	**Description**	**Symbol for Specific Case**
(x) Uncertainty	Deterministic day-ahead and hour-ahead forecasts	DD
(x) Uncertainty	Deterministic day-ahead and Stochastic hour-ahead forecasts	DS
(x) Uncertainty	Stochastic day-ahead forecast with within-day uncertainty	SS
(y) Marketing case	Marketing Wind	M
(y) Marketing case	Wind Following	F
(z) Wind Effect on day-ahead price	No effect	N
(z) Wind Effect on day-ahead price	As modeled in Equation (4.22)	W

The hydro system in Figure 4-1 is run for a 7-day period using historical storage, inflow, and customer load data for December 2011. The storage of the Lower Reservoir in Figure 4-1 is fixed for the entire optimization horizon, so the only reservoir state variable to keep track of is the storage at the larger Upper Reservoir. The reservoir storage level at the Upper Reservoir (GCL) is discretized into four levels between 48% and 49.2% of its capacity, which is the typical starting storage of the reservoir in refill operations for the system that this case study is based on. This range represents a volume of 2.8 billion cubic feet of water, which could generate up to 173 GWh per day. Recall that the radial basis function approximation is being implemented to create a response surface so that the solution can be accurate with relatively few levels per state variable.

The first stage optimal policy is discussed for each *Scenario (x, y, z)* in the following Sections. We show the first stage optimal policy because this is the action that would be immediately performed by the hydro utility after running the optimization. By considering

different *Scenario(x, y, z)*, various components of the modeling described in Section 4.3 can be demonstrated.

Section 4.4.2 describes deterministic wind *Scenarios (DD, y, N)* with no wind effect on price where *y* can be Marketing Wind or Wind Following (*M* or *F*)as described in Table 4-1. In this section, we also show detailed operations of the hydropower system as a result of the benefit function calculation described in Section 4.2.2. The benefit function calculation is run several times for the DS and SS cases in which there are various wind generation outcomes, and so detailed operations are not shown in the later sections.

Section 4.4.3 describes *Scenarios (DS, y, N)* that have deterministic day-ahead wind forecast with within-Day deviations from the day-ahead wind forecast, where *y* can be *M* or *F* as described in Table 4-1. Section 4.4.4 describes stochastic day-ahead wind forecast with within-day deviations from the day-ahead forecast, *Scenarios (SS, y, N)* where *y* can be *M* or *F* as described in Table 4-1.

Sections 4.4.2, 4.4.3, and 4.4.4 assume the wind amplitude (past and future forecasts) have no impact on price. Finally, Section 4.4.5 summarizes the results where the wind effect on day-ahead price are considered, *Scenarios (x, y, W)* where *x* and *y* vary according to Table 4-1, and compares them against results found in Sections 4.4.1 through 4.4.4.

4.4.1 Scenario 0: No Wind

To set a baseline for comparison, a deterministic dynamic programming problem is solved without wind generation (*Scenario 0*). Under these assumptions, the Bellman equation in Equation (4.1) simplifies to Equation (4.27).

$$\textit{Scenario 0 Bellman eqn: } V_t(s_t) = \max_{\Gamma_t} \left\{ B(s_t, \Gamma_t) + V_{t+1}(s_{t+1}(\Gamma_t)) \right\} \tag{4.27}$$

Additionally, with no wind generation the load in the nonlinear programming formulation in Equation (4.3) simplifies to Equation (4.28)

$$\textit{Scenario 0 Load: } L_t^h(\Gamma_t, U_t) = U_t^h + \Gamma_t^h(\Gamma_t) \tag{4.28}$$

Figure 4-6 shows the resulting optimal day-ahead power commitment over the 7-day horizon $\{\Gamma_1, .., \Gamma_t, ... \Gamma_7\}$ for *Scenario 0* for lowest (48% full) and highest (49.2% full) storage levels modeled. The policy shows that when there is more water available in the reservoir, the day-ahead commitment is always higher. This indicates that the system is not constrained in terms of operation and will always try to sell more power if possible.

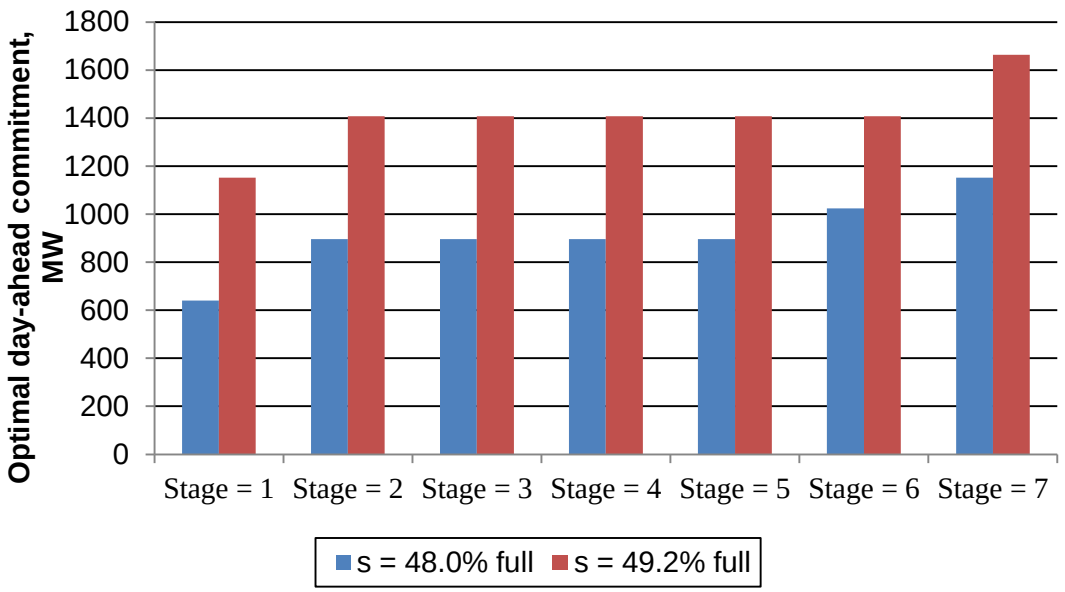

Figure 4- 6: The Scenario 0 optimal day-ahead commitment policy for each of the 7-days in the optimization horizon without wind. A positive day-ahead commitment means that power is sold on the day-ahead wholesale electricity market while a negative day-ahead commitment that power is bought on the day-ahead market.

4.4.2 Scenarios (DD, y, N): Deterministic Wind

Next, we consider the *Scenario (DD, y, N)* where the wind power generation w_t^h is assumed to be known for every hour $h = 1, \dots, 24$ over the entire horizon, $t = 1, . . ,7$. Recall y can be M for the marketing wind or F for the wind following defined in Table 4-1. The discrete wind levels are also discretized into four different levels, based on historical wind power generation for the month of December, ranging from 4% to 31% of the hydropower generation capacity. No wind effect on the day-ahead price is modeled.

Under the deterministic wind assumption, the Bellman equation in Equation (4.1) simplifies to Equation (4.29).

Scenario (DD, y, z) Bellman equation:

$$V_t(s_t, w_t) = \max_{\Gamma_t}\{B(s_t, \Gamma_t, w_t) + V_{t+1}(s_{t+1}, w_t)\} \quad (4.29)$$

Here, the transition between w_t to w_{t+1} is deterministic. The known hourly wind generation w_t^h simplifies the load in the *Scenario (DD, M, z)* (Marketing Wind) and *Scenario (DD, F, z)* (Wind Following) cases as described by Equations (4.23) and (4.24), to Equations (4.30) and (4.31).

Scenario (DD, M, z) load: $$L_t^h(\Gamma_t, U_h^t, w_t) = \mathrm{U}_t^h + \Gamma_t^h(\Gamma_t) - w_t^h \quad (4.30)$$

Scenario (DD, F, z) load: $$L_t^h(\Gamma_t, U_h^t) = \mathrm{U}_t^h + \Gamma_t^h(\Gamma_t) \quad (4.31)$$

The deterministic wind generation for the 7-day horizon is the "expected" wind generation of a Markov chain representation of the wind generation forecast (described in more detail in Section 4.4.4) starting from a particular discrete wind state $\widehat{w}_t$. An example of the deterministic wind generation for each day starting from the lowest and highest wind states $\widehat{w}_t$ is shown in Figure 4-7. The figure shows that the expected wind generation of both paths converges over time to the average of 10% of the hydro generation by day 5.

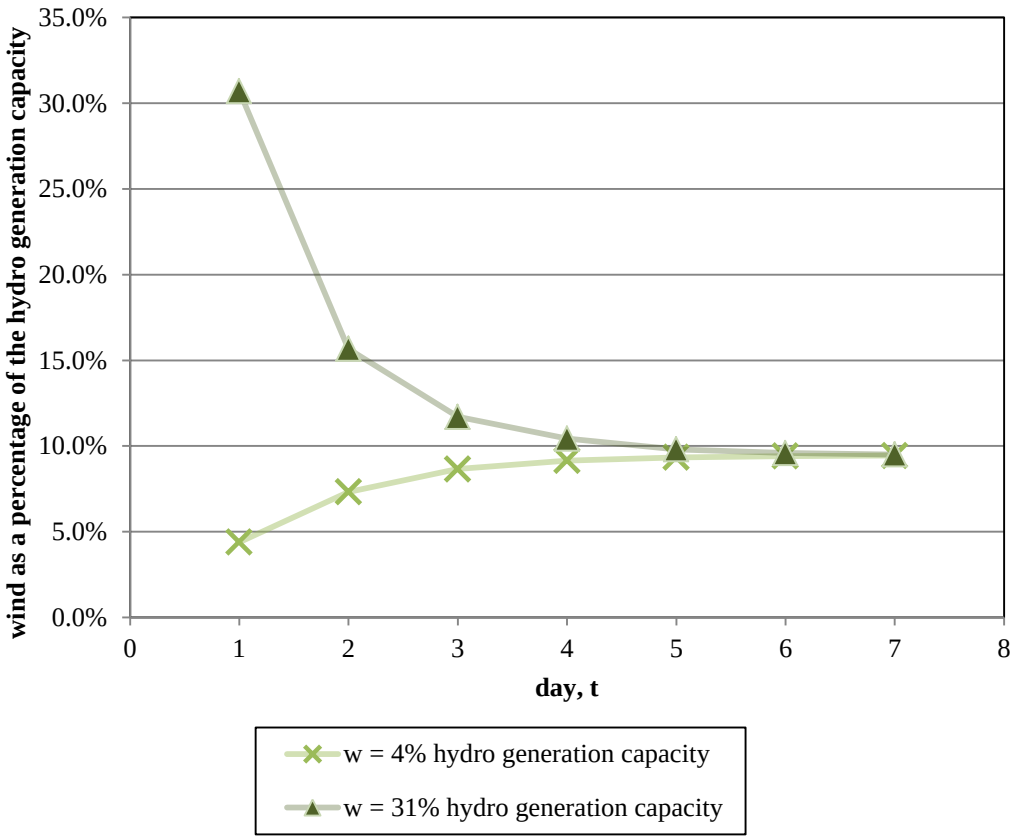

Figure 4- 7: The deterministic7-day wind forecast for two different starting values of the four discrete wind states described in Section 4.3.2. The wind generation for the 7-day horizon is the "expected" wind generation of a Markov chain representation of the wind generation forecast (described in more detail in Section 4.4.4)

Figure 4-8 shows the values computed by the dynamic programming model using Equations (4.29), and (4.30) or (4.31) for the stage 1 day-ahead power commitment policy Γ_1 for two different values of the starting wind state w_1 for the upper reservoir at 48.0% full, the lowest of the 4 discrete storage states. From Table 0-1, we see DD= known Day ahead and hour ahead forecast and N= no effect of wind amplitude on price. In *Scenario (DD, M, N),* Γ_1 for the *Deterministic Wind* uncertainty scenario is higher than the baseline Γ_1 in *Scenario 0,* shown as the solid black line. This is because the wind generation contributes to the power sold on the day-ahead and hour-ahead wholesale electricity markets, as described in Equation (4.30).

For *Scenario (DD, F, N) in* Figure 4-8, the operations are the same as for *Scenario 0*. This is because wind generation is not marketed by the hydro utility and there is no uncertainty in the wind generation.

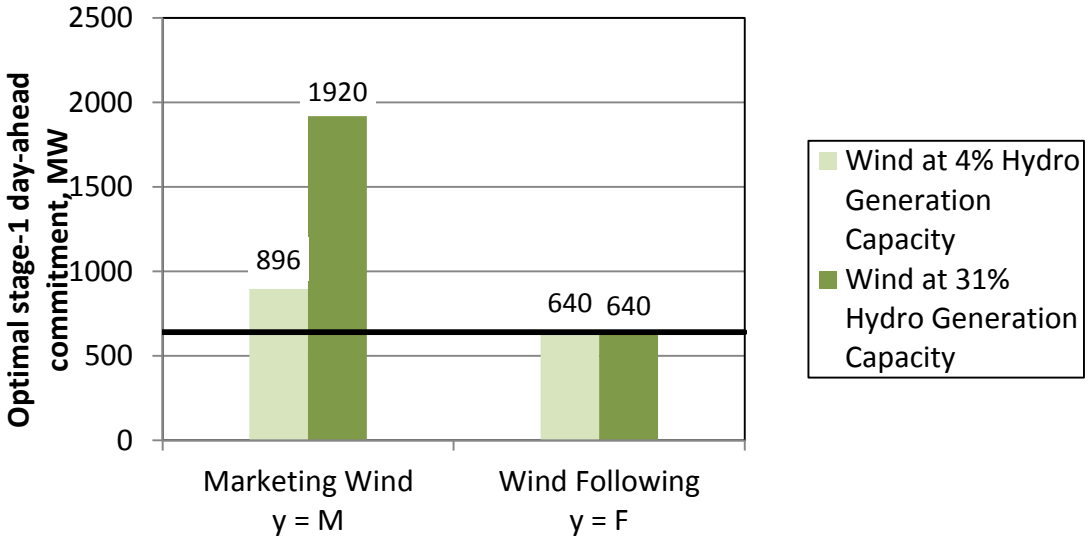

Figure 4- 8: The Scenario (DD, y, N) optimal stage 1 day-ahead commitment policy at different wind generation levels for the upper reservoir at 48.0% full on day 1 of the 7-day optimization horizon. DD and N are defined in Table 0-1. The black line shows the optimal stage 1 day-ahead commitment for Scenario 0.

In this section, we also show detailed operations of the hydropower system as a result of the benefit function calculation described in Section 4.2.2. This detailed operation can be interpreted as a realization of one of the many wind traces that would be considered in the stochastic runs in Sections 4.4.3 and later. Detailed operations are not shown in the later sections.

Table 4-2: The Scenario (DD, M, N) optimal policy and operation of the hydropower system for each of the different wind levels for a 7-day planning horizon. Refer to Table 4-1 for scenario definitions. Low wind means the wind starts at 4% of the hydro generation capacity, high wind means the wind start at 31% of the hydro generation capacity. In each of the cases shown the storage at the upper reservoir is at 48% full.

	A **Optimal stage-1 DA[1] commitment MW**	**B** **Average HA[2] power sold, MW**	**C** **Value function, $ M**	**D** **change in storage, %**	**E** **Total Hydropower system generation, GWh**
Scenario 0 (deterministic, no wind)	640	35	8.92	-7.7%	113
***Scenario (DD, M, N),* Low wind**	896	58	11.14	-7.7%	113
***Scenario (DD, M, N),* High wind**	1,920	107	11.73	-6.7%	63

[1] day-ahead
[2] hour-ahead

Table 4-2 provides a summary of the daily operation of the hydropower system for low (4% of hydro generation) and high (31% of hydro generation) wind generation in *Scenario (DD, M, N).* The optimal stage 1 day-ahead commitments Γ_1 shown in column A increase with increasing wind, as discussed previously. The average hour-ahead power sold (column B) is calculated by taking the average of the hour-ahead power sold over the entire 7-day planning horizon. This value also increases with the increasing wind generation. The value function at stage 1 in column C, $V_1(S_1)$ increases corresponding to the increasing Γ_1 in column A and average hour-ahead power sold in column B. However, the change in storage (and consequently, the total hydropower generation in column E) does not increase with the increasing Γ_1. In fact, there is less drawdown when the wind generation is high, indicating that the difference in the

day-ahead commitment from *Scenario 0* to the different *Scenarios (DD, M, N)* is met by the wind generation.

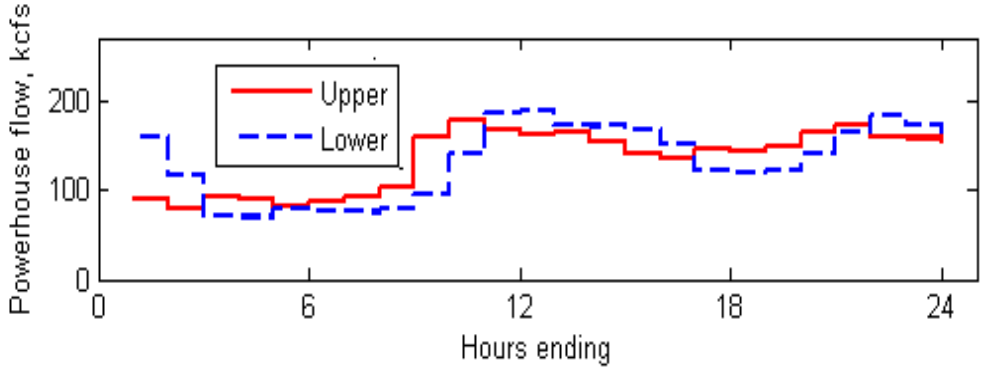

Figure 4- 9: The optimal Scenario (DD, M, N) within-day powerhouse flows for the cascaded two-reservoir system with the upper reservoir storage at 48% full, a day-ahead commitment of 896MW, and a wind generation of 410MW, or 4% of the hydro system generation capacity. There were no spills from either reservoir, and the reservoir levels had little change consistent with the restriction on the drawdown levels of both reservoirs. The optimal solution is obtained through the nonlinear programming formulation in Equations (4.8) through (4.13) and load described in Equation (4.30).

Figure 4-9 shows the values of the nonlinear programming decision variables $s_i^h, r_{i,PH}^h$ and $r_{i,spill}^h$ corresponding to *Scenario (DD, M, N)* with low wind, row 2 in Table 4-2, for the two-reservoir system in Figure 4-1. Since the storage at the lower reservoir is not a state variable in the SDP, it is maintained at a constant elevation while the elevation of the upper reservoir is allowed to vary. The upper reservoir level is drawn down slightly in the day. The flows through the powerhouse at the upper and lower reservoirs correspond very closely to the customer load profile shown in Figure 4-5. Note that the release at the lower reservoir lags the releases at the upper reservoir by about an hour. This corresponds to the travel time between the two reservoirs. In the optimization for *Scenario (DD, M, N)*, there is no spill at either the upper or lower

reservoir.

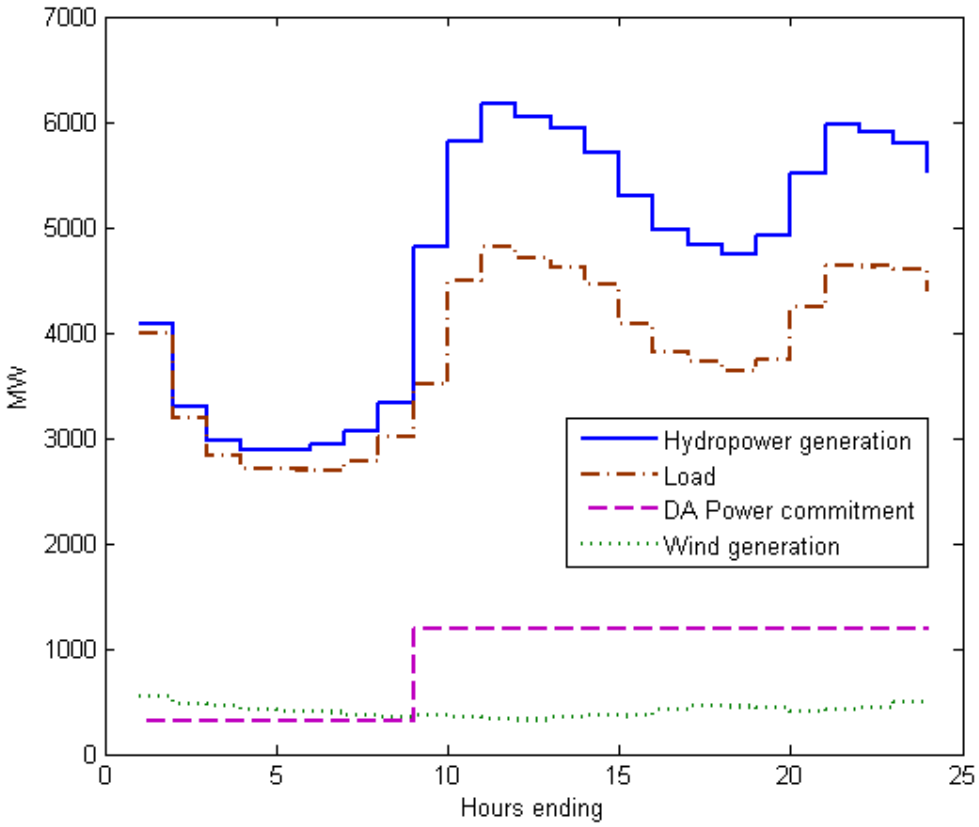

Figure 4- 10: Scenario (DD, M, N) optimal hydropower system generation, customer load, day-ahead (DA) power commitment, and wind generation with upper reservoir storage at 48% full, a day-ahead commitment of 896MW, and a wind generation of 410MW, or 4% of the hydro system generation capacity. Optimal policy is computed using nonlinear programming, Equations (4.8) *through* (4.13) *and load described in Equation* (4.30)

Figure 4-10 shows the relative magnitude of the hydropower system generation, customer load, day-ahead power commitment and the wind power generation corresponding to the operations in Figure 4-9. Observe that the hydropower generation is higher than the load due to the day-ahead power commitment, although less than the sum of the day-ahead commitment and load due to the ability of the hydro utility to market some of the wind to meet the day-ahead power commitment.

4.4.3 *Scenarios (DS, y, N): Deterministic Day-ahead Wind Forecast with Within-Day Deviations from the Day-ahead Wind Forecast*

Now we consider *Scenarios (DS, y, N)* where the day-to-day wind generation $\widehat{w} = (\widehat{w}_1, \dots \widehat{w}_t, \dots, \widehat{w}_7)$ forecast is deterministic, but that within-day deviations in the forecast Δw_t occur. Recall y can be M for the marketing wind or F for the wind following defined in Table 4-1. Under these assumptions, the Bellman equation in Equation (4.1) simplifies to Equation (4.32).

Scenario (DS, y, z) Bellman equation:

$$V_t(\vec{s}_t, \widehat{w}_t) = \max_{\Gamma_t} \left\{ \mathop{\mathbb{E}}_{\Delta w_t} [B(\vec{s}_t, \Gamma_t, \widehat{w}_t, \Delta w_t) + V_{t+1}(\vec{s}_{t+1}, \widehat{w}_{t+1})] \right\} \quad (4.32)$$

Additionally, the load in the *Scenario (DS, M, z)* (Marketing Wind) and *Scenario (DS, F, z)* (Wind Following) cases are described by Equations (4.23) and (4.24), which account for the within-day uncertainty in wind being modeled.

We show the results for two different deterministic day-ahead wind forecasts $\widehat{w}$, for the entire horizon that were shown in Figure 4- 7. These wind forecasts are differentiated by their starting values, $\widehat{w}_1$ at 4% and 31% of the hydro generation capacity. The upper reservoir is at 48.0% of its capacity. The expected benefit over seven different within-day wind-deviation scenarios is calculated where $\Delta w_t = (-0.77, -0.49, -0.24, 0.03, 0.28, 0.57, 0.94)$ with a probability of $\Pr(\Delta w_t) = (8.6\%, 15\%, 25\%, 25\%, 15\%, 9\%, 0.9\%)$. The expected value of The wind generation outcome for that day is described by Equation (4.16). Figure 4-11 shows the optimal stage-1 day-ahead commitment Γ_1 for *Scenarios (DS, y, N)* reflecting the assumptions as described above.

Figure 4-11 reveals that the stage-1 optimal decision Γ_1 in the *Marketing Wind* case, *Scenario (DS, M, N),*is higher than the Γ_1 in baseline case, *Scenario 0,* which is shown as the solid line. Again, this is because the wind generation contributes to the power sold on the day-ahead and hour-ahead markets, as described in Equation (4.30).

For the *Wind Following* case, *Scenario (DS, M, N),* shows that similarly, when $\widehat{w}_1$ is at 4% of the hydro system generation capacity, the within-day uncertainty does not appear to affect Γ_1. However, the within-day uncertainty does affect the day-ahead commitment when $\widehat{w}_1$ is at 31% of the hydro system generation capacity. This is because there is higher variability in wind generation due to the higher wind forecast and the hydro system has to make up for the wind generation when it ends up being lower than forecasted within the day. Thus, the optimal day-ahead commitment hedges for the wind uncertainty within the day in this scenario.

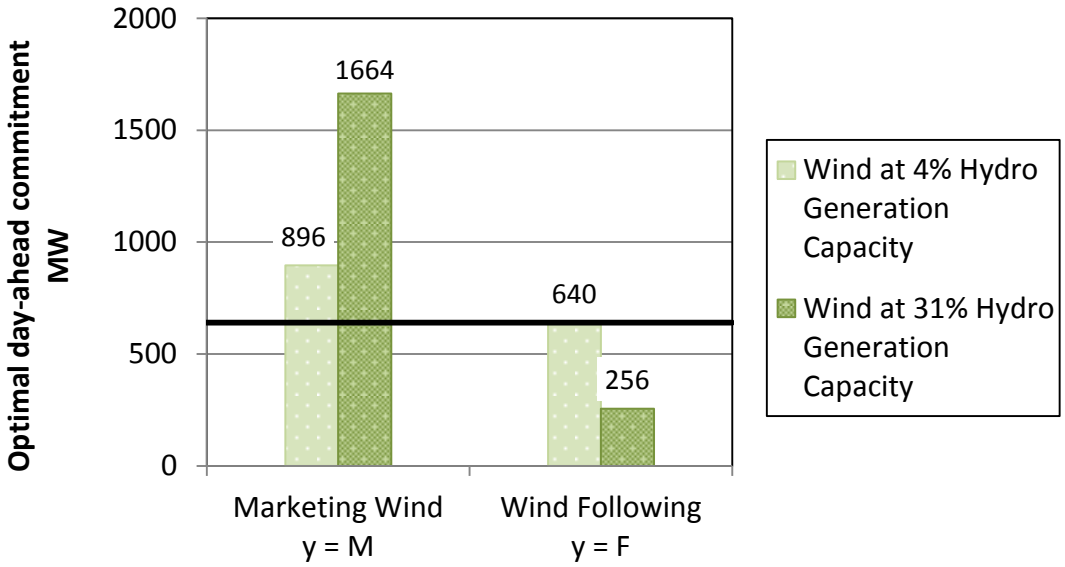

Figure 4- 11: The Scenario (DS, y, N) optimal day-ahead commitment policy at different wind generation levels for the Upper Reservoir at 48.0% full on day 1 of the 7-day optimization horizon. Table 0-1 defines DS and N. y=Marketing Wind (M) or Wind Following (F).The black line shows the day 1 optimal day-ahead commitment for Scenario 0.

4.4.4 Scenarios (SS, y, N) Stochastic Day-ahead Wind Forecast with Within-day Deviations from the Day-ahead Forecast

Next we show the results for *Scenarios (SS, y, N)* when both the day-to-day wind generation forecasts and within-day wind generation are uncertain (x = SS) and the wind generation does not affect the wholesale energy price (z = N). Under these assumptions the full Stochastic Dynamic Programming – Nonlinear Programming (SDP-NLP) formulation as described in Equations (4.1) and (4.3) is solved. The day-ahead wind generation forecast is modeled as a Markov chain with four discrete states and a Markov transition matrix as shown in Equation (4.33).

$$\mathbb{P} = \begin{bmatrix} 0.77 & 0.15 & 0.05 & 0.03 \\ 0.46 & 0.23 & 0.15 & 0.15 \\ 0.42 & 0.42 & 0.08 & 0.08 \\ 0.14 & 0.43 & 0.43 & 0 \end{bmatrix} \tag{4.33}$$

The matrix $\mathbb{P}$ is obtained from historical wind power production data for the month of December. Each row in the transition matrix $\mathbb{P}$ represents $\widehat{w}_t$, the state of the day-ahead wind forecast at time t, with the top row being 4% of the hydro system generation capacity and the bottom row being 31% of the hydro system generation capacity. Each column represents $\widehat{w}_{t+1}$, the state of the day-ahead wind forecast at time t+1 with the leftmost column being 4% of the hydro system generation capacity and the rightmost column being 31% of the hydro system generation capacity. For example, observe from the top row that $\widehat{w}_{t+1}$ tends to be low when $\widehat{w}_t$ is low, since there is a 77% of remaining at the lowest wind level. The bottom row shows that at the highest level of $\widehat{w}_t = 31\%$ of the hydro system generation capacity, $\widehat{w}_{t+1}$will probably be at a lower generation level (since there is only a 14% probability of remaining at the highest level), and is likely to reach the lowest generation wind level of $\widehat{w} = 4\%$ of the hydro system generation capacity in two stages (days). Note that the "deterministic" wind forecasts mentioned in sections 4.4.2 and 4.4.3 and Figure 4- 7 are actually the expected wind outcomes as described by the transition matrix $\mathbb{P}$ starting from 4% or 31% of the hydro generation capacity.

The optimal stage-1 day-ahead commitment Γ_1 and corresponding value $V_1$for the different *Scenarios (x, y, N)* considered thus far from Sections 4.4.1 through this section are summarized in Table 4-3. In this table, the stage 1 wind level $\widehat{w}_1$ is at 31% of the hydro system generation capacity for all *Scenarios (x, y, N)*. Recall that *Scenarios (DS, y, N)* and *Scenarios*

(SS, y, N) incorporate some uncertainty, compared to *Scenarios (DD, y, N)* and *Scenario 0* that are deterministic.

Table 4-3: The optimal stage-1 day-ahead commitment Γ_1 and corresponding stage 1 value function V_1 for under different scenarios when no wind generation effect on wholesale energy price is modeled. Table 0-1 defines the scenario designations. Two Upper Reservoir initial storage levels are shown, 48.0% and 49.2% full. The wind at stage 1 is at 31% of the hydro system generation.

		A Scenario 0	**B Scenario (DD, y, N)**	**C Scenario (DS, y, N)**	**D Scenario (SS, y, N)**
***y = M*, Upper Res at 48.0%**	Γ_1 (MW)	640	1920	1664	1664
	V_1 ($M)	8.9	11.7	10.4	10.1
***y = M*, Upper Res at 49.2%**	Γ_1 (MW)	1152	1920	1792	1792
	V_1 ($M)	11.2	12.1	11.2	11.1
***y = F* , Upper Res at 48.0%**	Γ_1 (MW)	640	640	256	256
	V_1 ($M)	8.9	8.9	6.8	6.7
***y = F*, Upper Res at 49.2%**	Γ_1 (MW)	1152	1152	640	640
	V_1 ($M)	11.2	11.2	9.2	9.2

In general, Table 4-3 shows that when there is more water in storage (i.e. when the upper reservoir starts at 49.2% full), the optimal stage-1 day-ahead commitment $\Gamma_1$is also higher. Since wind generation does not affect the price for scenarios with *z = N*, the commitment and value seen in columns B through D are greater than or equal to the *Scenario 0* base case with no wind. As more uncertainty in the wind generation is considered going from Column B to Column D however, Γ_1 becomes more conservative and V_1 decreases. This is because in *Scenarios (DS, y, N)* and *Scenarios (SS, y, N)*, the algorithm is choosing policies that would result in the best expected value over the different possible wind generation outcomes.

Recall that the wind forecast shown in Figure 4-7 for the *Scenarios (DS, y, N)* (column C in Table 4-3) is the expected wind trace for the Markov chain starting at $\widehat{w}_1 = 31\%$ of the hydro

generation capacity in the *Markov Wind* uncertainty scenario. This results in very similar values in the optimal Γ_1 and V_1 between the *Scenarios (DS, y, N)* and the *Scenarios (SS, y, N)* (column D). In fact, the Γ_1 between these two scenario groups are the same, but the values seen of Scenarios(SS, y, n) are lower than the values seen in *Scenarios(DS, y, n)* because of the additional uncertainty in the day-to-day wind generation forecast.

Observe that in *Scenarios (x, M, N)* in the first two rows in Table 4-3, the optimal Γ_1 is higher than the *Scenario 0* base case with no wind, regardless of the way uncertainty is represented. The corresponding optimal stage-1 value function V_1 is generally equal to or greater than the *Scenario 0* base case with no wind. Clearly, when there is extra generation in the system (as modeled in Equation (4.23)) and there is a market for it, the hydro utility will try to make more money by selling more power on the day-ahead wholesale electricity market The difference in values between column D and column A show the additional value the ability to sell the wind generation provides to the hydro utility under the assumptions we have made. It is worth noting that in some cases the value added by selling wind generation is close to zero or that there is a loss to the hydro utility. This is because even though the hydro utility can sell the wind generation, there are additional risks from the uncertainty in wind generation that is captured by the full modeling of uncertainty in *Scenario (SS, M, N).*

In contrast, for *Scenarios (x, F, N)* in the last two rows in Table 4-3, the optimal Γ_1 and V_1 are the same or lower than the *Scenario 0* base case with no wind shown in column A. In *Scenarios (DD, F, N)*, the optimal Γ_1 and V_1 are the same as in the baseline *Scenario 0*. This is because the wind does not contribute to or subtract from the load in the system, as shown in

Equation (4.24). However, in *Scenarios (DS, F, N)* and the *Scenarios (SS, F, N)* under different starting reservoir storage levels, the optimal day-ahead commitment Γ_1 decreases to hedge for the different possible wind generation outcomes considered. The wind generation in this case will contribute to or subtract from the required load to be met, due to the deviation of the within-day wind generation from the forecasted wind generation for that day, as modeled in Equation (4.24). As a result, the hydro utility can expect lower V_1values in the *Wind Following (y = F)* marketing case. The difference in values between column D and column A show the economic impact of balancing the hourly wind deviation from forecasts to the hydro utility under the assumptions we have made. This may be used to inform the payments that the hydro utility would seek from the wind generation owner to cover the losses incurred by the hydro utility compared to if it did not have to consider wind in its operations at all.

4.4.5 Scenarios (x, y, W): Add Wind effect on Day-Ahead Price

Now we will consider the results when there are effects on the day-ahead price based on the wind forecast, as described in Section 4.3.3. Recall that in Equation (4.19), increasing wind generation can be modeled to have a downward effect on the day-ahead wholesale energy prices. This change in day-ahead prices happens independently of whether or not we are able to use the wind power generation to help meet the load, i.e. the same price change occurs for the *Marketing Wind (y = M)* and *Wind Following (y = F)* cases. Table 4-4 shows Γ_1 for the different Uncertainty Scenarios when there is a wind forecast effect on day-ahead price. The stage 1 wind level is at 31% of the hydro system generation capacity for all representations of uncertainty.

We see similar trends to what was seen before in Section 4.4.4 when there was no wind effect on day-ahead price. When there is more water in storage (rows 1 and 3 in Table 4-4), the optimal Γ_1 is also higher. As more uncertainty in the wind generation is considered going from column B to column D in Table 4-4, the optimal Γ_1 is always lower than when the *Scenario 0* base case with no wind generation in the system.

Table 4-4 The optimal stage-1 day-ahead commitment Γ_1 and corresponding stage 1 value function V_1 for under different scenarios when the wind generation effect on price as described in Equation (4.19). Table 0-1 defines the scenario designations. Two upper reservoir initial storage levels are shown, 48.0% and 49.2% full. The wind at stage 1 is at 31% of the hydro system generation.

		A Scenario 0	**B Scenario (DD, y, W)**	**C Scenario (DS, y, W)**	**D Scenario (SS, y, W)**
***y = M*, Upper Res at 48.0%**	Γ_1 (MW)	640	1920	1408	1408
	V_1 ($M)	8.9	9.8	8.7	8.5
***y = F* , Upper Res at 48.0%**	Γ_1 (MW)	640	384	-384	-384
	V_1 ($M)	8.9	7.7	6.0	6.1
***y = M*, Upper Res at 49.2%**	Γ_1 (MW)	1152	1920	1792	1792
	V_1 ($M)	11.2	10.2	9.4	9.4
***y = F*, Upper Res at 49.2%**	Γ_1 (MW)	1152	1024	128	128
	V_1 ($M)	11.2	9.5	7.9	8.0

In comparing Table 4-3 to Table 4-4, when there is a wind effect on the day-ahead price, the optimal Γ_1 and V_1 is always lower. In fact, Table 4-4 shows that for *Scenario (DS, F, W)* and *Scenario (SS, F, W)* when the upper reservoir is at 48% of its capacity, the hydro utility has to purchase power on the day-ahead market to meet the storage targets and the customer load. This is optimal because the starting wind generation level (31% of hydro generation capacity) has a lower base and water in the reservoir may have more value on a later time step.

4.4.6 Discussion

Several illustrative runs were presented in this chapter that illustrates the effect of each of the Marketing Cases and Uncertainty Scenarios. A deterministic optimization is performed to set a baseline for comparison, called *Scenario 0*.

The results show that having wind generation in the system may benefit the hydro utility that also owns and markets the wind generation as in the *Marketing Wind* case, as long as wind generation does not have a significant impact on day-ahead energy prices. However, if the hydro utility only serves to provide hour-by-hour balancing of the wind forecast deviations in the *Wind Following* case, then the hydro utility may actually then use the algorithm as an indicator of what the compensation for this transmission from the wind power generation owner to the hydro utility should be. Introducing increasing levels of uncertainty causes the model to hedge by decreasing its commitment to produce power to be sold on the wholesale electricity market.

The inferred model of the wind effect on day-ahead prices serves to inform the hydro utility on how their operations would be affected in the situation where high wind penetration affects the market. Results show that for our inferred wind effect on price model, the hydro utility generally suffers a loss compared to the *Scenario 0* base case because of the high level of wind generation in the system. This result, it must be cautioned, is highly assumption driven and thus careful study should be undertaken by the hydro utility before implementing any model of the impact wind generation would have on the day-ahead prices.

4.5 Conclusions

In this chapter we described an algorithm for optimization of a hydropower system under wind generation uncertainty. We applied the optimization framework to a hypothetical hydro utility operating a hydropower system with a large generation capacity, modeled after Grand Coulee and Chief Joseph dams in Washington State, U.SA. The optimization framework enables the realistic modeling of two ex-ante wholesale electricity markets on different time frames: the day-ahead wholesale electricity market and the real time (hourly) wholesale electricity market. The non-linear programming formulation of the benefit function allows for some recourse from the day-ahead decision made in the SDP formulation. The optimization framework also considers the effect of the utility's decisions on the prices and income in the day-ahead wholesale electricity market through a price curve reflecting other utilities' willingness to pay for the power sold by our hypothetical utility.

We believe the adaptive strategies produced by our optimization framework for not just the day-to-day uncertainty, but also within-day uncertainty warrants its consideration as a viable optimization framework. To further decrease the decision space and subsequently, the model run times, we have used a time-decomposition approach. Time decomposition results in fewer stages and will be more computationally efficient than traditional stochastic dynamic programming, which would treat each hour as a stage and thus require many stages to go out to a one week time horizon. The radial basis function interpolation to calculate the future value function allows for a sparse and scattered data set for interpolation and thus would require fewer points than a traditional spline. The benefit function is made up of two parts, the first of which calculates the

value of the day-ahead commitment by optimally allocating a daily value to hourly values before the optimization, saving fewer decision variables in the nonlinear programming environment.

In this chapter, we have shown the utility of our novel, feature-rich model for optimizing hydropower operations under wind generation uncertainty. We believe this optimization framework has a huge potential to help large utilities tackle the challenges of renewable generation integration.

4.6 References

Abreu, L. V. L., M. E. Khodayar, M. Shahidehpour, and L. Wu (2012), Risk-Constrained Coordination of Cascaded Hydro Units With Variable Wind Power Generation, IEEE Trans. Sustain. Energy, 3(3), 359–368.

Acker, T. L. (2011), Hydroelectric Industry's Role in Intergrating Wind Energy.

Angarita, J., and J. Usaola (2007), Combining hydro-generation and wind energyBiddings and operation on electricity spot markets, Electr. Power Syst. Res., 77(5-6), 393–400, doi:10.1016/j.epsr.2006.03.019.

Bakke, G. (2016), The Grid: The Fraying Wires Between Americans and Our Energy Future, Bloomsbury Publishing.

Barbose, G. (2016), U.S. Renewable Portfolio Standards: 2016 Annual Status Report.

Becker, L., and W. W.-G. Yeh (1974), Optimization of Real Time Operation of a Multiple-Reservoir System, Water Resour. Res., 10(6), 1107–1112.

Bonneville Power Administration (2014), Wind Installed Capacity, Available from: https://transmission.bpa.gov/business/operations/Wind/WIND_InstalledCapacity_Plot.pdf (Accessed 3 May 2017)

Bonneville Power Administration (n.d.), WIND GENERATION & Total Load in The BPA Balancing Authority, Available from: https://transmission.bpa.gov/Business/Operations/Wind/default.aspx

Buhmann, M. D. (2003), Radial Basis Functions: Theory and Implementations, Cambridge University Press.

Chen, V. C. P., D. Ruppert, and C. A. Shoemaker (1999), Applying Experimental Design and Regression Splines to High-Dimensional Continuous-State Stochastic Dynamic Programming, Oper. Res., 47(1), 38–53.

Fernandez, A., S. Blumsack, and P. Reed (2012), Evaluating wind-following and ecosystem services for hydroelectric dams in PJM, J. Regul. Econ., 41(1), 139–154, doi:10.1007/s11149-011-9177-9.

Hamann, A., and G. Hug (2016), Using Cascaded Hydropower Like a Battery to Firm Variable Wind Generation, in Power Energy Society General Meeting, pp. 0–4.

Howard, C. D. D., and J. R. Stedinger (2012), Hydroelectric Power and the Future, in Toward a Sustainable Water Future, edited by W. Grayman, D. P. Loucks, and L. Saito, pp. 234–242, ASCE Press.

St. John, J. (2016), The California Duck Curve is Real, and Bigger Than Expected, Green Tech Media.

Johnson, S. A., J. R. Stedinger, C. A. Shoemaker, Y. Li, and J. A. Tejada-Guibert (1993), Numerical Solution of Continuous-State Dynamic Programs using Linear and Spline Interpolation, Oper. Res., 41(3), 484–500.

Labadie, J. W. (2004), Optimal Operation of Multireservoir Systems : State-of-the-Art Review, J. Water Resour. Plan. Manag., 130(2), 93–111.

Matevosyan, J., M. Olsson, and L. Söder (2009), Hydropower planning coordinated with wind power in areas with congestion problems for trading on the spot and the regulating market, Electr. Power Syst. Res., 79(1), 39–48, doi:10.1016/j.epsr.2008.05.019.

Miranda, V., H. Martins, and V. Palma (2014), Optimizing Large Scale Problems With Metaheuristics in a Reduced Space Mapped by Autoencoders — Application to the Wind-Hydro Coordination, IEEE Trans. Power Syst., 29(6), 3078–3085.

Regis, R. G., and C. a. Shoemaker (2007), A Stochastic Radial Basis Function Method for the Global Optimization of Expensive Functions, INFORMS J. Comput., 19(4), 497–509, doi:10.1287/ijoc.1060.0182.

Regis, R. G., and C. A. Shoemaker (2009), Parallel stochastic global optimization using radial basis functions, INFORMS J. Comput., 21(3), 411–426, doi:10.1287/ijoc.1090.0325.

Stedinger, J. R., B. F. Sule, and D. P. Loucks (1984), Stochastic dynamic programming models for reservoir operation optimization, Water Resour. Res., 20(11), 1499 – 1505, doi:10.1029/WR020i011p01499.

Trezos, T., and W. W.-G. Yeh (1987), Use of Stochastic Dynamic Programming for Reservoir Management, Water Resour. Res., 23(6), 983–996.

Tuohy, A., P. Meibom, E. Denny, and M. O. Malley (2009), Unit Commitment for Systems with Significant Wind Penetration, IEEE Trans. Power Syst., 24(2), 592–601.

Turgeon, A. (1980), Optimal Operation of Multireservoir Power Systems with Stochastic Inflows, Water Resour. Res., 16(2), 275–283.

U.S. Army Corps of Engineers (n.d.), Columbia River Basin Water Management, Available from: http://www.nwd.usace.army.mil/Missions/Water/Columbia/ (Accessed 3 May 2017)

U.S. Energy Information Administration (2012), Negative prices in wholesale electricity markets indicate supply inflexibilities, Today in Energy. Available from: http://www.eia.gov/todayinenergy/detail.cfm?id=5110# (Accessed 4 January 2014)

Wangdee, W., W. Li, and R. Billinton (2010), Coordinating Wind and Hydro Generation to Increase the Effective Load Carrying Capability, in IEEE 11th International Conference on Probabilistic Methods Applied to Power Systems (PMAPS), pp. 337–342.

Zima-Bockarjova, M., J. Matevosyan, M. Zima, and L. Söder (2010), Sharing of Profit From Coordinated Operation Planning and Bidding of Hydro and Wind Power, IEEE Trans. Power Syst., 25(3), 1663–1673.

CHAPTER 5

CONCLUSIONS

A goal for this research project was to develop efficient methods for optimizing hydropower operations incorporating critical hydraulic parameters, energy production relationships, environmental constraints, and economic issues including energy market price effects. Efficient methods employ precomputed powerhouse functions and operating rules, and an appropriate mix of optimization algorithms. The resulting optimization models address concerns of computational efficiency and renewable energy integration using relatively flexible hydro generation. Additionally, the research introduced a method of modeling environmental constraints in both powerhouse and spillway operations. This allows for the model to investigate the maximization of hydropower generation value while meeting complex release and environmental obligations.

Chapter 2 develops an algorithm to provide precompute optimized multi-turbine Powerhouse Generation Functions for each reservoir in the 10-reservoir Federal Columbia River Power System. This new algorithm to generate precomputed powerhouse functions reduces the many dispatch and loading decisions for multiple turbines at a hydropower project into a powerhouse function that depends on total flow. The dispatch and loading rules were simplified by a heuristic that loaded the turbines at their most efficient operating point, and continues to load turbines (with the latest running part of the period) at the same marginal generation rate until they all reach the capacity.

We showed that this dispatch and loading is optimal, i.e. no reallocation of releases among turbines can increase the overall generation for a given total release. The powerhouse functions can also incorporate turbine availability and operations when there is a need to incorporate fish passage considerations that mandate turbine dispatch order. The difference in generation between the actual and approximate Fish Dispatch powerhouse generation functions is negligible. Generation differences are much less than 5 MW in any period at any powerhouse, which is assumed to be acceptable; the automatic generation control within the reservoir power plant can only adjust to within 5MW of precision. Finally, the algorithm produces concave powerhouse generation functions or concave approximations of the powerhouse generation functions to ensure a convergence of the sequential quadratic programming algorithm to a global maximum. This algorithm provides a simple description of the maximum generation of a project with many turbines of different types for a give flow can greatly simplify hydropower system models.

Chapter 3 considers the computationally efficient of deterministic optimization model for the 10-reservoir Federal Columbia River System operation. The model incorporates expected inflow, hydropower plant operation, contracted energy loads, and the hydropower utility's interaction with wholesale energy markets. When applicable the model also includes special seasonal constraints for fish addressing location and volume of flow released from specified turbines or reservoirs. This enables the model to demonstrate the opportunity cost to the system by having to operate under Fish Operations.

Our objective function takes into account the hydro utility's opportunities as a large player in the hydropower markets and thus participation in the day-ahead wholesale energy markets to minimize the regional cost of energy generation. The parameters for the objective function are the price forecast for a particular volume of power transacted in the market. We showed that for an entity with market power, maximizing revenue will result in prices that are not balanced across periods, which would be the economically efficient solution. By maximizing avoided cost, the entity generates such that the cost of energy is lowered for all.

Altogether,Chapter 3 presents a multi-reservoir scheduling models with many unique features including variable time step flow routing between reservoirs, precomputed powerhouse functions, project release functions to honor complicated fish-operational requirements related to turbine dispatch and upper and lower bounds on spills as well as energy generation, market reactions to variation is energy sales, and an avoided-cost objective to identify a socially optimal solution.

Finally, Chapter 4 describes a feature-rich optimization algorithm for optimization of a hydropower system under wind generation uncertainty. The optimization framework is implemented with a hypothetical utility operating a wind and hydropower system with a large generation capacity, modeled after the Mid-Columbia projects (Grand Coulee and Chief Joseph) in the Federal Columbia River Power System. The optimization framework simulates a reality where the utility would hedge for uncertainty by participating in various wholesale energy markets to meet its commitment. The non-linear programming formulation of the benefit function allows for recourse from the day-ahead decision. The optimization framework also

considers the effect the utility's decisions on the prices and income in the day-ahead market through a demand curve reflecting other utilities' willingness to pay for the power sold by our hypothetical utility.

The results from the optimization in Chapter 4 show that if there is a market for it, having wind in the system will benefit the hydro utility that also markets the wind generation. Conversely, if the hydro utility only serves to provide the transmission of the wind power to other locations, then the algorithm provides an indicator of what the compensation for this transmission from the wind power generation owner to the hydro utility should be. Introducing increasing levels of uncertainty causes the model to hedge by decreasing its commitment to produce power to be sold on the wholesale electricity market.

There are opportunities for future research in the hydropower area, especially as it pertains to renewable generation integration. First, an investigation is needed into a better functional form of the demand curve to better capture the wholesale price of energy as a result of a large hydro utility's participation in the wholesale day-ahead energy market. Additionally, we could investigate whether the day-ahead market is a good representation of energy sales that can be anticipated days and weeks ahead of time. Expansion on this research would incorporate a larger, more complex reservoir system into the stochastic optimization framework with wind generation uncertainty. Finally, a better representation of the uncertainty in hourly wind generation such as a cluster analysis on available wind generation data or a more diverse geographical representation of wind generation rather than simply scaling the average hourly

wind generation profile would improve the stochastic algorithm. These topics are presented as research ideas that can be pursued and which should be worthwhile.

Hydropower systems optimization continues to be an important and challenging optimization problem. This research addresses new requirements associated with the incorporation of renewal energy sources and the increasing constraints associated with preserving fish populations, applying it to a 10-reservoir cascaded hydropower system. This research has a huge potential to help large utilities address the competing priorities of renewable generation integration and environmental stewardship, while still being able to maximize the value of wind and hydropower generation.

APPENDIX A

TAIL WATER EFFECTS

Power generation at a project is typically a function of releases through the powerhouse as well as the net head, or the difference in elevation between the forebay and tailwater elevations. Generally, the tailwater elevation LTW_t^i for project *i* at time *t* also depends on the total outflows of the project.

The project tailwater elevation-discharge relationship has been found to be reasonably approximated using simple linear relationships. For all projects except Bonneville, the tailwater elevation is a linear function of the releases from the project at time *t* and the forebay elevation at the downstream project, described in the equation below. The values of the coefficients at each of the projects are summarized in Table A-1.

$$LTW^i_t = A^i + B^i * \mathrm{R}^i_t + C * \mathrm{LFB}^{i+1}_{t-1}$$

A Chief Joseph is a special case: releases flows into the forebay of Wells, a nonfederal project. For this project, we assume the Wells elevation to be a fixed value.

Table A-1: Coefficients of regression for the tailwater functions for projects modeled in the Columbia River Power System

Reservoir	A^i	B^i	C^i
Grand Coulee (GCL)	436.02	0.0909	0.5412
Chief Joseph (CHJ)	293.88	0.0497	0.6205
Lower Granite (LWG)	119.01	0.0211	0.8119
Little Goose (LGS)	230.27	-0.0040	0.5726
Lower Monumental (LMN)	-128.88	0.0447	1.2914
Ice Harbor (IHR)	199.57	0.0736	0.4090
McNary (MCN)	18.53	0.0202	0.9237
John Day (JDA)	50.00	0.0219	0.6773
The Dalles (TDA)	12.59	0.0331	0.8048

Bonneville is the terminus of the system, and therefore has no downstream forebay elevation. But the tailwater elevation is influenced by tidal effects, and is hard to model. In this iteration of the model, the tailwater elevation at Bonneville is a linear function of the tailwater elevation at the previous time step, and the project releases at time *t* and at time *t-1*, as specified in the equation below.

$$LTW_t^{BON} = TW_{t-1}^{BON} + \frac{1\,ft}{25kcfs} * (R_t^{BON} - R_{t-1}^{BON})$$

APPENDIX B

END OF HORIZON CONSTRAINTS

Oftentimes optimizers run into an end-of horizon issue where there is no more benefit to storing water so the algorithm tries to empty the reservoir as much as it can. Additionally, because we are modeling the travel time of flow in the system, the flow in transit is not kept track of in the last time period, resulting in water as "lost flow" at the last time period. We provide several solutions, which can be employed jointly and separately.

First, we can modify the flow transition matrices so that flows that would have been in transit at the end of the planning horizon instead arrive in the last modeled period. This partly resolves the "lost flow" problem because there are no longer flows in transit at the end of the modeled period at most of the projects. An exception is the flow between Chief Joseph and McNary in the 4- and 8-hour time periods. In this case, we allow the flow to be routed as usual. However, we will show that a caveat is that this solution distorts the dynamics in the last period modeled, which has too much inflow. Thus some care needs to be exercised when implementing this solution. We further mitigated this by having routing over 24-hour time steps at the last time interval, which has less distortion in general.

Second, one can specify a marginal value for flows in transit at the end of the last time period or a value of being at a particular elevation level at the end of the time period. This would be an estimate of the value of water in storage in the reservoir to which the flow is headed. The caveat to this method is that there has to be some estimation of the marginal, which requires expert judgement.

Lastly, one can specify minimum, maximum or an exact value on the daily release rate for each project for the periods for which a portion of the day's release will be in transit at the end of the final period. Thus with an 8-hour time step, one would specify a constant daily release rate out of Chief Joseph for the last three 8-hour periods. Chief Joseph is the worst case because of the 17-hour time between Chief Joseph and the closest downstream reservoir McNary. If the transit time is equal to or less than the period length, then only the flow in the last period needs to be constrained. For the Chief Joseph case, with a 24 hour time step, only the last period is a concern; with a 17 hour transit time an 8-hour time steps is more than 2 periods requiring that the release in the last 3 periods be constrained. For a 4 hour time step, one would need to constrain 5 periods correspond to 20 hours, which is less than a day. Thus across all projects, it is only the flows in the last day of the model that will be distorted by this end-of-horizon fix.

In this chapter, we only discuss results implemented using the first end-of-horizon fix, which is to modify the flow transition matrices. The implementation of the second and third solutions can be done using results from a mid-term model. We will show that these produce satisfactory results for a 21-day optimization horizon.

APPENDIX C

FITTING A RADIAL BASIS FUNCTION TO DISCRETE FUTURE STATES

For K distinct states $S_k = (\vec{s}_t, \widehat{w}_t),\ S_1, \dots, S_K \in \mathbb{R}^d$, where the future value function V_{t+1} is known, a Radial Basis Function (RBF) interpolant of the form in Equation (1.1) is used. The following derivation is based on that outlined in Regis and Shoemaker [2007].

$$V_{t+1}(S) = \sum_{k=1}^{K} \lambda_k * \phi(\| S - S_k \|) + \mathrm{p(S)} \tag{1.1}$$

Where
$\lambda_k \in \mathbb{R}\ for\ k = 1, \dots, K$ are the weights on the basis function $\phi(\cdot)$,
$|| \cdot ||$ is the Euclidean norm, and
$p \in \Pi_m^d$, the linear space of polynomials in *d* variables of degrees less than or equal to *m*, where m is defined for a different basis function $\phi(\cdot)$.
$\phi(r) = r^3$ is the cubic RBF

To fit an RBF to the available data $V_{t+1}(\vec{s}_{t+1}, \widehat{w}_{t+1})$, define the $K \times K$ matrix Φ by Equation (1.2)

$$\Phi_{ij} = \phi\left(\left\|S_i - S_j\right\|\right) = \left(\left\|S_i - S_j\right\|\right)^3 \qquad i, j = 1, \dots, \mathrm{K} \tag{1.2}$$

Define $m_\phi = \frac{3}{2}$ for a cubic spline and select $m > m_\phi$ to be the dimension of the linear space Π_m^d. Also, let $p_1, \dots, p_m$ be a basis of Π_m^d and define matrix $\mathcal{P} \in \mathbb{R}^{n \times m}$ as in Equation (1.3)

$$\mathcal{P}_{ij} \equiv p_j(S_i) \quad i = 1, \dots, l \ \ j = 1, \dots, m \tag{1.3}$$

The RBF model that interpolates the points $\left(S_1, V_{t+1}(S_1)\right), \dots, \left(S_K, V_{t+1}(S_K)\right)$ is obtained by solving the system of equations for $\begin{pmatrix} \lambda \\ c \end{pmatrix}$ in Equation (1.4).

$$\begin{bmatrix} \Phi & \mathcal{P} \\ \mathcal{P} & \mathbf{0} \end{bmatrix} \begin{bmatrix} \lambda \\ c \end{bmatrix} = \begin{bmatrix} V_{t+1} \\ \mathbf{0}_m \end{bmatrix} \tag{1.4}$$

Where
$V_{t+1} = [V_{t+1}(S_1), \dots, V_{t+1}(S_K)]'$
$\lambda = (\lambda_1, \dots, \lambda_K)^T$
$c = (c_1, \dots, c_m)^T \in \mathbb{R}^m$
The coefficient matrix $\begin{bmatrix} \Phi & \mathcal{P} \\ \mathcal{P} & \mathbf{0} \end{bmatrix}$ in Equation (1.4) is invertible if and only if $rank(\mathcal{P}) = m$, where $\mathcal{P}$ is the matrix defined in Equation (1.3), and $m = \dim(\Pi_m^d)$.